Synthesis and characterization of ten new 1D, 2D and 3D-coordination polymers with oxygen or nitrogen containing ligands by using different metal cations.

DISSERTATION

zur Erlangung des akademischen Grades doctor rerum naturalium

(Dr. rer. nat.)

FRIEDRICH-SCHILLER-
UNIVERSITÄT
JENA

vorgelegt dem Rat der Chemisch-Geowissenschaftlichen Fakultät der

Friedrich-Schiller-Universität Jena

von **M.Sc. Mona Feizbakhsh Bazargani**

geboren am 21. September 1982 in Tehran (Iran)

Gutachter

1. Prof. Dr. Christian Robl

2. Prof. Dr. Kurt Mertzweiler

Tag der Verteidigung, 23.01.2019

Contents

Acknowledgments

My deepest gratitude goes firstly to my supervisor Prof. Dr. Christian Robl who excellently guided me during my study and also for his motivation, immense Knowledge and patience. His continuous support always convinced me to do my best in all of time of research and finally writing this thesis. Besides my supervisor, my appreciation also extends to my research group and my laboratory colleagues and I am so much grateful for their assistance and suggestion.

I would specially like to thank Mrs. Antje Wermann and Mrs. Christina Apfel for their generous supports. Actually I have learnt very much from them. They helped me to improve my german language skill and many other things. I am also thankful them for special instrumental analysis which is relevant to my work such as TG and XRD analysis.

My sincere thanks also go to Prof. Dr. Wolfgang Weigand because of his kind support during my Ph.D study, in particular for my scholarship (DAAD) extension.

The financial assistance from DAAD (Deutscher akademischer Austauschdienst) in the form of scholarship as research fellowship is gratefully acknowledged.

Last but not the least, I would like to thank my family: my parents, my best friends and to my brother and my little son for their love and encouragements. They supported spiritually me throughout writing this thesis and my life in general to pursue my interests. This work is simply impossible without them.

Chapter 1

1. General Introduction

1.1. Definition of Coordination polymer

Coordination polymers (CPs) are defined as large molecules, or macromolecules, composed of several repeated metal ions and organic ligands as fundamental subunits which are linked by covalent bonds and other weak chemical bonds [1]. The research area of coordination compounds (also known as metal-organic framework (MOFs) as porous coordination polymers) has turned out as a great research area over the past two decades. Moreover, it also takes significant attention to the realm of various applications of molecular magnetism, photoluminescence, catalysis, non linear optics (NLO) materials, spin-crossover materials, micro magnets, medical applications like drug delivery and implantable devices, gas storage/adsorption and materials science [2–11]. Actually, special interest in design of coordination polymers is the search for their interesting properties and applications. The one of an early example is coordination polymers of formula $[M(Pc)X]_{\infty}$ (M=Si, Ge; X= O), (Pc= Phthalocyanine) which was first synthesized in the early 1960s by Joyner and kenney [12]. Similar polymeric structures of M= Al, Ga, Cr; X= F [12] and compound $[Ga(Pc)F]_{\infty}$ had also been reported. The electrical conductivity of these coordination polymers was vastly investigated by kenney and co-workers [12].

The luminescent effect of polymeric networks has attracted much interest because of their potential applications for photoelectronic devices or as fluorescent sensors and probes. Indeed, the coordination polymers often expose more stability (thermal- and solvent-resistant) than the pure organic ligands and may affect the emission wavelength of these organic molecules [13–16].The further example, can be third-order non linear optical materials (NLO) in the realms of CPs and MOFs which are currently interest of many research groups since they can be used for a number of photonic applications, for example, optical signal processing, optical communication, optical computing, electrooptic modulation, optical limiting effect and etc [17]. In principle, in comparison with traditional NLO materials, the metal atom in coordination polymers introduces more sublevels into the energy hierarchy, which makes it possible to take place more allowed electronic transition, hence a larger NLO effect could be observed [18–20]. In the perspective of magnetic effect, many coordination polymers and metal-organic frameworks of transition metals have been reported in past two

decades [21–28]. For instance, the magnetic properties of lanthanide coordination polymers have been studied because many Ln(III) ions, such as Tb(III), Dy(III) or Ho(III) exhibit the strong unquenched orbital angular momentum that results in magnetic anisotropy, originating from unpaired 4*f* electrons. Therefore, lanthanide ions have become good candidates for synthesizing single-molecule magnets (SMM) and single-chain magnets (SCM) [29–32]. Besides, many interesting properties of coordination polymers, it is worth to note that the metal organic frameworks (MOFs) have emerged as a strong potential adsorbent and being as catalysts due to their porous nature, easily tunable and tailored structures and chemical functionality which ease diffusion and interfacial contact between active sites and reagents [33–35]. As a matter of interest, one of daily usage of coordination polymer is a cathode for sodium–ion batteries. Prussian blue (PB) mesocrystals with sodium ions as the alkaline metal have been synthesized and used as cathode materials in sodium–ion batteries. The mesocrystalline structure provided PB with very different phase change behavior and electrochemical performance in contrary to PB single-crystals in cyclic voltammograms and galvanostatic discharge/charge voltage profiles of PB/Na half-cells [36].Besides, many useful applications of coordination polymers and metal organic frameworks, it is worthy to describe the coordination polymers (CPs) and metal organic frameworks (MOFs) briefly.

The term “coordination polymer” was first used by J. C. Bailar in 1964, since he found the similarities between organic polymers with inorganic coordination compounds which can be considered as polymeric species. In comparison, he made the rules for the architecture and the required properties of new species which involved metal ions and organic ligands [1]. In addition a certain number of principal differences between CPs and polymers must be considered in order to avoid confusion: i) despite polymers usually exhibits a certain size distribution due to variable chain lengths, MOFs and CPs are usually characterized in the solid state and they possess infinite metal-ligand assemblies which extend into one-, two- or three- dimensional networks (Figure1.1) [37]; ii) a polymer is combined by many small molecules known as monomer units via covalent bonds, while a coordination polymer network is generally based on coordinative bonds. Coordinative bonds are formed into equilibrium which may be more on the side of the products and less of the starting materials. For both, weak intermolecular interactions may affect on the overall arrangement and influence the properties; iii) as a consequence, in solution, polymers may be identified by their chain length, while for MOFs or CPs the identity of polymeric structure depends on various factors. For instance, the solvent, the temperature, pH, the pressure and etc., i.e.,which influence stability; iv) The polymers may own properties which cause elastomers, duroplasts,

or thermoplastsdue due to the connection of an immense number of monomers while the coordination polymer networks are usually in solid state and crystalline, hence they are well-ordered in the long range.The latter leads to the fact that the structure of MOFs and CPs can be usually detected. Therefore, the structure can be shown by single crystal X-ray structural analysis technique [38].

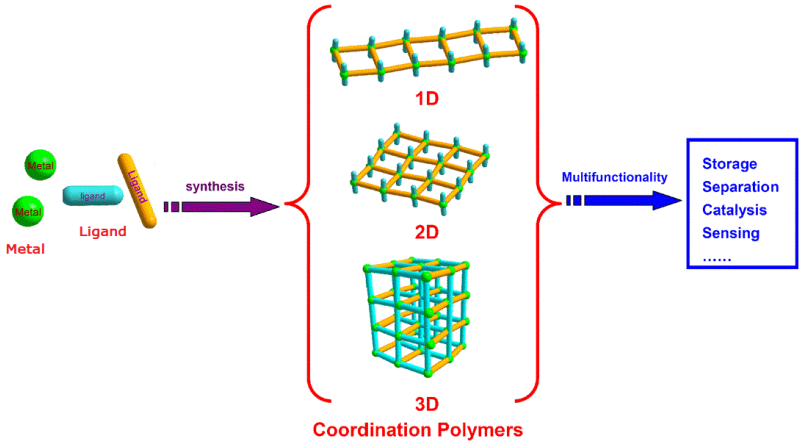

Figure 1.1: Schematic view of synthetic process of coordination polymers from starting materials [37]

Furthermore, there is another issue that makes CPs c different from organic polymers. They are highly crystalline and cannot be processed like organic counter parts.The metal-ligand bonds can be easily broken due to the solvation, so the species existing in solution does not need be true monomers or oligomers.

1.2. Chemical interactions in coordination polymers

In principle, coordination polymers and metal-organic frameworks are generally defined as compounds containing backbones constructed by metal ions as “nodes” and organic ligands as linkers into an infinite array.This infinite net must be defined by coordination bonds.Weaker noncovalent interactions like hydrogen bonds or π–π stacking play significant roles for packing of chains, two dimension net and three dimensions frameworks [39–40]. However, the multidimensional supramolecular structures of metal complexes which are merely constructed by hydrogen bonds are not considered as coordination polymer [41–43]. Furthermore, metallo-macrocycles, metallosupramolecular cubes, cages or capsules, [44–45], metallocatenanes, [46] coordination clusters [47] or helicates [48] which do not expose infinite metal-ligand assemblies, hence there are not considered as coordination polymers.

Coordination bonds are the donation of a lone electron pair of the ligand (Lewis base) to the metal cation (Lewis acid) and electrostatic attractions between the positively charged metal ion and a negatively polarized or charged donor atom of the ligand [49]. Weaker interactions also strongly influence the formation of coordination polymers such as hydrogen bond [50–53], metal–metal interaction [54], Metal-aromatic interactions [55] and π–π interaction [56–57]. An example of π–π stacking interaction illustrated with (Figure 1.2).

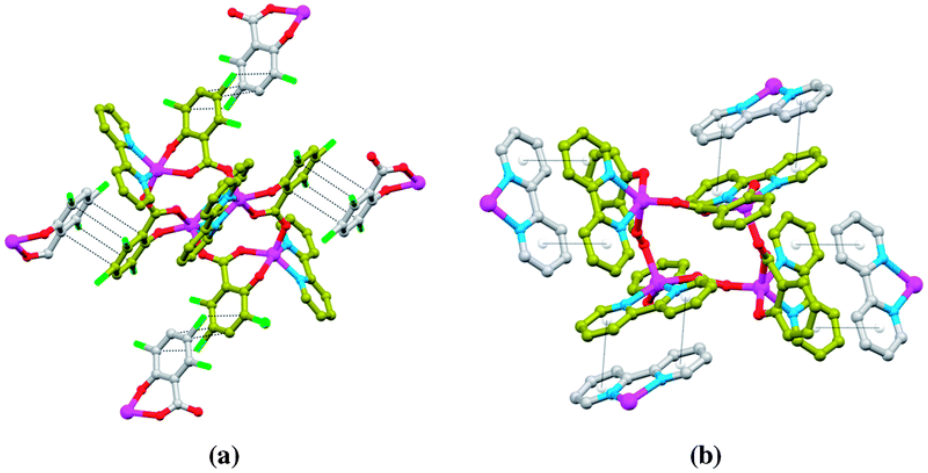

Figure 1.2: Crystal packing of two different side views of Zn complex and how the tetranuclear zinc complex self-assemble to generate 3D supramolecular framework with pair wise π–π stacking [57]

1.3. The ligands in coordination polymers

The ligands are used in the construction of coordination polymers act as a bridge between metal ions.This requires usually multidentate ligands with two or more donor atoms, called di-, tri-, tetra- which depends on the number of donor atoms.Special importance is relevant to rigid bridging ligands because they induce a certain steric consequences of the assembly process.The diversity of organic components basically affects on the variety of structural topologies.Moreover, selecting the suitable organic ligands also tunes the interesting physical properties and thus, attains various applications, such as catalysis, luminescence, magnetism, nonlinear optics. Popular ligands are depicted in (Figure 1.3), for constructing coordination polymers with these kinds of properties.As it can be concluded, nitrogen and oxygen donor ligands feature highly in the construction of coordination polymers [58–64].

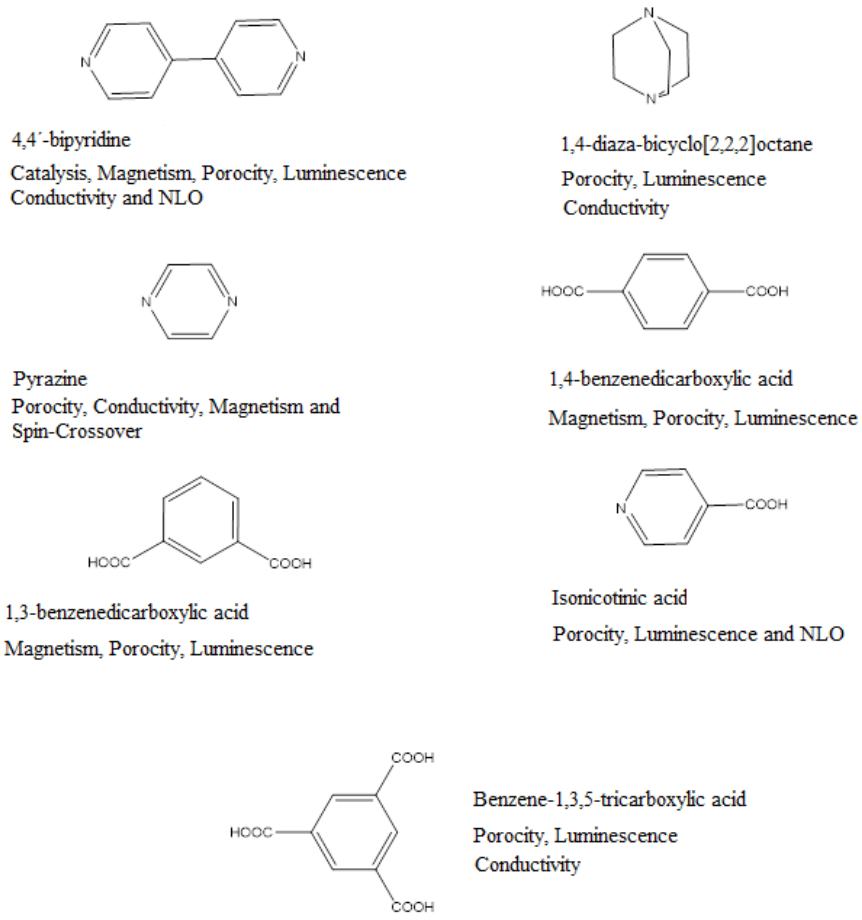

Figure 1.3: Some very famous and capable ligands and their application in the field of coordination polymers and metal-organic frameworks [64]

In the majority of coordination polymers, either the O-atoms of anions (carboxylates, nitrates, sulfates, phosphates, phenolates) or the N-atoms of cyanates, cyanides, amines, pyridines engage in the coordination bonds with transition metal ions. Hence, classification of ligands into inorganic and organic molecules can make it easier to investigate the ligand role in construction and properties of coordination polymers.

1.3.1. Inorganic Ligands

Divers metal-ligand assemblies can be formed into various inorganic bridging molecules such as halide Cl^-, Br^-, I^- or pseudohalide N_3^-, CN^-, SCN^-, OCN^-, $SeCN^-$ and other small inorganic species like H_2O, O^{2-}, O_2^{2-} , OH^-, S^{2-}, HS^-, Se^{2-}, HSe^-, Te^{2-}, HTe^-, TeS_3^{2-}, NO_3^-, NO_2^-, CO_3^{2-}, CO and NH_2^-. It is worth mentioning that metal clusters can also act as bridging ligand for construction coordination polymers, like large metal-oxygen clusters of polyoxometalate anions (POMs) which are either connected as guests, templates or counter

ions through noncovalent interactions (van der Waals interaction, hydrogen-bonding or ionic interactions) with the transition metal and organic moieties or coordinated to metal atoms as inorganic ligands through covalent bonds [65–68].

In between, short bridging pseudohalide ligands such as cyanides and azides have been merely used for construction coordination polymers and metal organic framework of transition metals. One of the very common examples of pseudohalide ligands is azide that exposes a number of various binding modes and has been incorporated into an array of 1D, 2D and 3D coordination polymers (Figure 1.6).As a matter of interest, the type of coordination modes can affect on the magnetic properties of coordination polymers. Normally, the end-to-end (EE) coordination mode gives antiferromagnetic coupling while the end-on (EO) causes ferromagnetic coupling [69].An example, compound $[Co(bmdt)(N_3)_2]\cdot MeCN$(1·MeCN) [bmdt = *N*,*N*‘-bis(4-methoxybenzyl)diethylenetriamine] exhibits 1D coordination polymer with well-isolated heterochiral chains (Figure 1.4). However, Magnetic data reveal ferromagnetic interactions between Co^{2+} ions within a chain mediated by single EE azides, which is very unusual because the EE mode mostly promotes antiferromagnetic coupling [70].

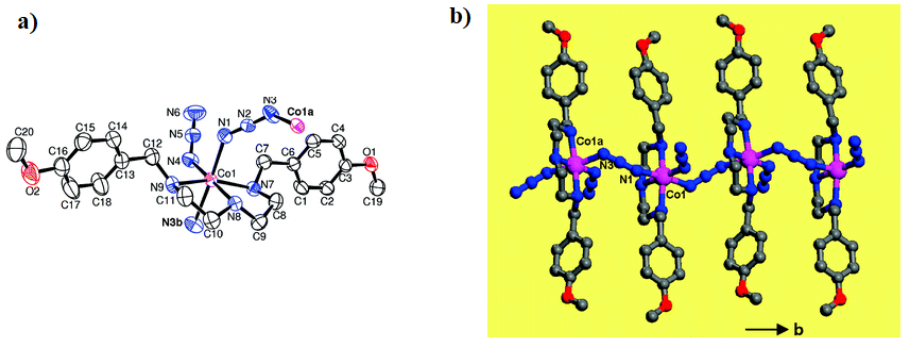

Figure 1.4 : The material $[Co(bmdt)(N_3)_2]\cdot MeCN$ (**1**·MeCN) shows polymeric chain with EE azide bridging ; **a)** 50% ellipsoid probability and the atom-labeling scheme; **b)** the chain structure running along the *b*-axis [70]

More example of azide EE bridging mode is in compound $[Co_2(N_3)_4(L)]_n\cdot 4nH_2O$ (L = tetrakis(3-pyridyloxymethylene) methane), the Co^{2+} chains are formed by double end-to-end (EE) azide bridges and are further linked by the tetrapyridyl ligands into a 3D network (Figure 1.5).Moreover, EE azide bridges transmit antiferromagnetic interactions along the chains within this compound [71].

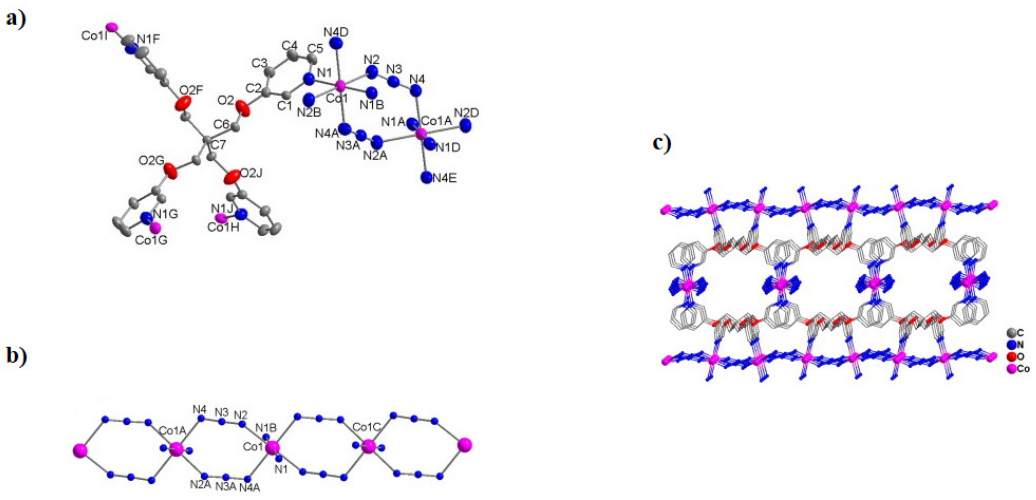

Figure 1.5: a) coordination environment around cobalt ions and the ligands in cobalt coordination polymer ; **b)** the chain along the *c*–axis in this compound ; **c)** 3D network is formed by bridging behavior of tetrapyridyl ligands [71]

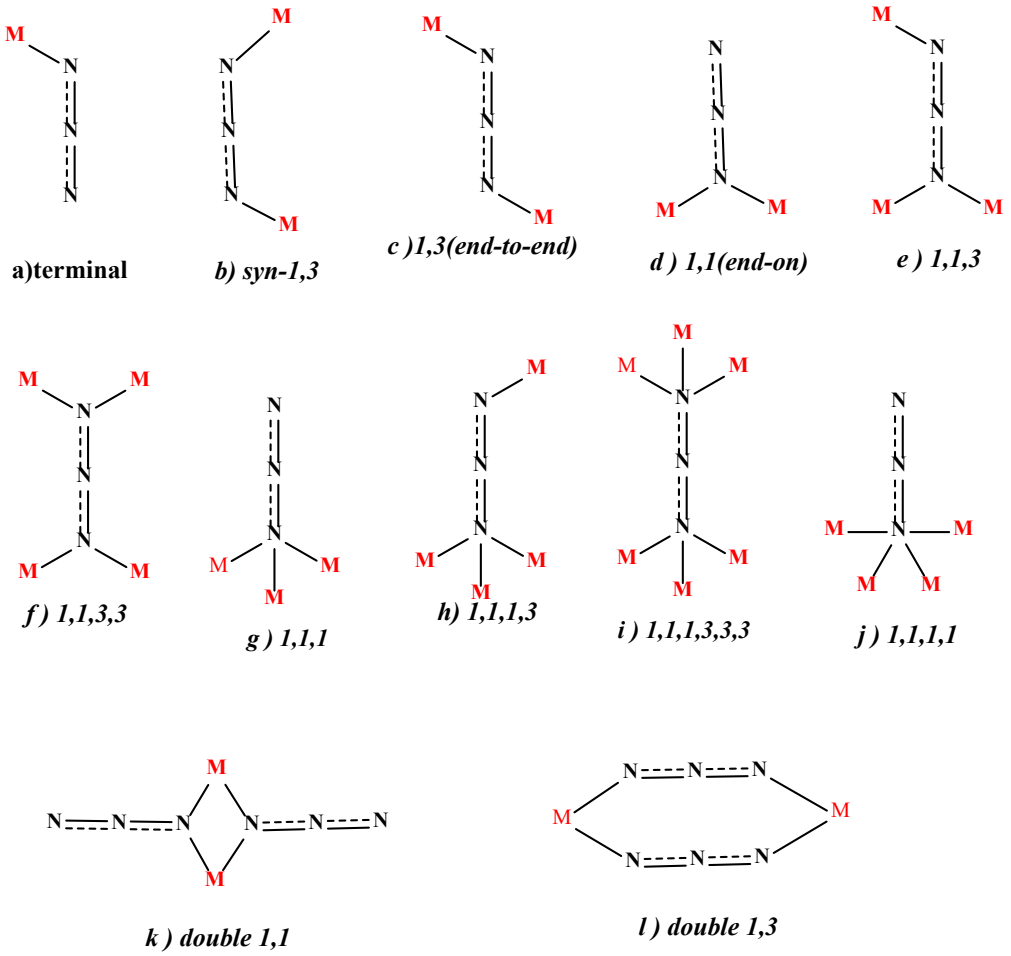

Figure 1.6: Different binding modes of azide ions (N_3^-)

Another example is copper coordination polymer of formula $[Cu_2(O_2CPh)(N_3)_2\{(py)_2C(OMe)O\}]_n$.The dinuclear units assemble with two EO azide ligands that bridge the Cu2 atoms to form a tetranuclear unit (Figure 1.7).The latter is further linked with the Cu1 centers of four EE azide ligands to form a 2D network [72].

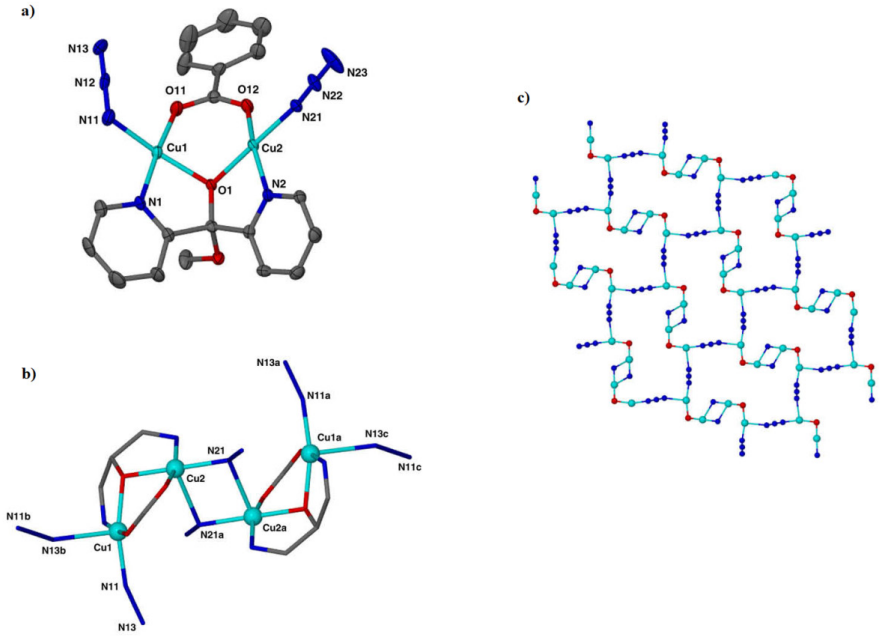

Figure 1.7: a) ORTEP view of the asymmetric unit; **b)** the assembly of two dinuclear units; **c)** the 2D network [72]

Further example of azide bridge in the EO fashion is an anion $\{[Cu_3(N_3)_7]^-\}_n$ shows 1D polymeric structure, where EO-azide ions bridge the Cu^{2+} ions to construct an anion chain $\{[Cu_3(N_3)_7]^-\}_n$.In such structure, the three crystallography independent Cu^{2+} ions (Cu1, Cu2, and Cu3) are connected by EO-azides to form a linearly arranged Cu_3 motifs and such a Cu_3 motif further links with a centrosymmetrically equivalent Cu_3 motif by two EO-azides at both ends, resulting in the formation of an elongated Cu_6 ring as the repeating unit of the chain. Additionally, the two adjacent rings are serially connected with Cu1 ions by double EO-azides along the chain [73]. In this compound, the canted ferromagnetism is induced through the $Cu–N_{azido}–Cu$ super exchange pathways with lower angles (Figure 1.8) [73].

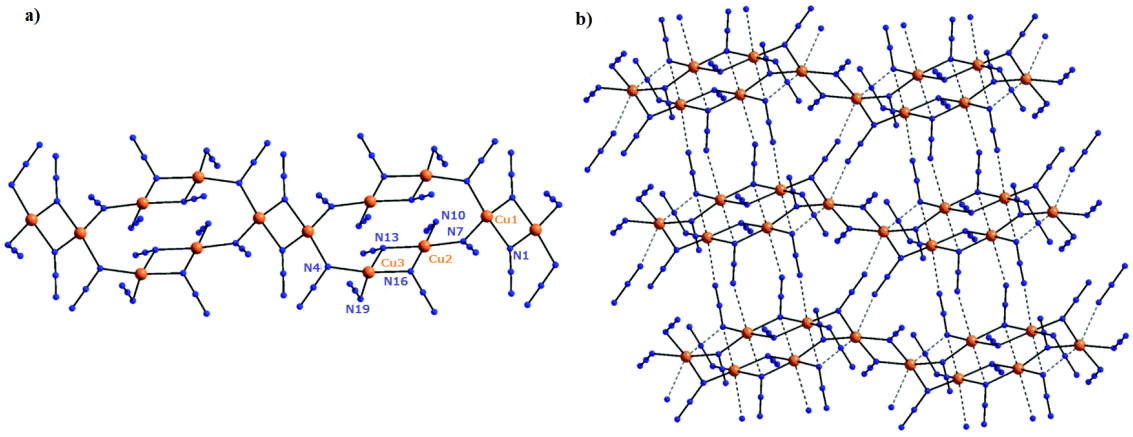

Figure 1.8 : a) View of the $\{[Cu_3(N_3)_7]^-\}_n$ chain along the *b*-axis, Cu^{2+} ions are bridged by double EO azide ligands**; b)** View of the supramolecular $\{[Cu_3(N_3)_7]^-\}_n$ layer [73]

Anionic ligands in the form of NCX^- (where X= O, S and Se) can be used for constructing coordination polymers as terminal or bridging ligands.These ligands can also act like azide in both EO and EE binding modes and can have implications for magnetic materials (Figure 1.9) [74–79].

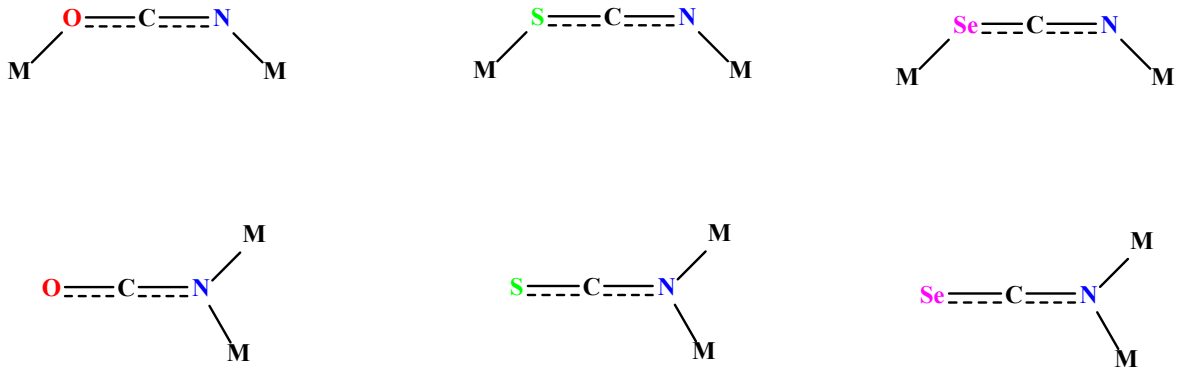

Figure 1.9: Coordination binding modes of NCX^- ligands

Small polynitrile ligands such as dicyanamide (dca) and tricyanomethanide (tem) are also used for the synthesis of coordination polymers with transition metals, since they exhibit a large range of binding modes (Figure 1.10).

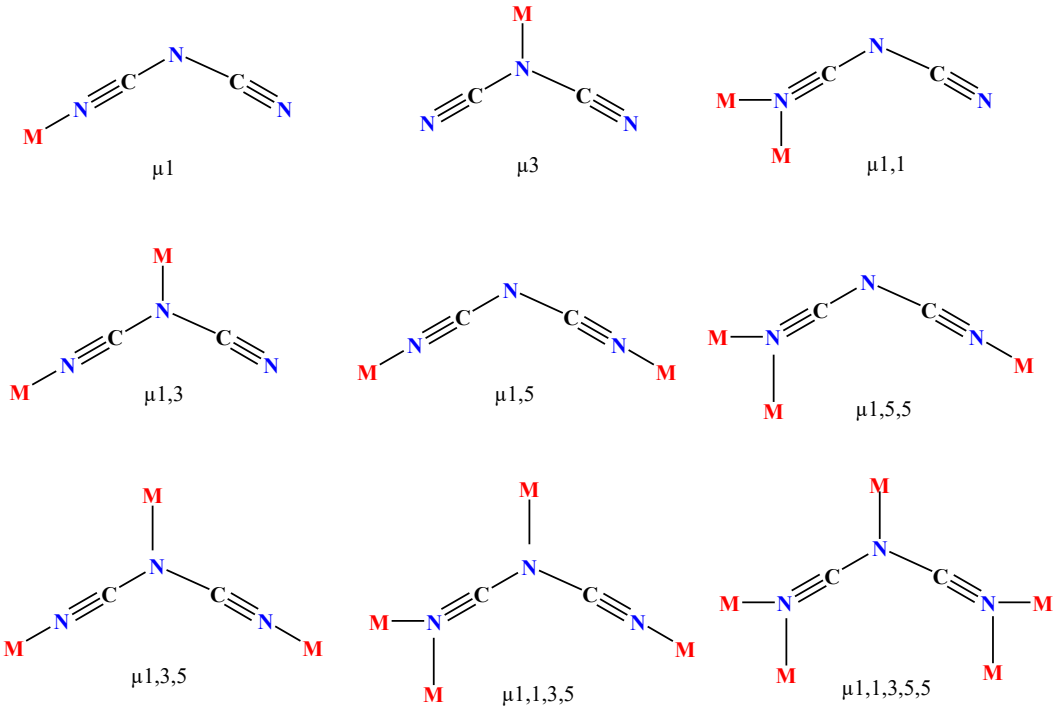

Figure 1.10: Various coordination modes of dca ligand

1.3.2. Organic molecules act as ligands in coordination polymers and metal organic framework

There are numerous reported organic compounds incorporating into coordination polymers and metal organic frameworks.Commonly used compounds include oxygen and nitrogen donor atoms, such as pyridine and its derivatives or carboxylic acids.In comparison, sulfonic acids, phosphonic acids, thiophen, furan, Schiff-bases (nitrogen- imin group) are rather less studied.Neutral polynitrile compounds are weak donor ligands and tend to bind well to soft metal ions such as Cu^{+} and Ag^{+}. For example, the the ligand 1,3,5-tricyanobenzene (TCB), 1,3,5-tris(4-ethynylbenzonitrile)benzene (TEB) and 1,3,5-tris(3-ethynylbenzonitrile)benzene (TEBB) have been already reported (Figure 1.11) [80–81].

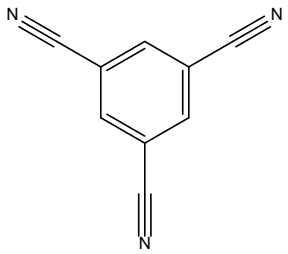

1,3,5-tricyanobenzene (TCB)

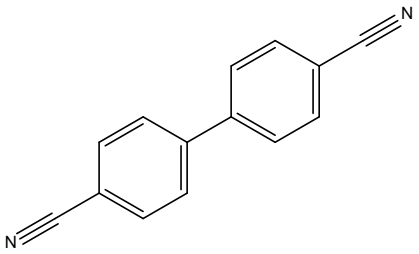

4,4′-biphenyldicarbonitrile (BPCN)

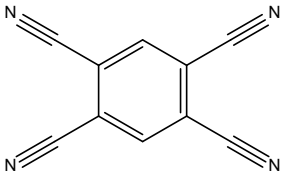

1,2,4,5-tetracyanobenzene (tcnb)

Figure 1.11: 2-connecting nitrile ligand 4,4′-biphenyldicarbonitrile (BPCN), 1,3,5-tricyanobenzene (TCB) and 1,2,4,5-tetracyanobenzene (tcnb)

Pyridine and its derivative are very often used for construction of coordination polymers and are very well established in three basic classes: 2-, 3- and 4-connecting modes. Examples of higher coordination pyridyl ligands (i.e. 5- and 6-connecting) are very rare. Some of the mostly used 2-connecting pyridyl ligands are depicted in (Figure 1.12).

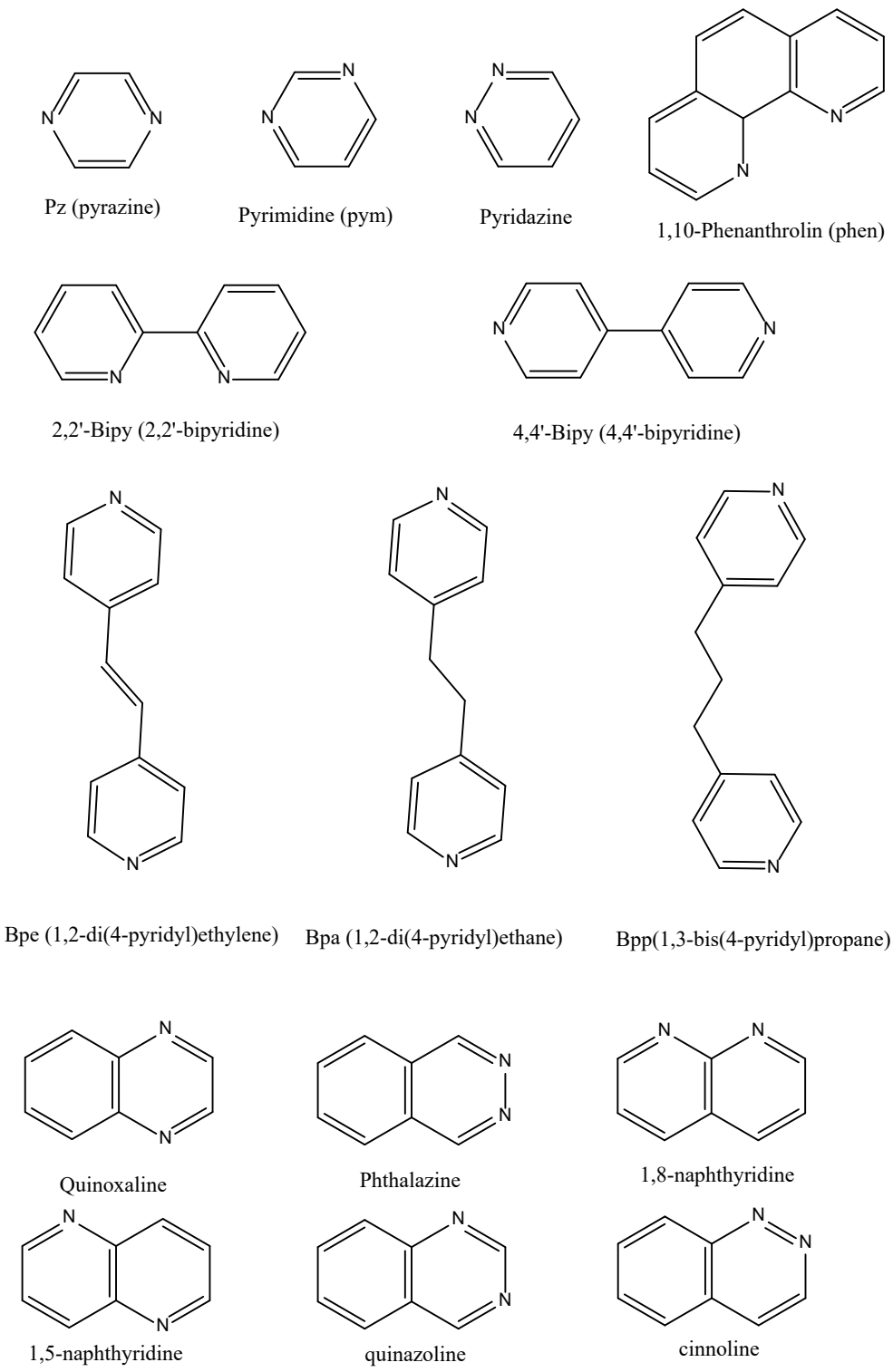

Figure 1.12: List of some suitable 2-connecting pyridyl ligands

One of the simplest 2-connecting pyridyle ligand is pyrazine (pyz) which provides a linear connection with transition metal ions. An example, compound $[Cu_2(pyz)_4](ClO_4)_2 \cdot HBz \cdot H_2O$ (HBz = Benzoic acid) presents a quartz-like topological net with a $(6^4.8^2)$ point group [82]. Pyrimidine (pym) and pyridazine (pydz) perform as a bent connectors, have been used in the

same way as pyrazine. Such ligands can also be functionalized as 2,3-pyrazinedicarboxylic acid or pyridazine-3-carboxylic acid which are very interesting for framework topologies. As longer linear 2-connecting pyridyl ligands, (4,4′-bipy) [4,4′-bipy = 4,4′-bipyridine] is a current choice to construct CPs and MFOs and has been reported in many coordination polymer articles. For example, in coordination compound $[Hg(4,4'\text{-bipy})(SCN)_2]_n$, Hg^{2+} ions are linked by the bridging (4,4′-bipy) ligands to yield a zigzag chain extending infinite 1D construction [83]. There are numerous coordination polymers based on 4,4′-bipy that may form frameworks with different topologies including simple 1D, 2D and 3D networks depending upon transition metal cations.

The three connecting pyridyl-based ligand, triazine (tri), 2,4,6-tris(4-pyridyl)-1,3,5-triazine (tpt) and 1,3,5-tri(4-pyridyle)-benzene (tpb) have been successfully applied for the the construction of frameworks with interesting topologies as well.

Compared to 2- and 3-connectors, there are fewer examples of 4-connecting pyridyl ligands and they have been mainly focused on porphyrin analogues, but several other ligands have been also applied (Figure 1.13). Since 4-connecting pyridyl ligands are mostly large, hence they usually produce frameworks of large cavities.

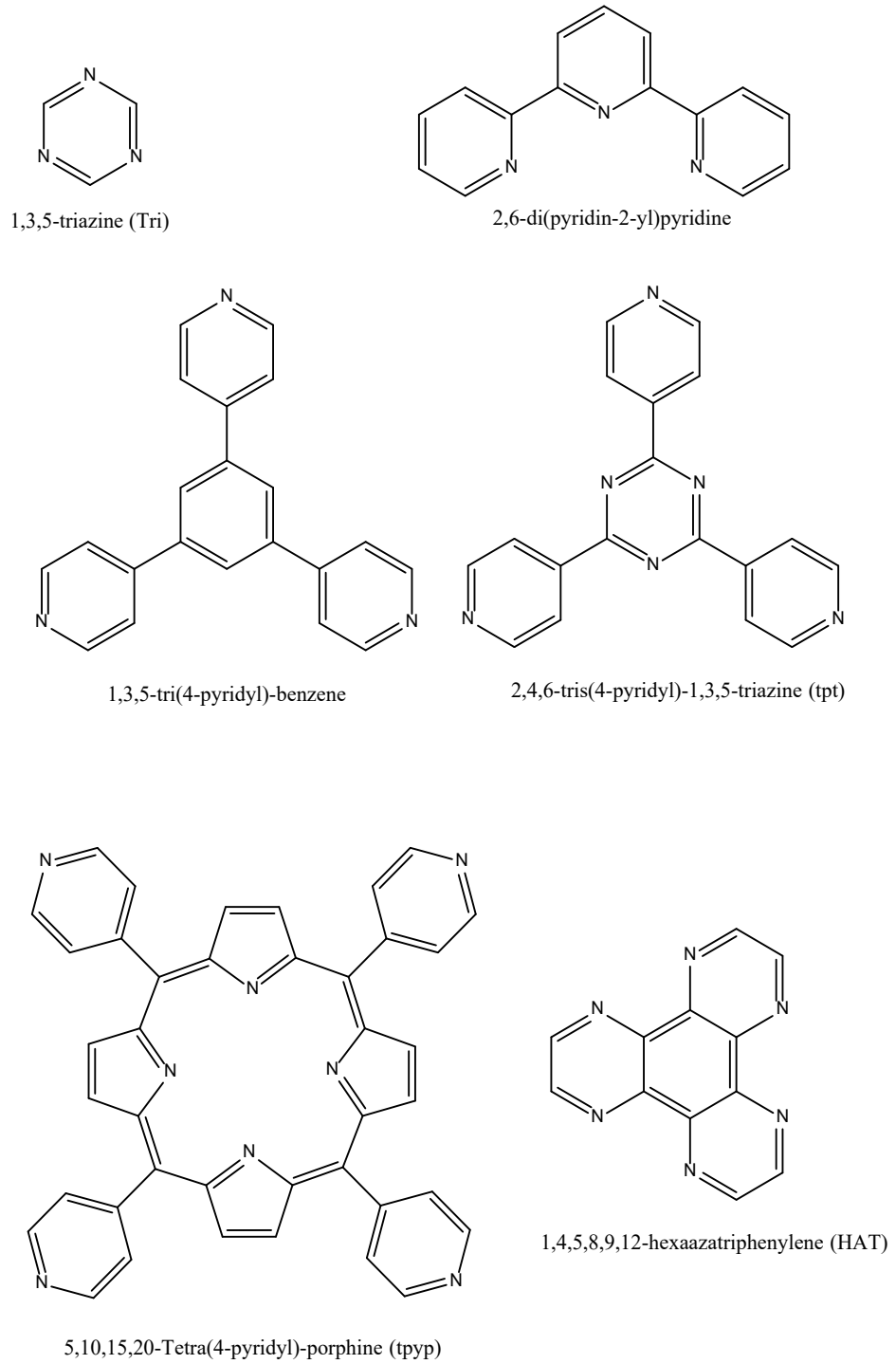

Figure 1.13: Some 3- and 4-connecting pyridyl ligands which have been commonly used in coordination polymer synthesis

N-donor an aromatic heterocyclic molecules are such as imidazole, triazole and pyrazole have been used as much as pyridyl donor ligands since they coordinate to transition metal ions with a similar affinity. Moreover, greater diversity of network topologies could be obtained by these of ligands. Some more usable heterocylic nitrogen donor ligands are shown in (Figure 1.14).

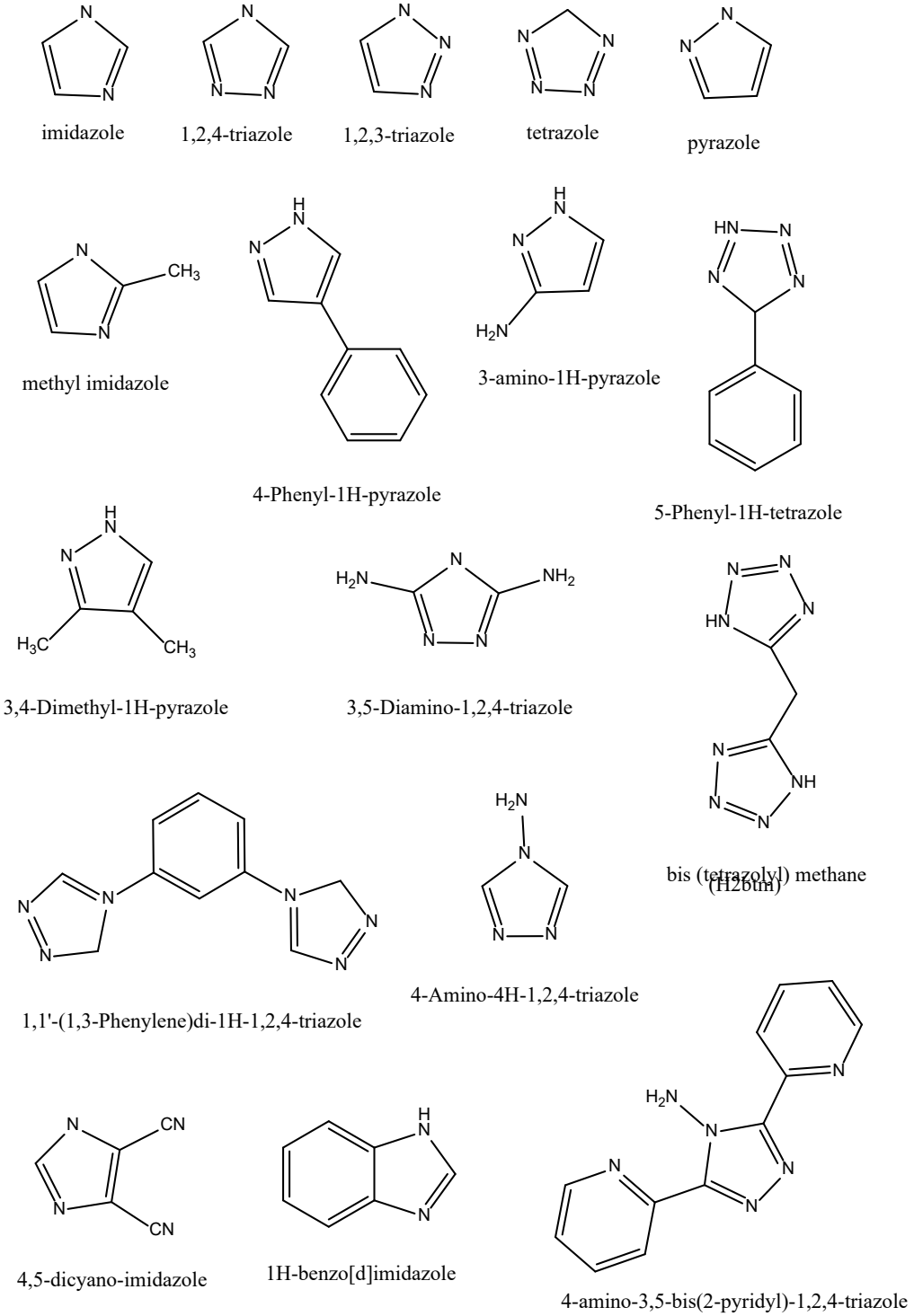

Figure 1.14: Some interesting and common used 5-memberd N-donor rings

An example, triazole (trz) ring is present in chain compound $[Cu(\mu_2\text{-}NH_2trz)_2Cl]Cl\cdot H_2O$ (NH_2trz = 4-amino-4*H*-1,2,4-triazole) where each Cu^{+2} ion is coordinated by two chlorine

atoms in *trans*-configuration and four nitrogen atoms arising from four different NH_2trz ligands (Figure 1.15) [84]. This results the formation of a distorted 1D coordination polymer.

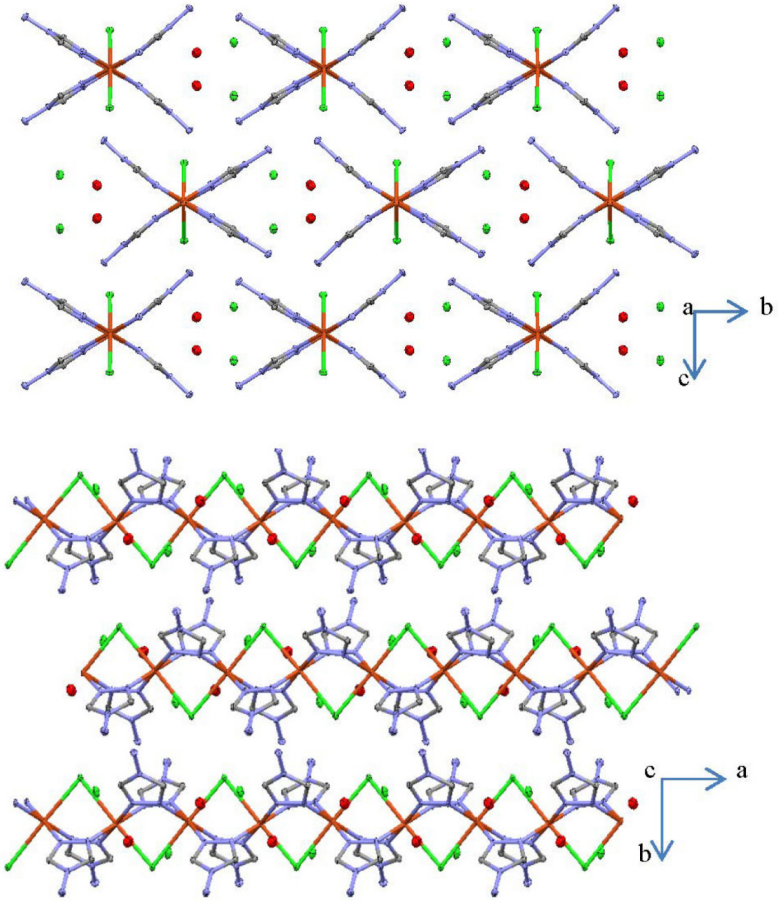

Figure 1.15: Thermal ellipsoid (50%) along the *a* (top) and *c*-axes (bottom). The nitrogen atoms are depicted in blue, the carbon atoms in grey, the chloride ions in green and the copper atoms in red. H-atoms were removed for clarity [84]

Another example involves ligand (bib) has been recently reported to a 2D structure of NLO properties in compound $[Ni(H_2O)_2(bib)_2].(H_2BTA)\cdot 2H_2O$ (H_4BTA = biphenyl-3,3′,4,4′-tetracarboxylic acid, bib= 1,2-bis(imidazole-l-yl methyl)benzene) as depicted in (Figure 1.16) [85].

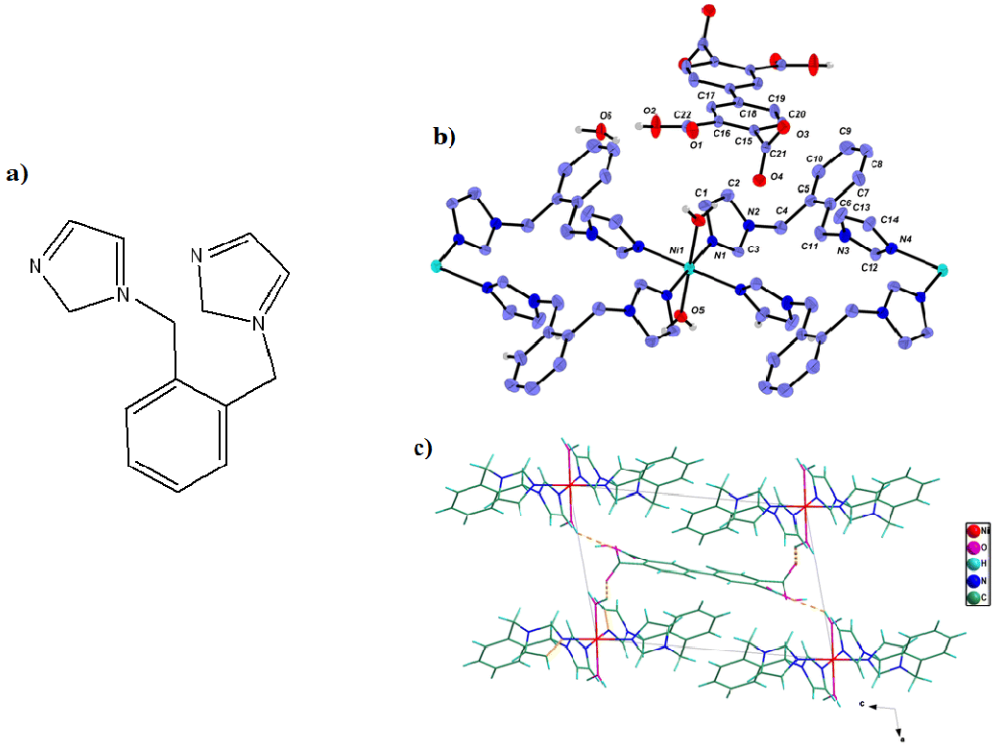

Figure 1.16 : The structure of ligand 1,2-bis(imidazole-l-yl methyl)benzene (bib) **(a)**; ORTEP representation of compound $[Ni(H_2O)_2(bib)_2].(H_2BTA)\cdot 2H_2O$ with 40 % probability displacement ellipsoids **(b)**;View of the structure of along the b axis **(c)** [85]

Apart from nitrogen donor ligand, many oxygen-donors organic compounds have been extensively used for the formation of coordination polymers and metal organic frameworks. Beside carboxylate ligands, other O-donor ligands such as N-oxides have caught considerable attention.An example is a compound $\{[Yb(4,4'\text{-bpdo})(NO_3)_3(CH_3OH)]\}_\infty$, each metal centre is nine-coordinated with YbO_9 coordination sphere and resulted in 1D coordination polymer built from repeating zigzag chains of linked Yb(III) cations (Figure 1.17) [86].

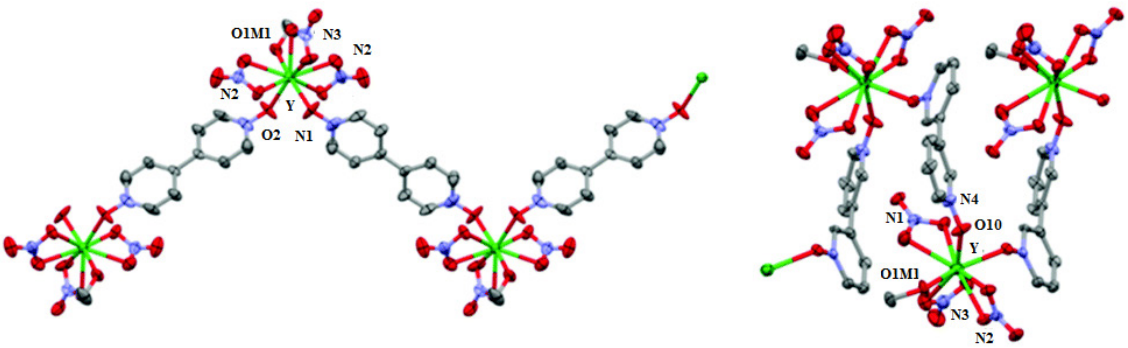

Figure 1.17: The structure of $\{[Yb(4,4'\text{-bpdo})(NO_3)_3(CH_3OH)]\}_\infty$ (left) and showing 1D coordination polymer chain(right) [86]

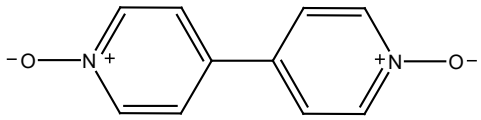

N,N′-oxide(o-4,4′-bipy)

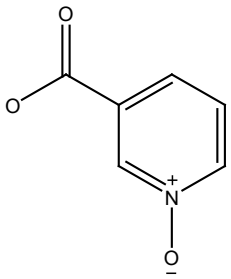

nicotinate N-oxide (NNO)

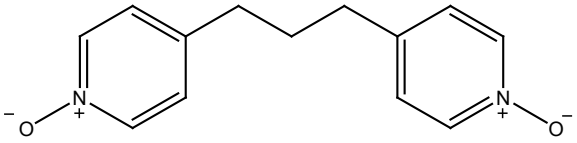

1,3-bis(4-pyridyl)propane N,N′-dioxide (o-bpp)

Figure 1.18: Structures of some very convenient *N*-oxide ligands

Carboxylate ligands can form strong bonds with metal ions with various binding modes in either a monodentate or bidentate. The common carboxylate coordination modes are shown in (Figure 1.19).

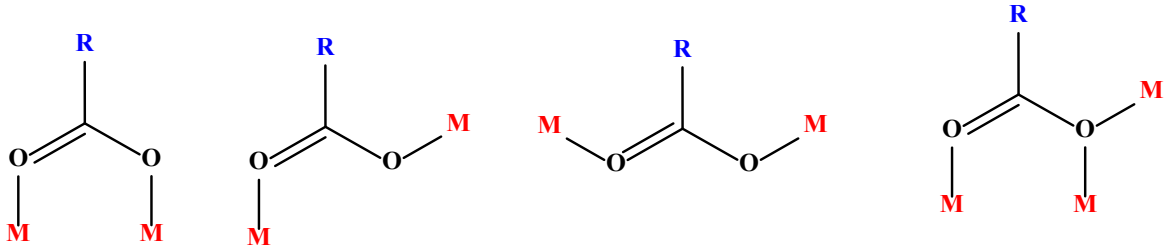

Figure 1.19: Carboxylate coordination modes

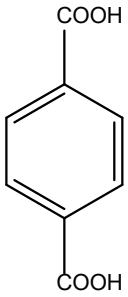

Terephthalic acid

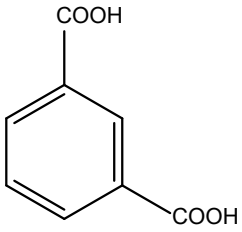

isophthalic acid

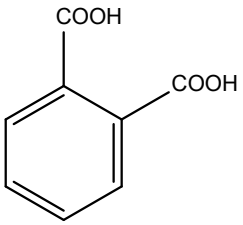

Phthalic acid

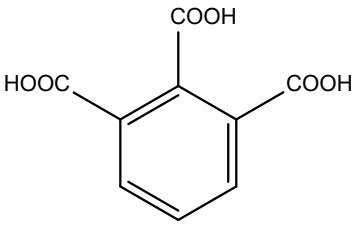

Hemimellitic acid

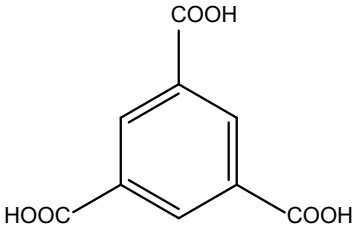

Trimesic acid

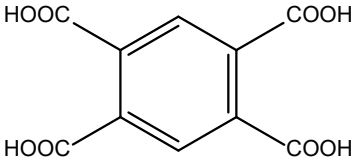

Pyromellitic acid

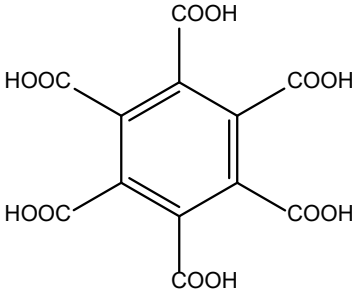

Mellitic acid

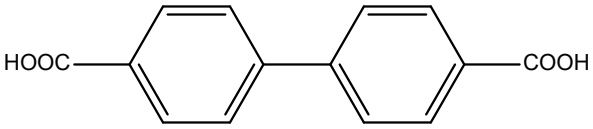

Biphenyl-4,4'-dicarboxylic acid

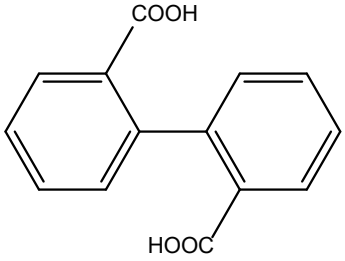

Diphenic acid

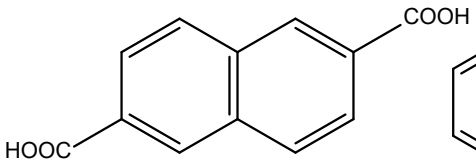

2,6-Naphthalenedicarboxylic acid

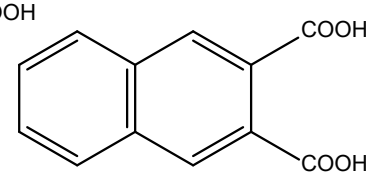

2,3-Naphthalenedicarboxylic acid

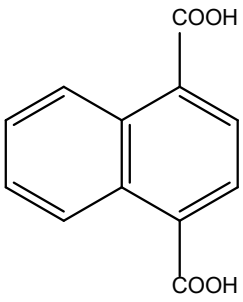

1,4-Naphthalenedicarboxylic acid

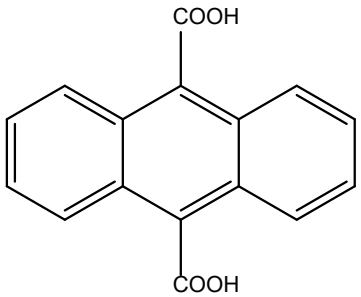

9,10-Anthracenedicarboxylic acid

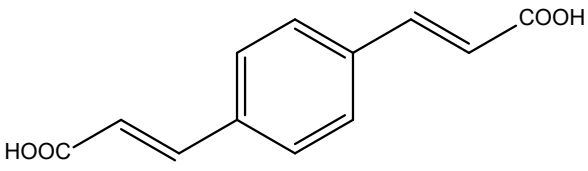

1,4-Phenylenediacrylic acid

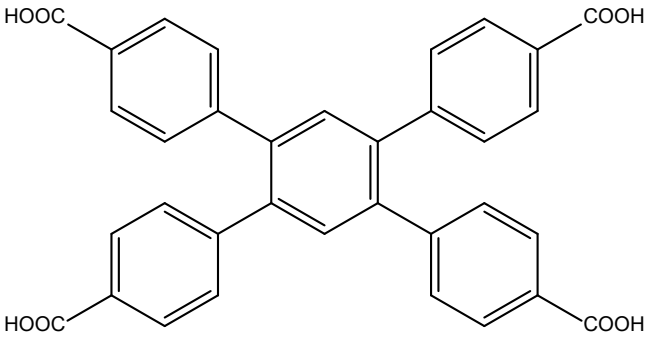

1,2,4,5-Tetrakis(4-carboxyphenyl)benzene

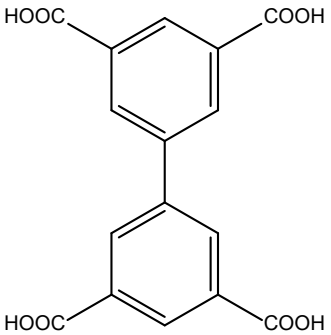

Biphenyl-3,3',5,5'-tetracarboxylic acid

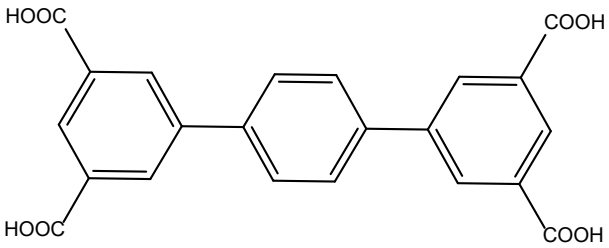

[1,1':4',1]Terphenyl- 3,3,5,5-tetracarboxylic acid

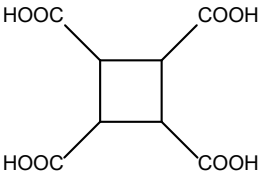

1,2,3,4-Cyclobutanetetracarboxylic acid

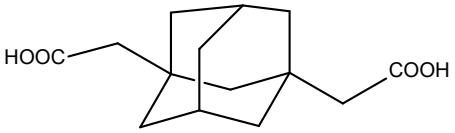

1,3-Adamantanediacetic acid

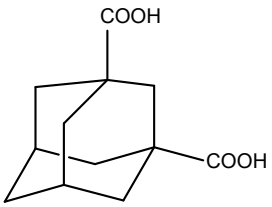

1,3-Adamantanedicarboxylic acid

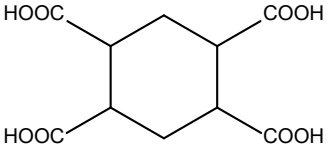

Cyclohexane-1,2,4,5-tetracarboxylic acid

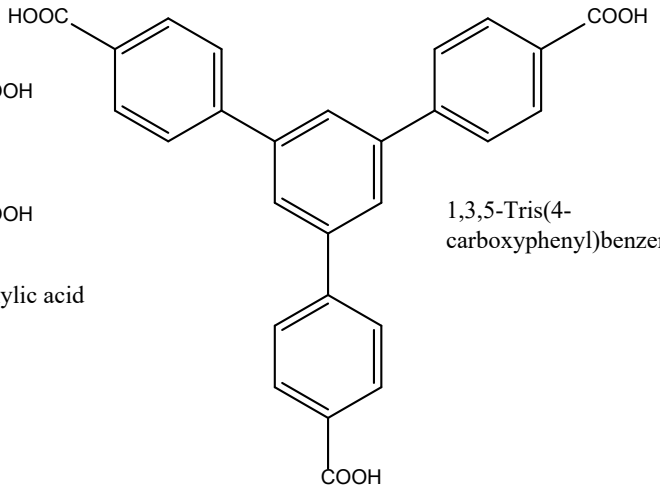

1,3,5-Tris(4-carboxyphenyl)benzene

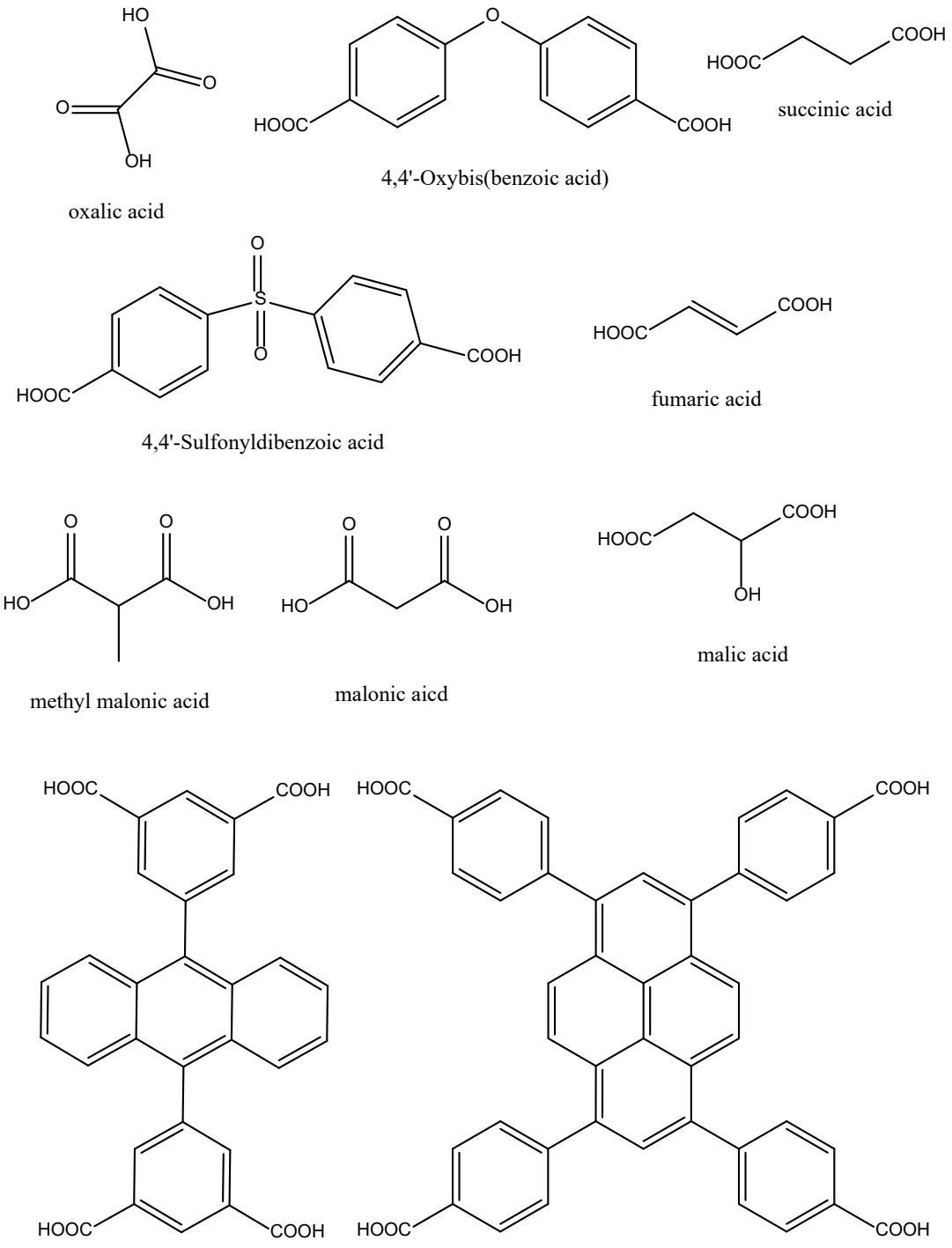

Figure 1.20: Carboxylate ligand structures that have been mostly used for coordination polymer synthesis

Indeed, 2-connecting carboxylate and 2-connecting pyridyl ligands are among the most studied types of ligands in CPs and MFOs field. For example, in the 3D coordination polymer [Cd(bdc)(bipm)] bipm = bis(4-imidazolphenoxy)methane, H_2bdc = 1,4-benzenedicarboxylic acid, where the Cd^{2+} ion adopts a highly distorted tetragonal pyramidal coordination sphere and is five-

coordinated by two nitrogen atoms from two bipm ligands and three oxygen atoms from two bdc^{2-} anions.The bdc^{2-} anion connects two Cd^{2+} ions *via* one monodentate carboxylate and one chelating carboxylate moieties (Figure 1.21) [87].

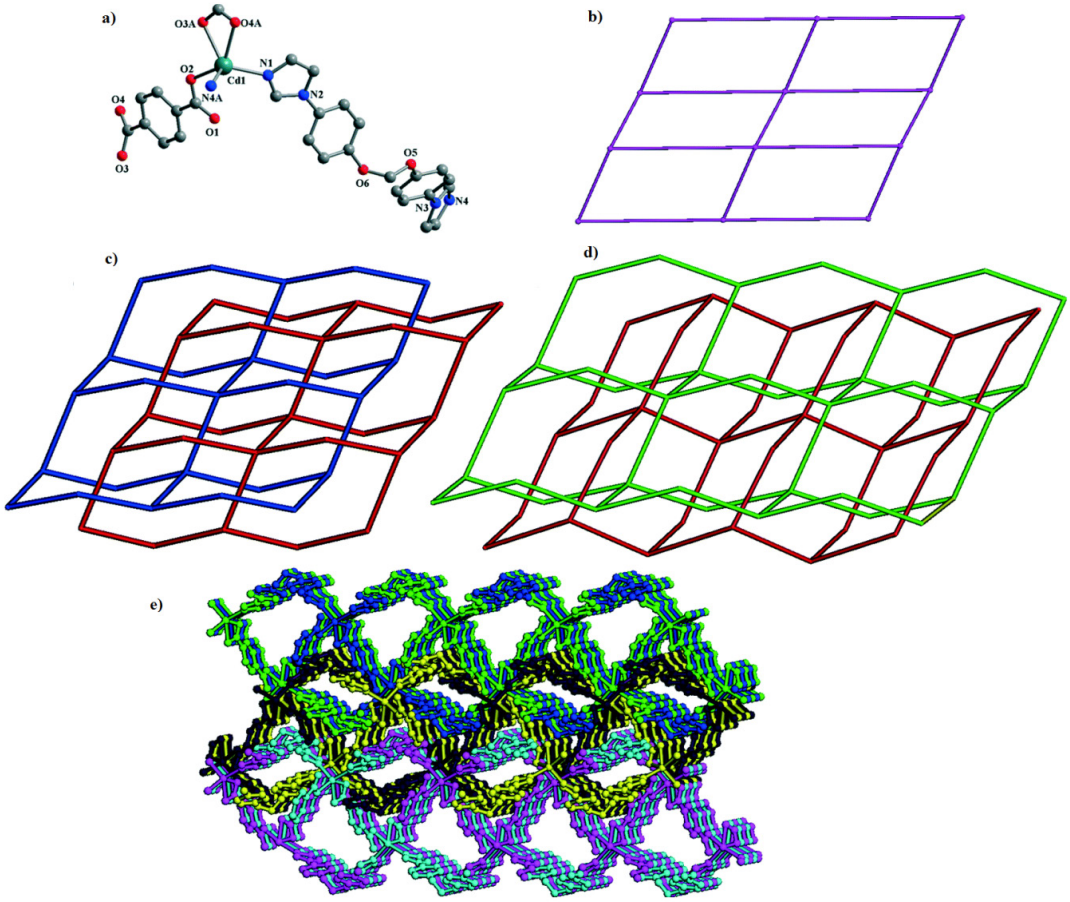

Figure 1.21 : Coordination environment of the Cd^{2+} ion in [Cd(bdc)(bipm)] **(a)** ; The schematic view of the square network in Cadmium complex **(b)** ; The schematic view of the 2D → 2D parallel interpenetration of pairs of sheets **(c)**; The schematic view of the interpenetration of two sheets from adjacent layers; note the different orientations of the two sheets**(d)**; The perspective view of the 2D → 2D parallel → 3D parallel interpenetration **(e)** [87]

One of the recent reported MOFs based on a 3-connecting carboxylate ligand, benzene-1,3,5-tricarboxylic acid (btc), is a series of isoreticular lanthanide metal–organic frameworks, Ln-MOFs (Ln = Eu, Gd, and Tb), shown in (Figure 1.22) [88]. Another example of 3-connecting carboxylate ligand is 1,3,5-tris(carboxylphenyl)benzene which is analogue of (btc) ligand.

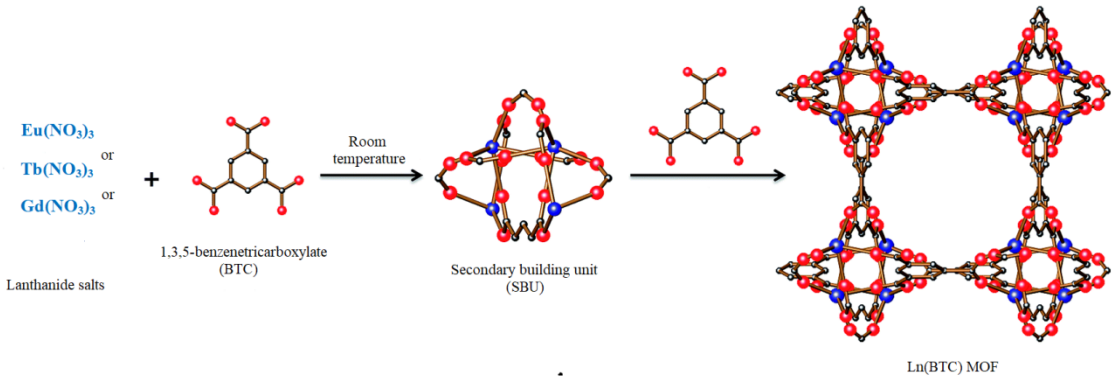

Figure 1.22: Schematic view for the synthesis of lanthanide metal–organic frameworks (Ln-MOFs) *via* Eu^{3+}, Gd^{3+}, or Tb^{3+} with equimolar benzene-1,3,5-tricarboxylic acid (BTC). Secondary building units (SBUs) are formed through rigid M–O–C core clusters [88]

Ligands containing both pyridyl and carboxylate functional groups such as pyrazine-2-carboxylate (2-pyc) and the longer version 4-(pyridine-4-yl)pyridine-2-carboxylic acid (ppca), have been successfully utilized for the formation of coordination compounds (Figure 1.23).

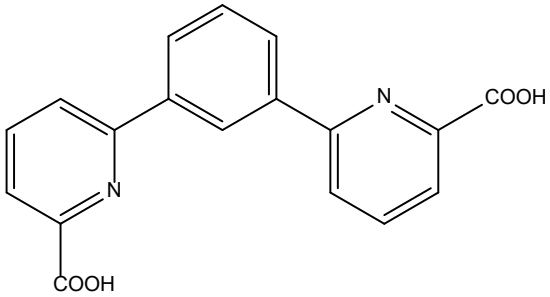

6,6'-(1,3-Phenylene)di(pyridine-2-carboxylic acid)

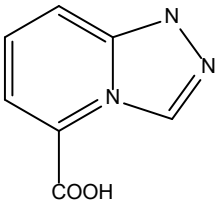

[1,2,4]triazolo[4,3-a]pyridine-5-carboxylic acid

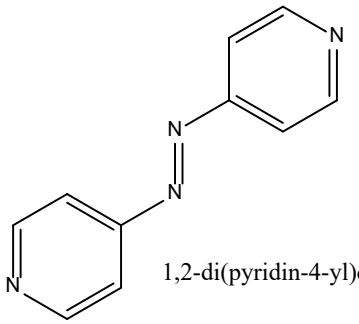

1,2-di(pyridin-4-yl)diazene

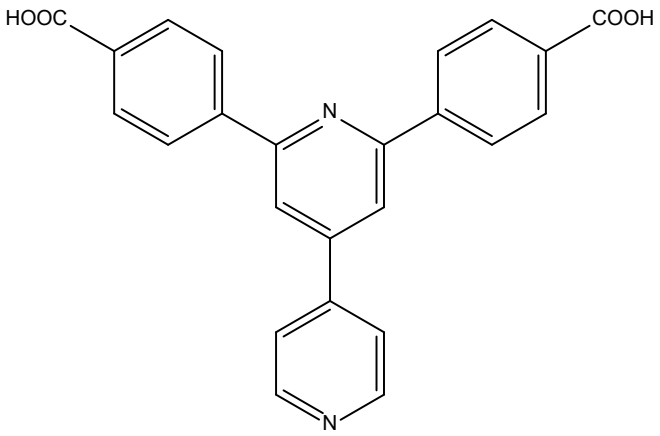

4,4'-(4,4'-bipyridine-2,6-diyl)dibenzoate(bpydb)

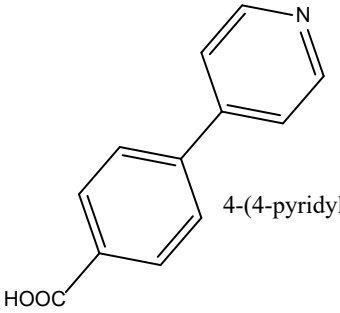

4-(4-pyridyl)benzoic acid

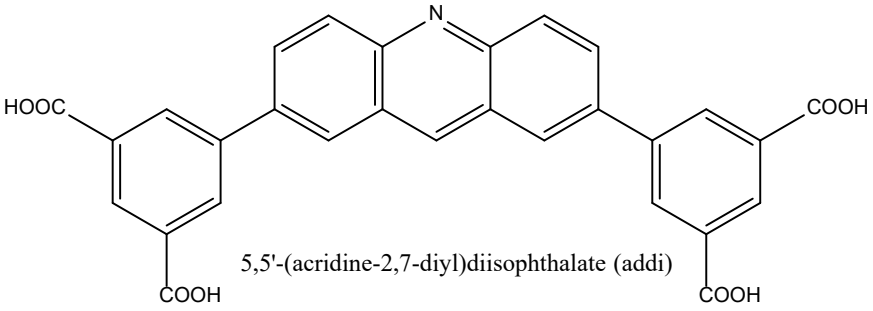

5,5'-(acridine-2,7-diyl)diisophthalate (addi)

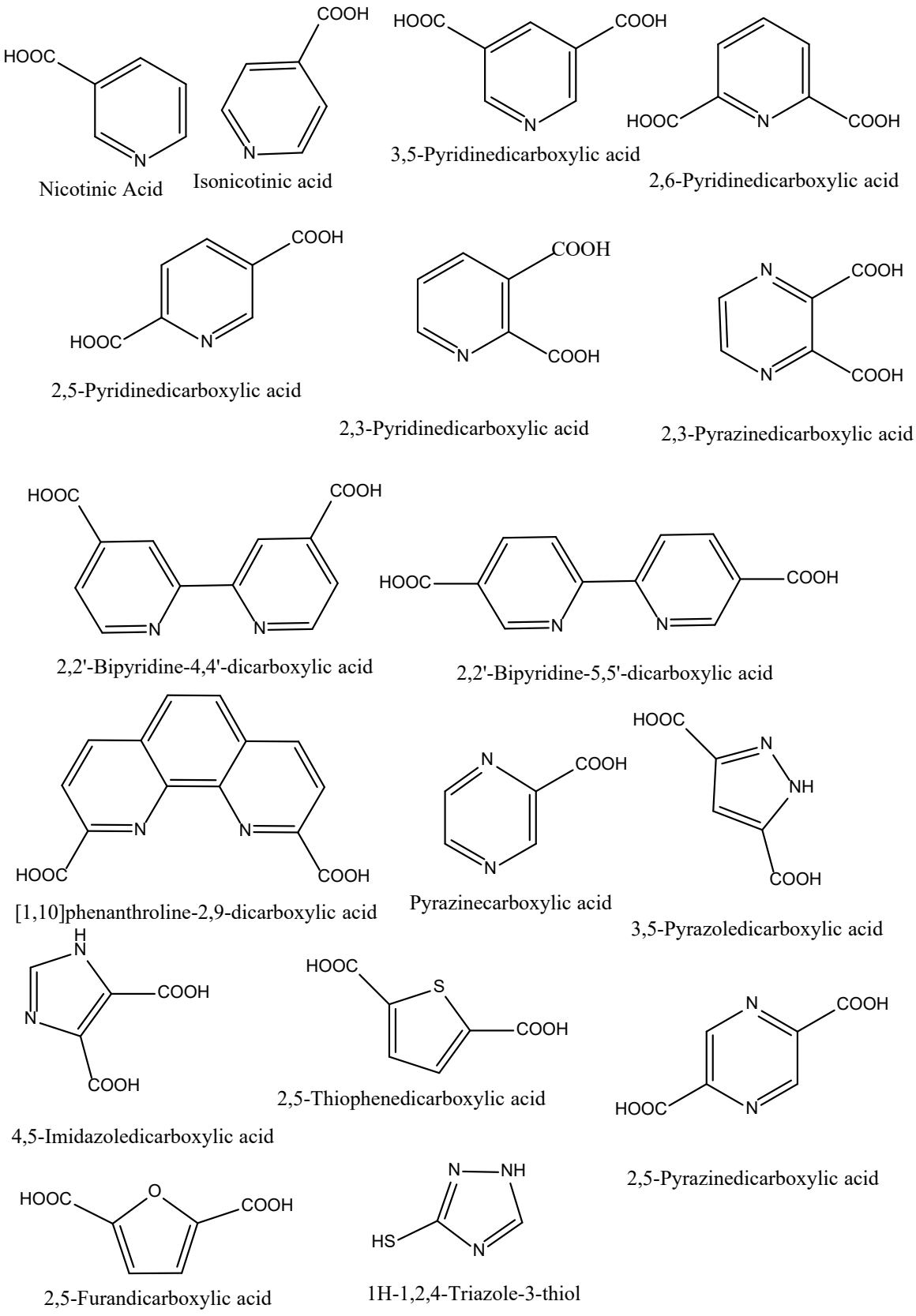

Figure 1.23: Most interesting five-membered N-donor rings ligand structure used for coordination polymer synthesis

Sulfonic acids, phosphonic acids, thiophen, furan, Schiff-bases (nitrogen- imin group), large aromatic ligands such as pentacene, benzanthracene, triptycene, pyrene and perylen and metal clusters have been also used to construct very interesting coordination networks (Figure 1.24).

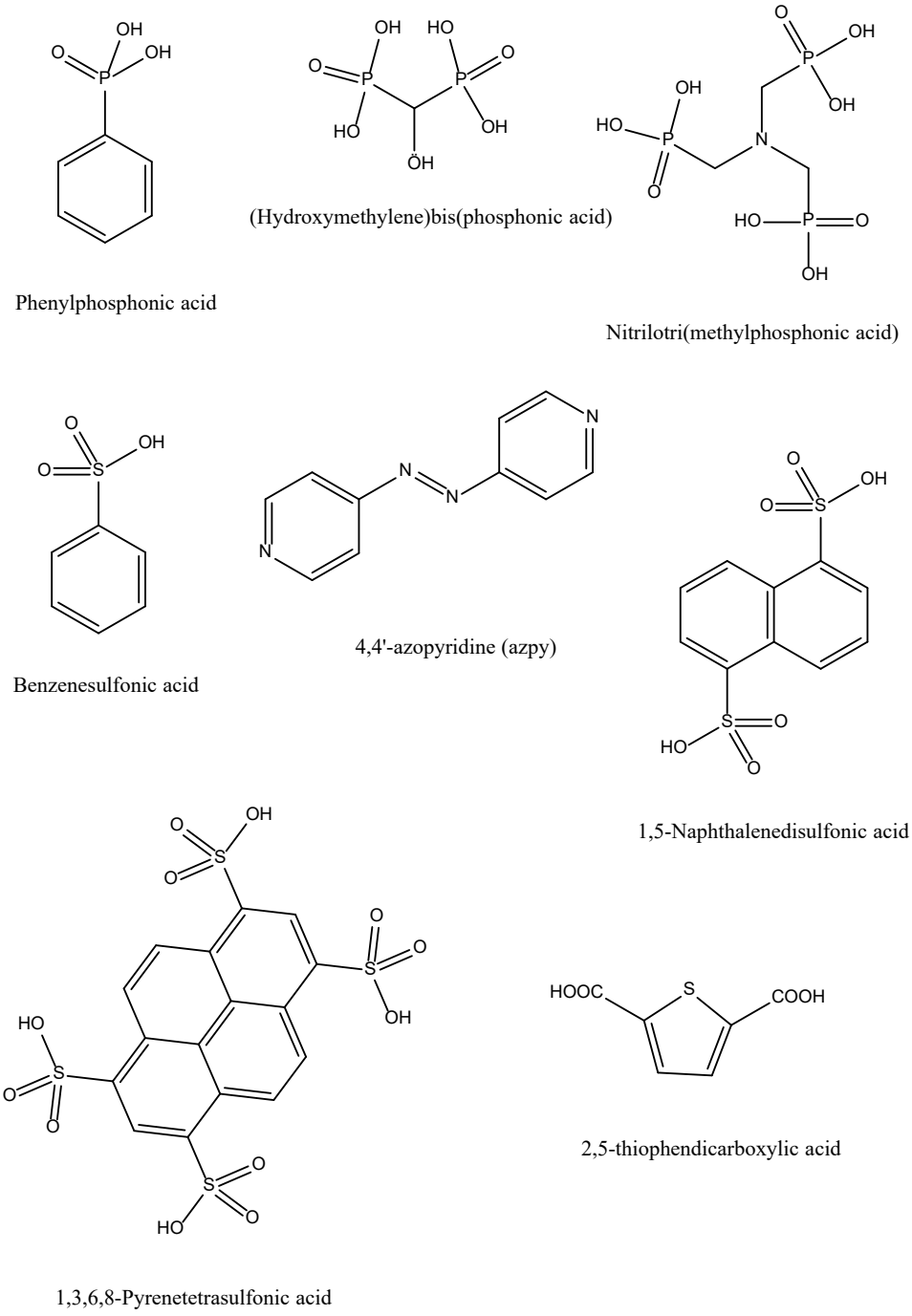

Figure 1.24: Some other convenient ligands that have been frequently use to construct coordination polymers

1.4. Synthesis method

As mentioned earlier, a coordination polymer is a complex of metal ions and ligand molecules extended in one, two and three dimensions and formed by self-assembly process.Self-assembly is very effective for the following reasons: (i) a wide variety of frameworks can be realized just from simple building blocks of metal ions, organic bridging ligands and counter anions; (ii) easy and rational modification of organic bridging ligands is possible; (iii) several interactions such as coordination bond, hydrogen bond, aromatic interaction, metal-metal bond and van der waals interaction are available; (iv) the reaction can be controlled by different factors such as temperature, pH, solvent, pressure, etc. For coordination polymers, the recrystallization method is not useful for obtaining high purity or large single crystals because they are insoluble in most solvents. Therefore, common techniques to synthesize pure coordination compounds are slow diffusion, hydrothermal and slow evaporation and many other methods. Moreover, a new synthetic approach has been developed as well [89]. It is well known that the crystallization, structure and morphology of MOFs and CPs do not only depend on the modules building blocks, but they are in control of many experimental conditions such as solvent type [90], pH value of reaction mixture [91], temperature [92], reagents concentration [93], time [94], molar ratios of starting materials [95], the nature of counter ions [96] and pressure [97].These parameters are divided into two main categories including a) compositional parameters like solvent type, pH, substituent of ligands, the molar ratio of starting materials, counter ions and concentration; and b) process parameters such as pressure, time and temperature (Figure 1.25) [98].Keeping in mind that these parameters have a deep influence on the structure of final framework and could lead to compounds with different particle sizes distributions and morphologies with different applications. In the following, some important synthetic routes will be mentioned here.

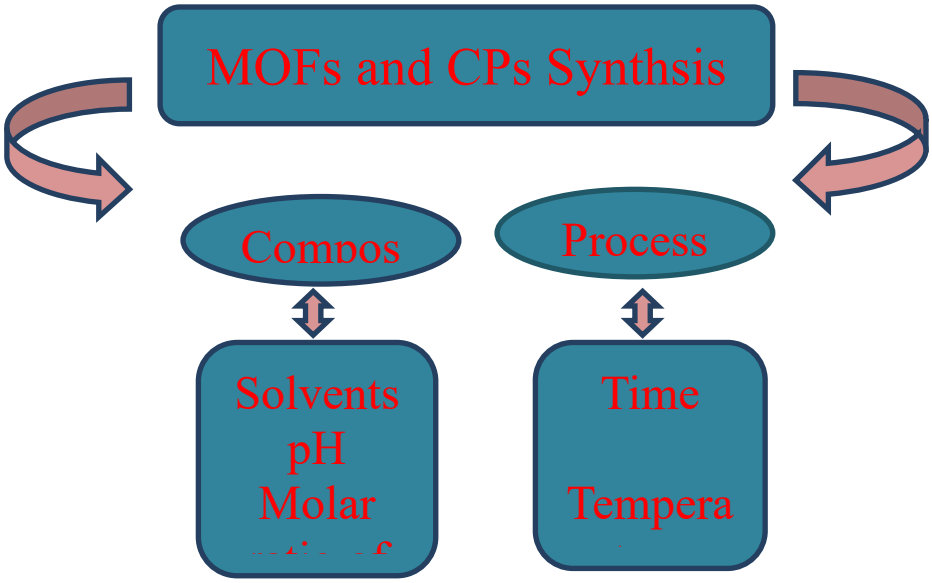

Figure 1.25: Schematic feature parameters which play roles in MOFs and CPs synthesis [98]

1.4.1 The slow evaporation method

Slow evaporation is implied as one of the typical methods for the synthesis of MOFs and CPs. In this method, evaporating of solvents occurs at room temperature and metal salts and organic linkers are mixed together in the liquid phase with or without auxiliary ligands (Figure 1.26).Highly soluble precursors are usually required in this method which should be concentrated by slow evaporation process. The great disadvantage of this method is that it is very time-consuming compared to the other conventional synthesis methods.This problem can be sometimes overcome by using low-boiling solvents [99–102]. In point of fact, this technique needs convenient conditions:

- Crystals growth in saturated solution.
- Solubility increases by temperature and crystal can appear during cooling step.

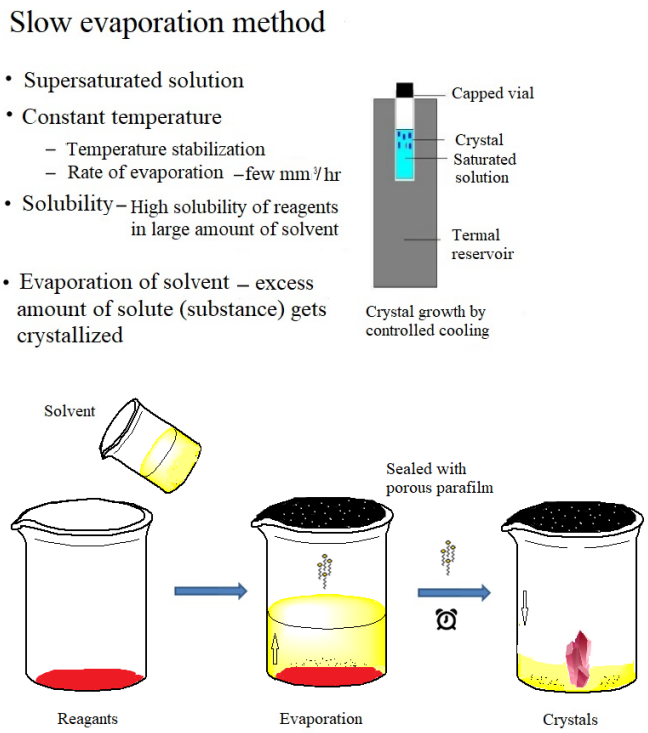

Figure 1.26: Slow evaporation method [103]

1.4.2 The slow diffusion method

Rapid mixing of metal ion with ligand solutions may result in microcrystal (powder) with size in the order of μm which is not suitable for X-ray single crystal structural analysis. To avoid precipitation, diffusion method is often used. Large single crystals suitable for X-ray structural analysis could be obtained by slow diffusion of the two above mentioned solutions [104].Various devices, such as straight-tube (test-tube) (Figure 1.27), NMR tube, H-tube (Figure 1.28) and Y-tube glass cell have been designed for this goal. In this technique, second solvent should be added slowly and carefully on top of the first solvent hence, the two liquid layers do not mix at all.During several days or even weeks, top solvent slowly diffuses into the first solvent, decreasing the solubility of product and producing large, good quality crystals. For this reason, either narrow Schlenk flasks or NMR tubes are preferred due to their smaller surface area of the boundary [104].This method could be utilized either for air-stable or air-sensitive compounds.This is worth to not that the Schlenk flask is normally used for air-sensitive materials.

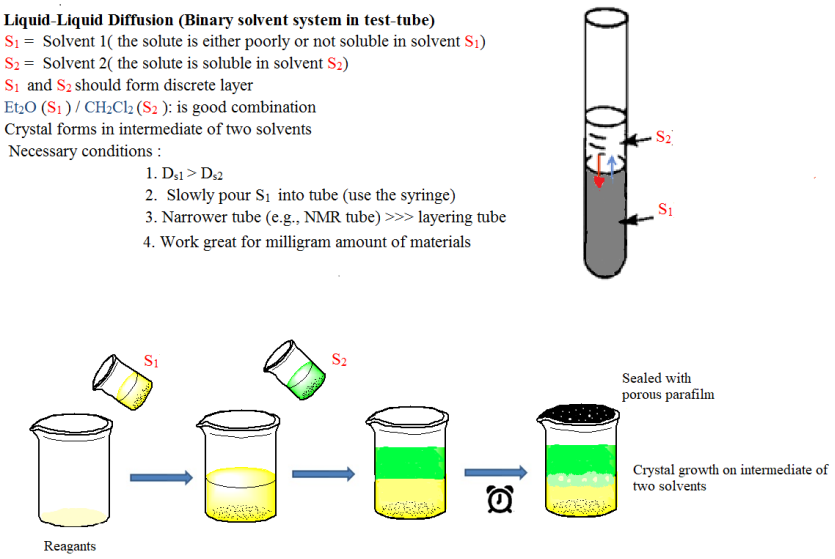

Figure 1.27: Slow diffusion in test-tube

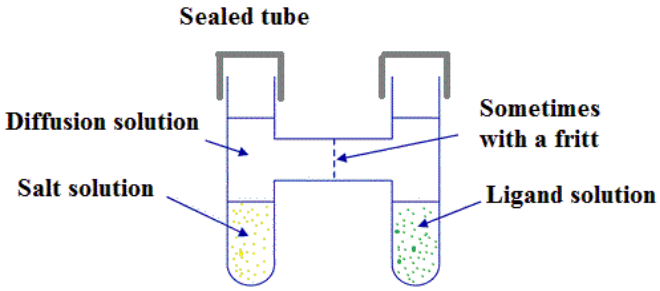

Figure 1.28 : Slow diffusion in H-tube [105]

1.4.3. Vapor Diffusion Technique

This method involves the diffusion of the vapor of a volatile solvent into the solution including sample. This gradually decreases the overall solubility of the product and forces the product to crystallize (Figure 1.29) [104a, 106].This method can be used for either air-stable or air-sensitive samples (Figure 1.30) [107].

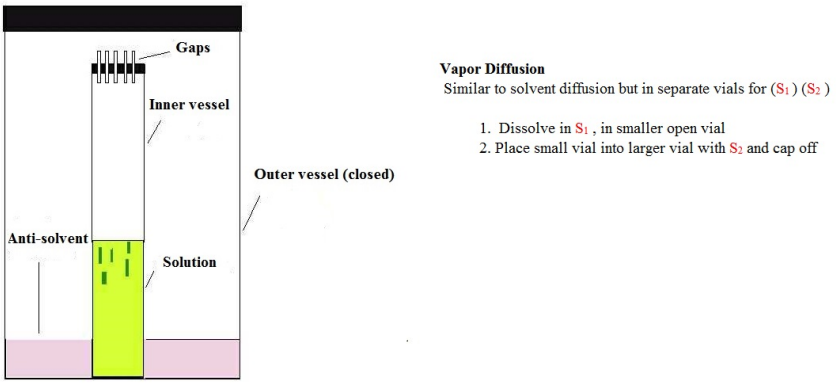

Figure 1.29: Vapor diffusion mechanism [106]

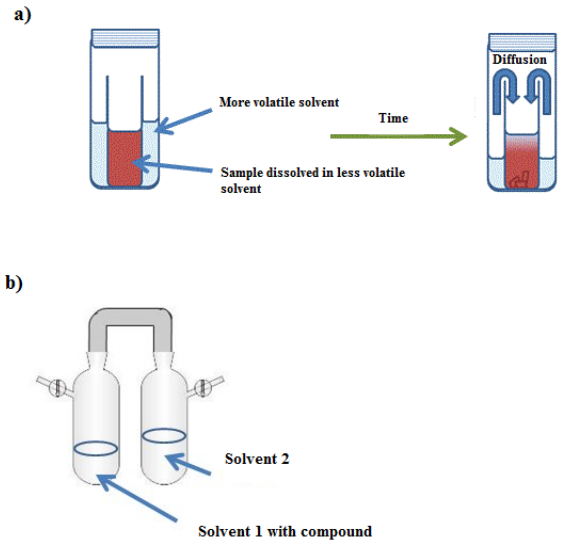

Figure 1.30: Vapor diffusion for air-stable samples **(a)**; for air-sensitive samples **(b)** [107]

1.4.4. Gel growth method

Large crystals with dimensions of several mm can be obtained via this technique within 3 to 4 weeks. Furthermore, crystals are very pure since the growth takes place at room temperature for several days and weeks. Growing crystals is usually carried out in a U-shaped Tube or test-tube as depicted in (Figure 1.31). Sodium metasilicate, also known as silica hydrogel, has been the mostly used [108–111].

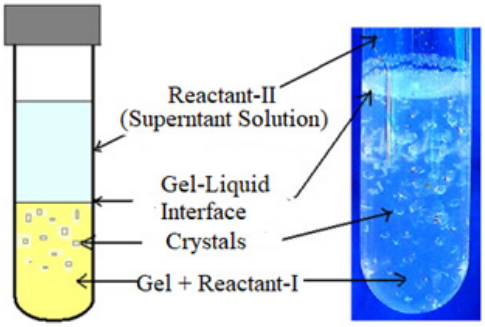

Figure 1.31: Schematic feature of gel growth method in test-tube and real sample [111]

1.4.5 Temperature gradient method

Tempereture gradient method is pointed as convenient way to grow large and high quality single crystal at a fixed temperature [112–115]. In this technique, a thermal gradient is obtained by local heating or cooling of a part of the tube and it causes the warmer portion of the solution is saturated more than the cooler part. In consequence, warmer solution can be transferred to the cooler part by convection currents where crystal grows. The polar solvents are normally used in this method such as water, ethanol, methanol and acetonitrile, hence the highest temperature must be adjusted up to boiling point of solvent. As a matter of fact, this method is applicable to moderate temperature, approximately up to 100 ˚C. Furthermore, this method is suitable for the reagents which are insoluble or slightly soluble.This method is commonly carried out in branched tube, either test tube or V-shaped tube as illustrated with (Figure 1.32).

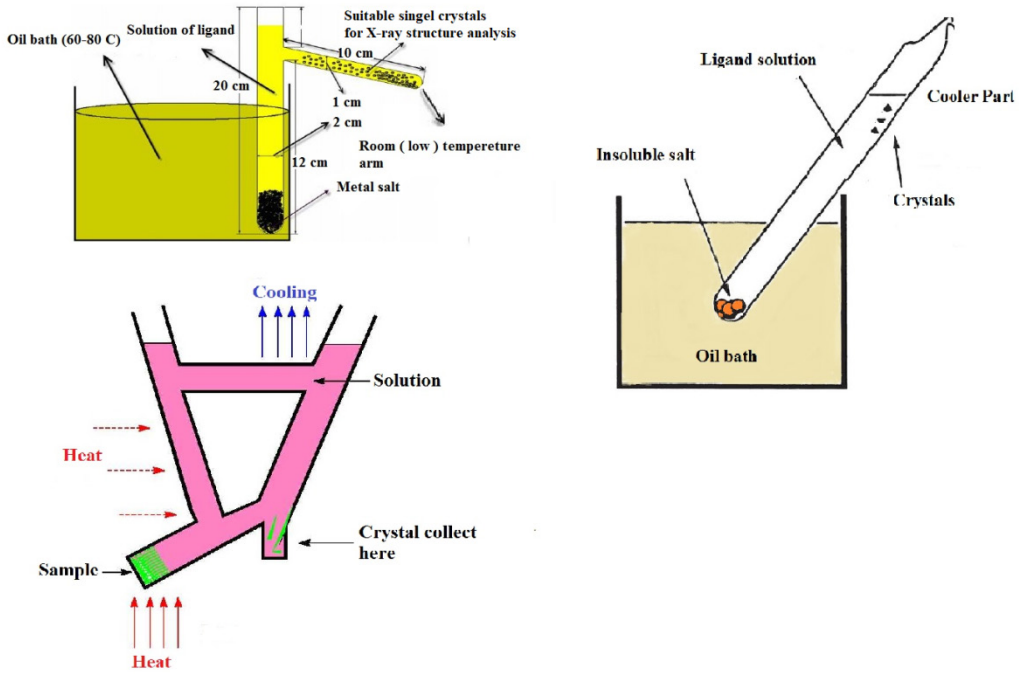

Figure 1.32: Thermal gradient method via different types of vessel . Branched tube **(a)**; test-tube **(b)**; V-shaped tube **(c)** [106,116]

1.4.6. Hydro (solvo)thermal methods

The hydrothermal technique performs as an important tool for advanced materials processing with a wide variety of technological applications such as electronics, catalysis, ceramics, magnetic data storage, biomedical, biophotonicsm and etc. Indeed, the hydrothermal technique is known an efficient technique for synthesizing nano-hybrid and nanocomposite compounds.

Hydrothermal processing is defined as heterogeneous reaction under high pressure and temperature between materials that are relatively insoluble under ordinary conditions to dissolve and recrystallize materials [117–118]. In this synthetic method, reactions are carried out at higher temperatures (temperature higher than 100 ˚C) and pressure for several hours or days into the well-sealed vessels. Usually, Teflon-lined autoclaves are used.The reactants are taken in polar and high boiling point solvents such as DMF, DEF, DMSO, H_2O, acetone, acetonitrile and alcohols or sometimes a mixture of these solvents when the solubility of the starting materials are different. The major advantage of this method is that it offers high solubility of the precursors and formation of crystals with good quality suitable for structural characterization [119].The running temperature range is commonly between 100–260 ˚C inside autoclave under autogenous pressure. Under these conditions, water properties undergo significant changes and its viscosity and polarity (dielectric constant) decrease, but pressure,

ion production and also the diffusion process increase. So, crystal growth of this solution is favored. As a result, hydrothermal method can be an excellent alternative to boost solubilities of starting materials (Figure 1.33, 1.34) [120]. It is worth to notice that solvothermal technique is very similar to the hydrothermal concepts. But the only difference is that the precursor solution is not aqueous.

Figure 1.33: Different size and shape of hydrothermal tubes which are produced via environment friendly materials [121]

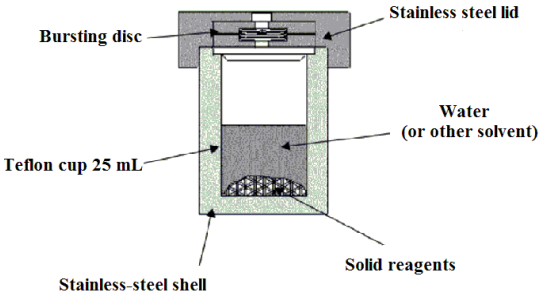

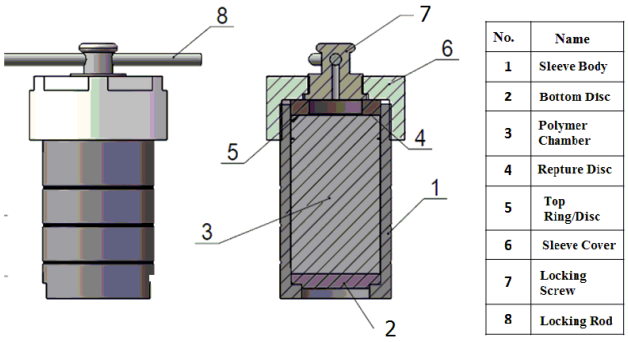

No.	Name
1	Sleeve Body
2	Bottom Disc
3	Polymer Chamber
4	Repture Disc
5	Top Ring/Disc
6	Sleeve Cover
7	Locking Screw
8	Locking Rod

Figure 1.34: Schematic feature of hydrothermal tube.

1.4.7. Solvent-free method

Solvent-free synthesis is an advantageous method, since it could explain the role of solvent molecules in template microporous structures, giving access to large scale green production processes, and even providing more convenient lab-scale preparative methods. Recently, there have been several reports on using of mechanochemical methods (grinding) to produce various coordination complexes [122–125], and three reports of the synthesis of one- and two-dimensional coordination polymers [126–128].The 3D coordination polymer [Cu (isonicotinate)$_2$]$_n$, which is an example of permanent open porosity, is produced by grinding [129].The solvent-free method is quick and gives a quantitative yield, without the need for solvents or external heating. Clearly, it can expose higher efficiency in terms of materials, energy, and time compared to solvothermal method (Figure 1.35).

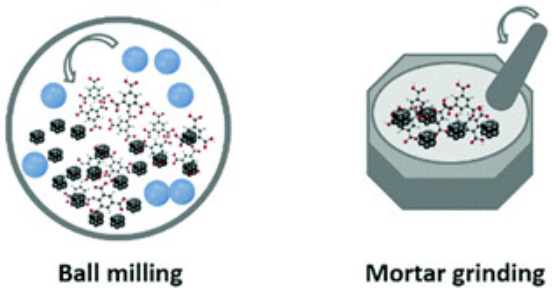

Figure 1.35: Synthesizing coordination polymer by solvent-free method [130]

1.5. Structural modulation by reaction condition

A polymeric metal-organic compounds and coordination polymers are usually insoluble, because coordination bonds are usually stronger and have better directionality than hydrogen bonding and other weak supramolecular interactions.However, structural diversity and uncertainty is an intrinsic problem for crystallization and construction of coordination polymers due to the coordination flexibility of the metal ions and organic ligands, as well as the presence of other chemical variable such as solvent molecules [131]. Among a number of factors that may contribute to the structures of coordination polymers, temperature, pH, solvent, counterion, and template (or additive) play an important role in the formation of products.To continue, some of them will be discussed here to illustrate their significance of modulation of the structures [131].

1.5.1. Temperature Effect

Temperature plays an important role in formation of kinetic and thermodynamic product. The thermodynamically favored product that can usually be obtained at higher reaction temperature and can be even synthesized more remarkably under hydro(solvo)thermal reactions, in which metastable kinetic phases can be more controlled. Furthermore, higher temperatures can raise the solubility of reagents which might reduce the kinetics of crystal growth and lead to bigger and better quality of particles [132–133]. Moreover, selecting an appropriate reaction temperature can provide possibility to control on the evaluation of colloidal solution [134].

1.5.2. pH Effect

Acid-base reactions are usually involved in the assembly of coordination polymers. It is well-known that crystallization and growth of inorganic-organic hybrid materials are highly affected by the acidity/basicity of reaction media.The deprotonation of an organic ligand and sometimes generation of an OH^- ligand in aqueous solution by changing of pH of reaction will provide connectivity of polycarboxylate ligands to metal ion based on acid-base concept. Moreover, the reaction kinetics can be influenced by altering pH conditions in some cases [135].

1.5.3. Solvent Effect

Solvent molecule determines the solubilities of both reactants and products which simulates the supersaturation and kinetics of crystal formation, determining the final particle shape and dimensions.Besides their role in dissolving the reactants and products, they can also impact on the superstructures of the intermediates and final products through supramolecular interactions between the products and solvents, Therefore, solvent molecules can have effect not only on the crystallization process, but also on the configurations of the certain groups of the products, leading to different structures.They play a role of template and occupy the voids of the products and also they only serve as the crystallization environment and do not exist on the products [136–138].

1.5.4. Counter ion effect

Counterions usually are attributed as the anions that are not involved in the inner coordination sphere. But still they can affect the crystallization of coordination polymer products, leading to different coordination structures. In addition, charge is an important factor of rational construction of functional coordination polymers. Because most transition metal ions exist on a positive charge in the framework, an anionic source must be included to neutralize the overall charge. Many N-containing heterocyclic ligands are electrically neutral and, therefore, counter anions are included in the crystal. Frequently used anionic sources are inorganic anions, such as ClO_4^-, BF_4^-, NO_3^-, NCS^-, PF_6^-, NO_2^-, SiF_6^{2-}, CN^-, $CF_3SO_3^-$, SO_4^{2-}, N_3^- and halides, which are introduced together with metal ions from the corresponding metal, sodium and potassium salts. The inorganic anions exist as (i) free guests; (ii) hydrogen-bond acceptor; and (iii) coordination unit. An important characteristic of inorganic anions is their ability to act as hydrogen-bond acceptor sites through their O and F atoms. In some cases, especially in silver (I) coordination polymers [139], the counter-ion can play a key role in formation of final supramolecular structure. Indeed, the different counter-ions have different coordination interactions with metal ions due to the different H-bonding interaction with the other components and the different influence on crystallization speed for different supramolecular products.Besides supramolecular interactions, counter anions also play important roles in the self-assembly. For example, in sliver (I) coordination polymers, changing anions often alters the structural topologies, sometime even the overall physical properties of polymeric Ag^+ complexes [140].The anions can usually exist on coordinating, weakly coordinating, noncoordinating silver(I) polymeric complexes. Among the commonly used anions, BH_4^-, ClO_4^-, NO_3^-, $CF_3SO_3^-$ and $CF_3CO_2^-$, PF_6^- and SbF_6^- are usually uncoordinated.

1.6. Lanthanides

The lanthanides (Ln) are composed of lanthanum (La) and 14 other elements (Ce, Pr, Nd, Pm, Sm, Eu, Gd, Tb, Dy, Ho, Er, Tm, Yb, and Lu).These elements are stable in the III oxidation state and are simply characterized by the electronic structure of the 4*f* orbitals.Since, 4*f* orbitals are shielded by the outer 5s and 5p orbitals, there is a slight shift in their electronic transitions.The energy levels of the trivalent lanthanide ions are given in (Figure 1.36) [141–142].

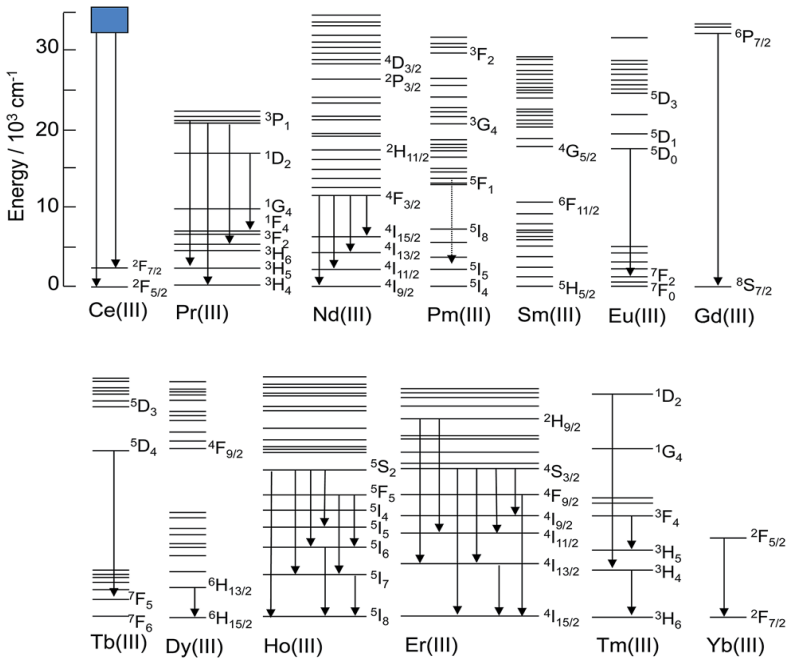

Figure 1.36: The diagram of energy levels of the trivalent lanthanide ions [142]

The energy levels presented in (Figure 1.36) are splitted by the crystal or ligand field. Although the ligand field strength of transition metal ions (*d*) is basically several tens of thousands of cm^{-1}, the ligand field strength for Ln (III) ions (*f*) amounts to several hundreds of cm^{-1}. In a configurational coordination diagram, energy levels in 4*f* orbital appear as parallel parabolas (small off–set case) because the 4*f* electrons are well-shielded from 5s and 5p orbitals [142]. Thus, electronic transitions in absorption and emission processes exhibit sharp spectral lines.The radiative emission of Ln (III) ions originates principally from the electric dipole transition.The electric transitions to the inner 4*f* orbital of free ions are forbidden because they do not correspond to a change of parity. However, the transitions are partially allowed by mixing of the 4*f* orbital (odd parity) and 5*d* orbital (even parity) under the ligand shield. The parity does not change significantly in such a transition; therefore, the lifetime of the excited state is long (ca.10 ms). Lanthanides with characteristic 4*f* orbitals show very fascinating photophysical properties [142].Inorganic phosphors and coordination compounds including lanthanide ions have also been synthesized and their resulting emission properties have been investigated. Recently, metal organic frameworks (MOFs) composed of lanthanide ions and organic ligands, Ln-MOFs, have been extensively studied [143–146]. By this time, various types of luminescent Ln-MOFs have been reported. MOFs provide characteristic frameworks with three-dimensional cavities that act to encapsulate metal cations and/or molecules (Figure 1.37) [99,147–157].

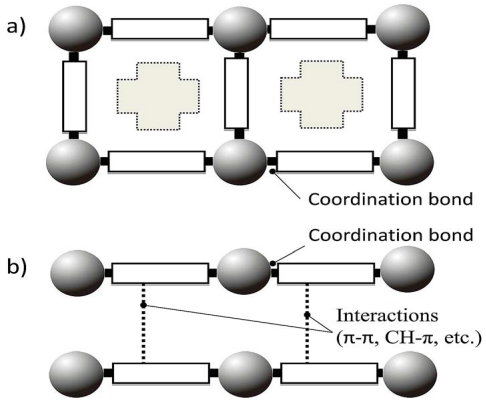

Figure 1.37: Structure of Ln-MOFs **(a)**; the structure of Ln coordination polymers are constructed by metal ions and organic ligands **(b)** [142]

Such cavities are utilized as nanoscale sensors for metal ions and gas or organic molecules based on the host-guest chemistry. Chandler et al. described CO_2 gas sensors that employ luminescent Ln-MOFs [158]. Liu et al. and Pan et al. have demonstrated Ag^+ sensors based on Ln-MOFs [159–160]. In addition, Rocha and Carlos have provided a review on luminescent multifunctional lanthanides-based Ln-MOFs [161]. On the other hand, coordination polymers composed of lanthanide ions and organic ligands have also attracted considerable attention in the coordination chemistry, inorganic chemistry, supramolecular chemistry, polymer and material science. One-, two- and three-dimensional alternating sequences of metal ions and organic ligands (Figure 1.37) exhibit remarkable characteristics as novel organic–inorganic hybrid materials with various structures, and individual physical properties that can be prepared by the combination of lanthanide ions and organic ligands. Moreover, the characteristic network structure results in photonic applications. Luminescent lanthanide coordination polymers have characteristic network structures built of lanthanide ions and functional organic linkers.The luminescence properties depend upon the coordination structures around the lanthanide ions, causes significant photophysical properties. In next the section, photonic application, photofunctional materials, and the photophysical properties of lanthanide coordination polymers are introduced.

1.6.1. Luminescence in lanthanide MOFs and CPs

Luminescence is described as spontaneous emission of radiation stimulated by an absorption of an electronically or vibrationally energy. Although the excitation energy is frequently in form of light (photon), but it could also be achieved in number of different ways, such as electronical field, ionizing radiations, chemical or electrode reactions, within biological systems and through

mechanical forces. A general distinction between semiconductor-based luminescence and the luminescence stems from the metal ions, organic molecules or coordination complexes.The general mechanisms for these two types are depicted in (Figure 1.38a) [162–163]. Both ground and excited states evolve from the MOs of organic molecules and coordination complexes. The fundamental mechanism is similar in all cases, to excite an electron from the ground to an excited state and the consecutive return to the ground state through emitting of a photon that is with nanoparticles spanning the gap between molecules and semiconductors. Generally, a distinction can be defined between two main luminescence phenomena: fluorescence and phosphorescence which shown in (Figure 1.38b) [163].

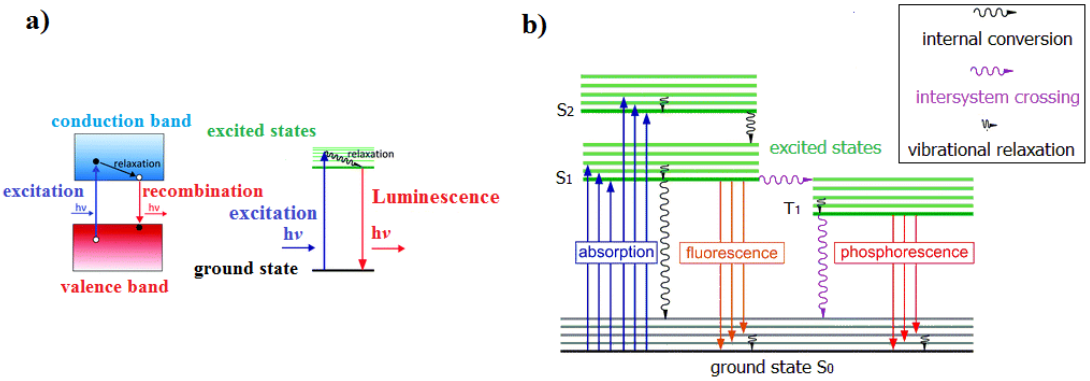

Figure 1.38 : Simplified mechanisms of semiconductor (electronic bands; left) and molecular based excitation/emission processes (discrete energy levels; right) **(a)** ; Jablonski diagram showing basic photophysical processes; S denotes singlet, T triplet states; internal conversion and intersystem crossing are nonradiative processes; intersystem crossings are accompanied by a forbidden change in the spin state **(b)** [163]

Lanthanide-based luminescence has proven its versatility in many areas including solid state lighting and biomedicine [164]. Different lanthanide elements in their trivalent state expose various luminescence colors and characteristics (Figure 1.39). A huge number of luminescent lanthanide materials are relevant to Tb (III) and Eu(III) which provide green or red 4*f*–4*f* emissions, respectively. Furthermore, Tb (III) and Eu(III) ions identify an energy gap between their main emissive and receiving states that is large enough to avoid pronounced vibrational quenching. Lanthanide ions such as Nd(III), Er(III) or Yb(III) can provide 4*f*–4*f* emissions in technologically relevant ranges such as NIR [186] or show up conversion effects where two or more NIR photons are combined into one shorter wavelength [163].

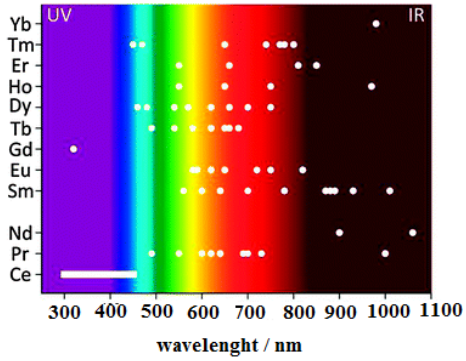

Figure 1.39: Wavelength of the main emissive transitions of the trivalent lanthanide coordination compounds in the near-UV to near-IR range; the relative intensities of transitions and thus the overall emission color of a lanthanide (III) compound may vary and that Ce(III) emissions are 5d–4f in nature, covering the indicated range depending on the chemical environment of the cerium ion [163]

So far, lanthanides show much richer photophysics, as they are not generally restricted to MC 4*f*–4*f* luminescence [165]. Evidently, Ce(III) can show 5*d*–4*f* transitions due to an emission in the visible range, as the energetic level of the d states is dropped by ligand and crystal fields. These transitions exhibit a much higher dependence on the coordination environment of the metal ion than 4*f*–4*f* transitions, due to participation of 5*d* states. They cause broad absorption and emission bands that do not require an antenna effect to improve brightness, as the transitions *f*–*d* and *d*–*f* are parity allowed. This is also observed for divalent lanthanide ions like Eu(II), because they can also commit 5*d* levels in luminescence processes. Reduction of energy of 5*d* states depends on chemical surrounding and the crystal field dominates broad band processes that are parity allowed and as strong as for Ce (III). Hence, transitions involving *d* and *f* states significantly differ from 4*f*–4*f* transitions [163].

The construction of lanthanide CPs and MOFs vary in some aspects from those containing transition metals. Moreover, under different synthetic thermal conditions involving room temperature or solvothermal which leads to CP formation, the co-coordination of water or other oxygen-containing solvents often cannot be avoided. Nevertheless, lanthanide CPs mostly possesses interesting and unusual topologies and often forming iso-structural series. Luminescent lanthanide CPs and MOFs represent a well-established area, which has already been developed towards applications [166–167]. Although Eu(III) and Tb(III) are often selected for luminescence studies, almost of the lanthanides exhibit photoluminescent properties. The energy levels of some commonly used lanthanides are shown in (Figure 1.39). Except Gd(III), the highest labeled energy level for each element is the level from which luminescence occurs. In fact, the lifetimes of nearly all lanthanides emissive transitions are very long, on the order of hundreds of microseconds. This

prevents their use in applications requiring fast emission, such as scintillation and displays. When the luminescence is sensitized through the antenna effect, the lifetime is even longer, usually close to a millisecond [167–168].

1.7. Lead coordination chemistry

According to the general rule concerning oxidation states of the p block elements, lead shows the oxidation states II and IV. However, Lead exposes oxidation state II more than IV in coordination compounds due to effect of the so-called “inert electron-pair”[169]. This property was explained by the relativistic stabilization of the 6s orbital, caused by the direct relativistic effect and the presence of the filled 4f subshell.The lead (IV) compounds are strong oxidants in aqueous systems, being spontaneously reduced to lead (II) under formation of oxygen gas.

The lead (II) displays the broad range of coordination numbers from 2 to 12. Therefore, a large variety of configurations of its complexes and compounds results [170]. According to the valence bond theory, the inert electron-pair can either occupy a hybrid orbital formed by mixing the 6s and 6p orbitals on the metal ion and as such becoming stereochemically active or be a pure s^2 electron-pair and thereby stereochemically inactive. In terms of coordination number, this means that the hybrid orbital with a lone electron-pair can be considered an additional ligand in the coordination sphere normally even taking up *more* space than that of an ordinary ligand [171]. However, according to molecular orbital theory the classical conception of 6s/6p orbital hybridization on the lead (II) ion is regarded as incorrect. This is because the energy levels of these orbitals are too unsimilar and the different spatial distribution of their corresponding wave functions [172–175]. Instead, the stereochemical activity observed in lead (II) complexes should be noticed as a result of an antibonding lead 6s-ligand np (6s/np) interaction which causes structural distortions to energetically minimize these unfavorable covalent interactions [172–175]. Two general structural types of lead (II) complexes are determined, *hemidirected* and *holodirected*, as introduced by Shimoni-Livny et al (Figure 1.40) [176]. In the former, the electron distribution around the metal ion is greatly unevenly distributed, caused by antibonding metal−ligand interactions creating a visual gap in the coordination sphere [177].

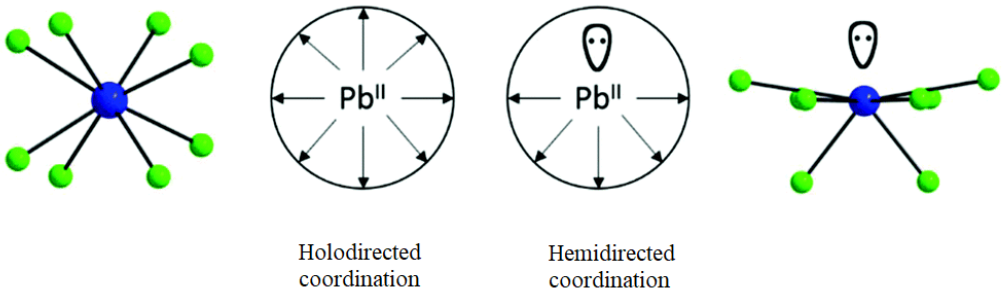

Figure 1.40: Pb (II) complexes can be either hemidirected (right) or holodirected (left) [178]

The lead coordination sphere can be defined as holodirected in complexes in which the bonds to ligand atoms are directed toward the surface of encompassing sphere, while hemidirected refers to those cases where the bonds to ligand atoms are directed only to a part of the coordination sphere, leaving a gap in the distribution of bonds to the ligand [179–183]. Lone pair activity may depend on the following factors: (i) low or high coordination number, (ii) hard or soft ligands, (iii) attractive versus repulsive interactions among ligands, (iv) fewer or more electron donation from ligands to metal [184].

Chapter 2

2. Materials and instruments and methods

2.1. Instruments and softwares and materials

2.1.1. Instruments

(i) Elemental analysis (CHNS) were performed on a Hekatech elemental analyzer for C, N, H and S analyses of samples.

(ii) The ATR-IR spectra were recorded in the range 400–4000 cm^{-1} on a Bruker Alpha spectrometer.

(iii) X-ray diffraction measurements were performed using a *Siemens P4* diffractometer with monochromated Mo (Kα) radiation for lanthanide , silver, copper and lead compounds and Ag (Kα) radiation for lead compound of formula $[Pb_3(CH_3COO)_2(N_3)_4]_n$ at room temperature via Stoe IPDS diffractometer.

(iv) TGA and DSC analysis were carried down by using instrument netzsch sta 449 F1.

(v) Autoclave, general purpose acid digestion vessel 25 ml with PTFE cup and cover.

2.1.2. Software

i) 3D scheme of structures were drawn by *Mercury 3.7* and *Diamond 4.1.2.*

ii) The resolutions of 3D scheme of structures were improved by *POV-Ray 3.7.*

iii) Diagrams drawing have been done by means of *Origin Pro 8.5.*

2.1.3. Materials

All the starting materials and solvents for synthesis were purchased from commercial supplier Sigma–Aldrich and Merck and also used as received without purification.

2.2. Synthesis methods of compounds

2.2.1 Silver coordination polymer

Synthesis of complex $[Ag_2(HPO_3CH_2COOH)]_n$ (1)

Slow diffusion of aqueous solution of Ag (I) nitrate with ligand solution in H-Tube was carried out in light exclusion.$AgNO_3$ (2mmol) was dissolved in 3 ml water and carefully placed in right wing of H-tube.Phosphonoacetic acid (1mmol) and sodium hydroxide (2mmol) were dissolved in 3 ml water and carefully placed in left tube.The tube was slowly filled by EtOH and sealed. After several weeks the colorless crystals were formed on inner surface of tube and suitable for X–ray structural analysis.Yield: *Ca*. 69% based on Ag. Elemental analysis: *Anal*. Calc. for $Ag_2C_2H_3O_5P$ (353.75): C, 6.78 ; H, 0.848 ; O, 22.61 . Found: C, 6.70 ; H, 0,834 ; O, 22.61%. IR spectra: $\nu(cm^{-1})$ = 2369(w), 2221 (w), 2159 (w), 1522 (vs), 1410(s), 1363(m), 1207 (s), 1178 (m), 1158 (s), 1122 (m), 1041(m), 953 (m), 912 (s), 867 (m), 818 (m), 634 (s), 568 (s), 518 (m), 499 (s), 469 (s).

2.2.2 Lanthanide coordination polymers

2.2.2*a*. Neodymium coordination polymer $\{[Nd_2(FDA)_3(DMF)(H_2O)_2]\cdot DMF\cdot(H_2O)_2\}_n$ (2)

2,5-Furandicarboxylic acid (1.5 mmol) and neodymium nitrate (1mmol) were poured into capped tube.Then DMF (10 ml) was added into tube and the reagents were stirred powerfully. Afterwards, the tube was sealed and put into oil bath and heated around 120 ˚C.The pale pink-colored crystal was formed within five days.They were collected and washed by acetone and distilled water. Yield: *Ca*. 43% based on Nd. *Anal.* Calc. for $C_{24}H_{30}N_2Nd_2O_{22}$ (986.48) : C, 29.2; H, 3.04; N, 2.89. Found: C, 30.01; H, 3.06; N, 2.78 %. IR (cm^{-1}): 3560 (w), 3290 (m), 3115(w), 2271 (w), 2205 (w), 2075(w), 2044(w), 1983(w), 1651 (m), 1639 (m), 1623(m), 1562(vs), 1548(vs), 1438(w), 1366(vs), 1223(m), 1198(m), 1165(m), 1104(m), 1061(m), 1023(m), 832(m), 821(vs), 782(vs), 674(m) , 664(vs) , 615(s) , 491(s).

2.2.2*b*. Samarium coordination polymer $\{[Sm_2(FDA)_3(DMF)(H_2O)_2]\cdot DMF\cdot(H_2O)_2\}_n$ (3)

2,5-Furandicarboxylic acid (1.5 mmol) and samarium nitrate (1mmol) were poured into capped tube.Then DMF (10 ml) was added into tube and the reagents were stirred powerfully. Afterwards, the tube was sealed and put into oil bath and heated around 120 ˚C. The pale pink-colored crystal was formed within five days.They were collected and washed by acetone and distilled water.Yield:*Ca*. 50.05 % based on Sm. Elemental analysis: *Anal.* Calc. for

$C_{24}H_{30}N_2O_{22}Sm_2$ (998.72): C, 28.84; H, 3.004; N, 2.80. Found: C, 29.04; H, 3.00; N, 2.84 %. IR (cm^{-1}): 3365 (m), 2274 (w), 2214 (w), 2076(w), 2021(w), 1651(m), 1638 (m), 1623(m), 1561(vs), 1549(vs), 1375(vs), 1223(m), 1198(m), 1165(m), 1104(m), 1061(m), 1012(m), 833(m), 822(vs), 783(vs), 675(m) , 664(vs) , 615(s) , 491(s).

2.2.2*c*. Cerium coordination polymer $[Ce(pdc)(DMF)_2(NO_3)]_n$ (4)

Pyrazole-3,5-dicarboxylic acid (1.5 mmol) and cerium nitrate (1mmol) were dissolved in DMF (10 ml) and the mixture was stirred powerfully. Afterwards, the mixture was transferred into teflon-lined autoclave vessel (25 ml) and sealed and heated around 150 ˚C for 4 days. Subsequently, the mixture was moderately cooled down in rate of 5 ˚C per hour for 48 hours. The transparent crystals were formed and collected and washed by acetone and water.Yield: *Ca*. 72% based on Ce. Elemental analysis: *Anal.* Calc. for $C_{11}H_{16}Ce\,N_5O_9$ (642.23) : C, 20.55; H, 2.49 ; N, 10.90 %. Found: C, 20.64 ; H, 2.44 ; N, 10.85 %. IR (cm^{-1}): 3375 (m), 2300 (w), 2215 (w), 2040(w), 1674(vs), 1623(m), 1556 (s), 1489(vs), 1444(s), 1297(m), 1202(m), 853(w), 833(vs), 783(vs), 770 (m), 738 (m), 715(m).

2.2.3. Copper (I) and Schiff-base coordination polymer

a) Preparation of ligand 1. [N,N´- bis (4-methyl-benzylidene)butane-1,4-diamine] (L_1)

The solution of 4-Methoxy benzenaldehyde (10 mmol) in 40 mL methanol was stirred and heated gently (ca. 60 ˚C) for 10 min.The solution of 1,4-Diaminobutane (5 mmol) in 10 mL methanol was added dropwise with constant stirring.The mixture was heated for 2 hours and then allowed to cool over the night. The resulting crude solid was collected and filtered and washed several times with methanol.Yield:*Ca*. 97%. Elemental analysis: *Anal.* Calc. for $C_{20}H_{24}N_2O_2$ (324) : C, 74.07 ; H, 7.40 ; N, 8.63. Found: C, 74.17; H, 7.35; N, 8.60 %. IR (cm^{-1}): 3074 (w), 2832 (m), 2541 (m), 2909(m), 1644(s), 1605(s), 1578(s), 1508(m), 1441(m), 1379 (m), 1299 (s), 1177(m), 1165(m), 1045 (s), 1001(w), 830(vs), 769(w), 743(w), 609(m).

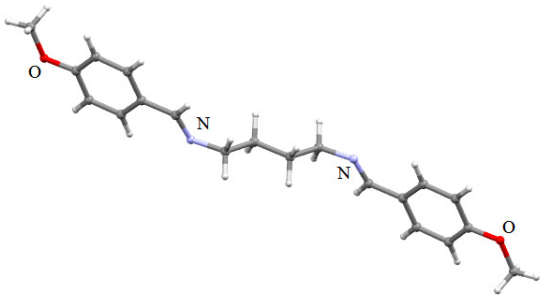

Figure 2.1: Schematic view of Schiff-base ligand [N,N′- bis (4-methyl-benzylidene)butane-1,4-diamine] (L_1)

b) Preparation of ligand 2. [N,N′- bis (4-chloro-benzylidene)butane-1,4-diamine] *(*L_2)

The solution of 4-Chlorobenzenaldehyde (10 mmol) in 40 mL methanol was under stirring and heating moderately for 15 min. 1,4-Diaminobutane (5 mmol) in 10 mL methanol was added dropwise with constant stirring.The mixture was heated around 50–60 ˚C for 2 hours and then allowed to cool overnight at room temperature.The resulting crystalline solids were collected and filtered and washed several times with methanol.The FT-IR analysis was carried out and the peak at 1646.51 cm^{-1} was assigned to C=N group. *Anal.* Calc. for $C_{18}H_{18}N_2Cl_2$ (332.9): C, 64.88; H, 5.41; N, 8.41. Found: C, 64.80; H, 5.40; N, 8.38 %. IR (cm^{-1}): 3067 (m), 2964 (m), 2939 (m), 2909(m), 2857(m), 2836(m), 1646(vs), 1592(s), 1570(m), 1483(m), 1448(w), 1403(m), 1372(m), 1335(m), 1212(w), 1185(vs), 1039(m), 1008(m), 849(vs), 775(w), 708(w), 544(s), 503(s).

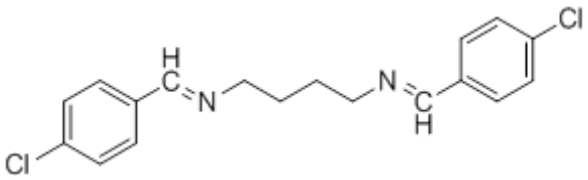

Figure 2.2: Schematic view of Schiff-base ligand [N,N′- bis (4-chloro-benzylidene)butane-1,4-diamine] *(*L_2)

2.2.3*a*. Preparation of $[Cu((\mu_{N,N'}\text{-4-MeO-ba})_2bn)Br]_n$ (5)

CuBr (3 mmol) was dissolved in 10 mL acetonitrile and L_1 (3mmol) was dissolved in 5 mL Chloroform.Method is combination of layering in test tube and slow evaporation.First at all, the acetonitrile solution was layered onto ligand solution in test tube and allowed them to diffuse slowly. After diffusion, the solution was put at room temperature to slow evaporation without any turbulence. After 2 days, the yellow crystals were formed. The FT–IR analysis was carried out and the peak at 1644 cm^{-1} was assigned to C=N which shifted to lower frequency around 1625 cm^{-1} in complex form. *Anal.* Calc. for $C_{20}H_{24}CuBrN_2O_2$ (467.45) : C,

51.34; H, 5.13; N, 6.00 %. Found: C, 51.30; H, 5.15; N, 5.97 %. IR (cm^{-1}): 3362(w), 3015(w), 2971(w), 2947(w), 2852(w), 1620 (s), 1598(s), 1461(m), 1443(m), 1420(w), 1351(m), 1303(s), 1255(m), 1171(vs), 1116(w), 1028(vs), 1014(m), 965(w), 861(vs), 831(w), 730(w), 524(s).

2.2.3*b*. Preparation of $[Cu((\mu_{N,N'}\text{-4-MeO-ba})_2bn)I]_n$ (6)

CuI (3 mmol) was dissolved in 10 mL acetonitrile and L_1 (3mmol) was dissolved in 5 mL Chloroform.The method is similar to preparation complex **(5)**. *Anal.* Calc. for $C_{20}H_{24}CuIN_2O_2$ (514.45): C, 46.65; H, 4.66; N, 5.44%. Found: C, 46.61; H, 4.62; N, 5.39 %. IR (cm^{-1}): 3067 (w), 2963(w), 1620 (m), 1601 (s), 1572 (m), 1510(s), 1458(w), 1393(m), 1309(vs), 1257(vs), 1024(vs), 1003(m), 962(w), 861(vs), 837(s), 809(w),739(w).

2.2.3*c*. Preparation of $[Cu((\mu_{N,N'}\text{-4-Cl-ba})_2bn)I]_n$ (7)

CuI (3 mmol) was dissolved in 10 mL acetonitrile and L_2 (3mmol) was dissolved in 5 mL Chloroform.The method is similar to preparation complex **(5)**. *Anal.* Calc. for $C_{18}H_{18}CuIN_2Cl_2$ (523.34): C, 47.43; H, 4.60; N, 7.37. Found: C, 46.59; H, 4.69; N, 7.19%. IR (cm^{-1}): 3055(w), 2039(w), 2907(w), 1624(s), 1585(m), 1478(s), 1454(m), 1408(w), 1354(w), 1296(w), 1169(m), 1089(s), 1008(w), 970(m), 857(vs), 835(vs), 749(w), 506(vs).

2.2.4. Lead coordination polymers

2.2.4a. Preparation lead compound $[Pb_3(CH_3COO)_2(N_3)_4]_n$ (8)

$Pb(CH_3COO)_2.3H_2O$(1mmol), and NaN_3 (2 mmol) were loaded into one arm of branched tube. Both arms were slowly filled by acetonitrile and the tube was completely sealed.The arm filled by reagents was immersed in oil bath at 68 ^{0}C while other arm was kept at room temperature.The colorless tiny crystals were formed on inside surface of cooler arm within one week in 25% base on lead. The crystals were collected and washed by acetone.Yield: *Ca*. 25% based on Pb. Elemental analysis: *Anal*. Calc. for $C_4H_6N_{12}O_4Pb_3$ (907.78) : C, 5.29 ; H, 0.66 ; N, 18.51 %. Found: C, 5.23; H, 0.65; N, 18.49 %. IR (in cm^{-1}): *v* 2019 (vs), 2001 (m), 1485 (m), 1395 (vs), 1334(s), 1147(w), 1016 (m), 935 (w), 843 (w), 683(w), 660 (s), 642 (s), 617 (s).

2.2.4b. Preparation of lead compound $[Na_2Pb_2(CH_3COO)_6]_n$ (9)

$Pb(CH_3COO)_2.3H_2O$ (1.5 mmol) and NaN_3 (1.5 mmol) were added to one arm of branched tube.The method is thermal gradient and similar to preparating method of complex **(8)**. The colorless cubic crystals were formed on inside surface of cooler arm within 2 weeks in 48 % base on lead.The crystal was filtered and washed by acetone and methanol. Yield: *Ca*. 48% based on Pb. Elemental analysis: *Anal*. Calc. for $C_{12}H_{18}O_{17}Pb_2Na_2$ (814.62): C, 17.68; H, 2.21; N, 0 %. Found: C, 17.68; H, 2.02; N, 0 %. IR (in cm^{-1}): *v* 1528 (vs), 1391 (vs), 1336 (m), 1047 (w), 1019 (m), 922 (w), 655 (m), 641 (vs), 616 (m), 482 (s), 467 (w).

2.2.4c. Preparation of lead compound $[Pb(DHBDA)]_n$ (10)

$Pb(NO_3)_2$ (1mmol) was dissolved in 7 ml deionized water. Ligand L= 2,5-Dihydroxy-1,4-benzenediacetic acid (1.25mmol) was dissolved in 7 mL ethanol.The metal ion solution was poured into a test-tube, then the ligand solution was carefully layered on it.The test-tube was perfectly sealed. After standing at room temperature for almost two weeks, the fine crystals were formed.The crystals were collected and washed by deionized water and ethanol.The yield was around 41 % based on lead. Elemental analysis: *Anal*. Calc. for $C_{10}H_8O_6Pb$ (431.35): C, 27.82; H, 1.85%. Found: C, 27.76; H, 1.94 %. IR (in cm^{-1}): *v* 3340(w), 3197 (w), 3035(w) 3016 (w), 3010 (w), 2345 (w), 2188 (w), 2069 (w), 2010 (w),1524 (s), 1498 (s), 1426 (vs), 1397 (vs), 1340 (s), 1281 (s), 1247 (s), 1221 (s), 1168 (m), 1147 (m), 946 (s), 908 (m), 886 (s), 852 (m), 775 (s), 662 (m), 572 (m), 487 (m).

Chapter 3

3. Results and disscution

3.1. Silver coordination polymer $[Ag_2(HO_3PCH_2COO)]_n$ (1)

3.1.1. Crystal structure determination

X-ray single-crystal diffraction analysis reveals that silver complex emerges as two-dimensional coordination polymer and there are two crystallographically non-equivalent silver atoms (Ag1 and Ag2) and one phosphonoacetic acid ligand in an asymmetric unit.This compound crystallizes in the triclinic system with Pī space group. The coordination sphere around the (Ag1) atom can be described as distorted tetrahedron, with four oxygen atoms (O1, O2, O3) from four individual ligands. The other silver atom (Ag2) possesses coordination number of four, formed by four coordinated oxygen atoms (O2, O3 and O5) from four different ligands, adopting distorted tetrahedron coordination sphere, (Figure 3.1 and 3.2). Crystallographic data are presented in (Table 1).In this compound, the Ag–O bonds are in range between 2.212(4) Å and 2,683(5) Å for Ag1–O and 2.364(4) Å to 2,856(5) for Ag2–O respectively which lie in normal ranges [185–193].In compound **(1)**, the argentophilic interactions between Ag1–Ag1, Ag1–Ag2 atoms are observed and the argentophilic distances are 3.0892(9) Å and 2.8733(9) Å respectively. [185–193] As matter of interest, The Ag1–Ag2 distance is slightly shorter than the Ag1–Ag1 interactions.But it is significantly less than twice the van der Waals radius for silver (3.44 Å) and therefore suggests a d^{10}–d^{10} closed shell argentophilic interaction. In comparison, the expected range for argentophilic interactions is between 2.96 Å and 3.66 Å [194–201]. In this network, the ligand behaves as bridging ligand as it coordinates to silver atoms via oxygen atoms of both carboxylate and phosphonate moieties. The carboxylate groups are coordinated to silver atoms through coordination mode (μ_4-η^2:η^2) [202–204] while the phosphonate moieties adopt coordination fashion {1M, 1M, 1H–1M} or (μ_3-η^1:η^1:η^1) to construct the framework [205–206]. It is also worth to notice that P atom has a near tetrahedral C–PO_3 coordination environment, with angles ∠O3–P–O4, ∠O3–P–O5 and ∠O4–P–O5 are 111.0°(3), 114.8°(3), 107.2°(3) and P–O bond lengths in the range 1.509(5)–1.562 (4) Å and a P–C bond length of 1.806(7) Å, respectively. Due to high bridging mode of oxygen atoms in the ligand, a two dimensional network is constructed, as illustrated with (Figure 3.2). The overall structure is best described as 2D neighboring layers

of silver complexes which are linked through O–H…O hydrogen-bonding interactions with short distances (O4…O3: 2.632 Å), to form a 3D supramolecular framework (Figure 3.3).

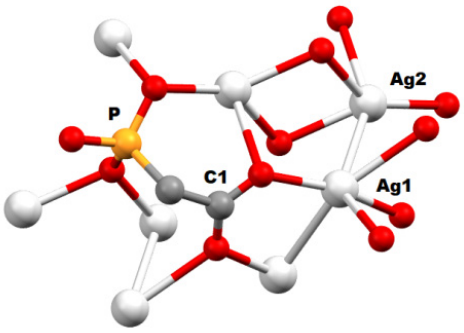

Figure 3.1: Molecular structure of silver compound

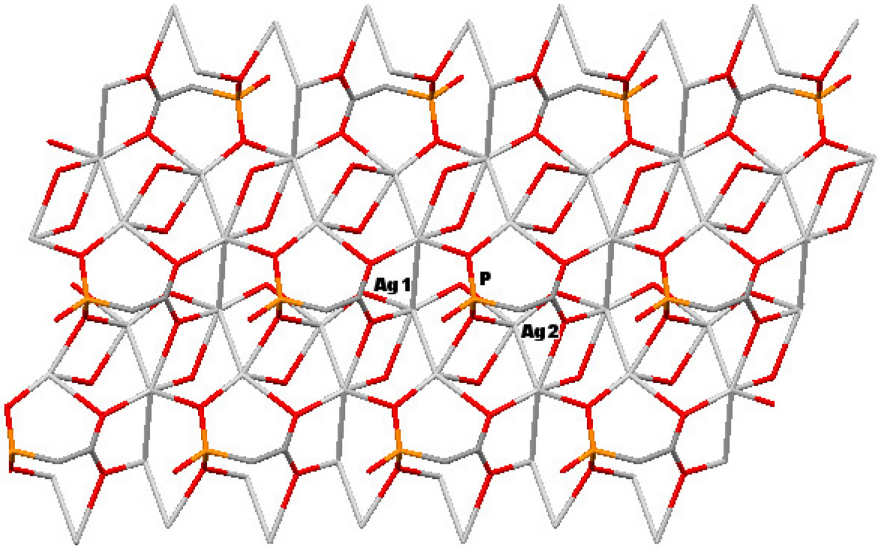

Figure 3.2: Schematic view of layered structure of compound **(1)**

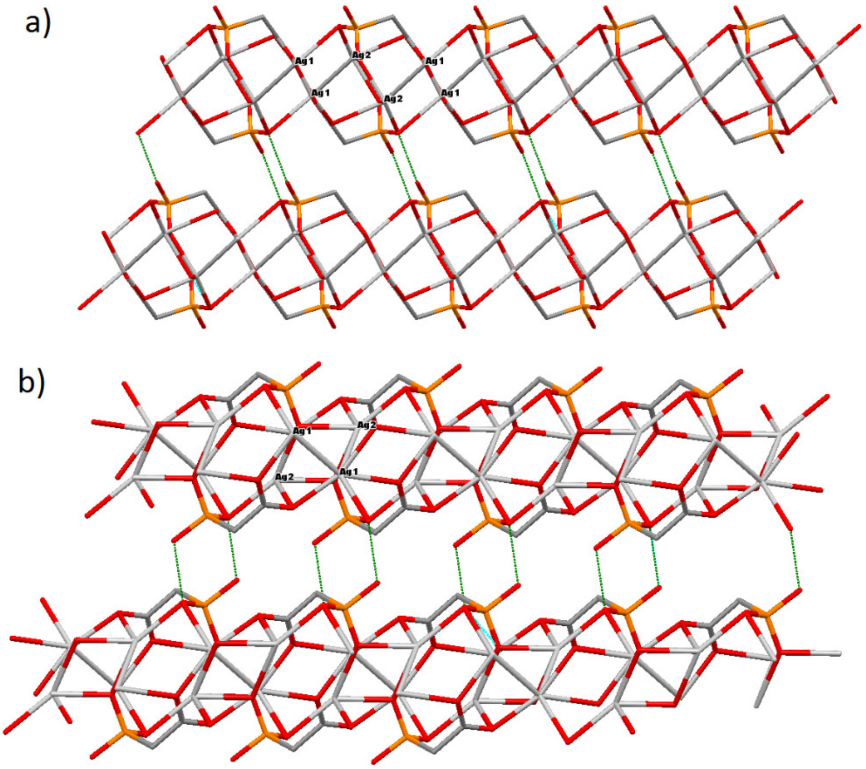

Figure 3.3: Two different view of packing arrangement in silver compound along crystallographic a) *a*-axis; b) *b*-axis; Available interchain hydrogen-bonding interactions are presented as green dotted lines between layers

To conclude, a new silver coordination polymer with phosphonoacetic has been synthesized via slow diffusion method in mixture of water and ethanol as solvents. Actually some coordination polymers of transition metals have been reported, in which phosphonoacetic acid has been utilized in combination with co-ligands [207–210]. A new silver coordination polymer exhibits very unique structure without any coordinated or guest solvent molecules, hence it has very robust and interesting polymeric structure.

Table 3.1: Crystal data and refinement details for the X-ray structure determinations of the silver compound **(1)**

	Silver compound **(1)**
Empirical formula	$C_2H_3Ag_2O_5P$
crystal system	triclinic
Space group	$P\bar{1}$
Formula weight /g.mol^{-1}	353.75
a/ Å	5.8730(10)
b/ Å	6.7370(10)
c/ Å	8.7310(10)
α/°	102.425(7)
β/°	98.813(6)
γ/°	115.395(6)
Cell volume/ Å^3	292.73(7)
Formulas in unit cell	2
Density (calcd.) / Mg·cm^{-3}	4.013
Wavelength / Å	0.71073
Absorption coefficient /mm^{-1}	6.912
Numerical absorption correction	min./max.Transmittance 0.22476/0.76058
Temperature/ K	293(2)
Crystal size/mm	0.04*0.24*0.34
F (000)	328
Θ range / °	3.53–25.00
Limiting indices	$-6 \le h \le 6$ $-7 \le k \le 7$ $-10 \le l \le 10$
Reflection collected	2006
Independent reflections	1003 (R_{int} = 0.0190)
Refinement method	Full–matrix least–squares on $\|F\|^2$
Goodness–of–fit on $\|F\|^2$	1.388
R indices (all data)	R1= 0.0308 , wR2 = 0.0764
Largest diff. Peak and hole	0.912 and –1.011 eÅ^{-3}

Table 3.2: Selected bonds and angles of silver compound **(1)**

Bond length (Å)			
Ag(1)–Ag(2)	3.0892(9)	Ag(2)–O(1)#1	2.913(5)
Ag(1)–O(2)	2.212(4)	Ag(2)–O(5)#4	2.364(4)
Ag(1)–Ag(1)#2	2.8733(11)	Ag(2)–O(2)#5	2.689(5)
Ag(1)–O(1)#2	2.568(4)	P–C(2)	1.806(7)
Ag(1)–O(1)#1	2.249(4)	P–O(3)	1.518(6)
Ag(1)–O(3)#3	2.683(4)	P–O(4)	1.562(4)
Ag(1)–O(5)#4	2.896(4)	P–O(5)	1.510(5)
Ag(1)–O(2)#2	2.568(4)	O(3)–Ag(1)#6	2.683(4)
Ag(1)–Ag(1)#1	2.8733(11)	O(1)–Ag(2)#1	2.913(5)
Ag(2)–O(3)#5	2.307(4)	O(3)–Ag(2)#5	2.30 (4)
Ag(2)–O(3)#2	2.406(4)	O(5)–Ag(2)#4	2.364(4)
Ag(2)–O(1)#2	2.856(5)	O(5)–Ag(1)#4	2.896(4)
Ag(2)–O(4)#4	3.019(5)	O(5)–Ag(2)#7	2.406(4)
P–Ag(2)#5	3.227(3)	P–Ag(1)#6	3.441(2)

Angles (°)			
O(2)–Ag(1)–O(1)#1	161.6(2)	O(5)–P–O(3)	114.5(2)
O(1)#1–Ag(1)–O(1)#2	71.1(2)	O(2)–Ag(1)–Ag(2)	114.92(12)
O(1)#1–Ag(1)–O(3)#3	99.8(2)	O(3)–P–O(4)	111.0(2)
O(2)–Ag(1)–Ag(1)#1	82.62(11)	O(5)–P–Ag(2)#5	88.6(2)
O(2)#2–Ag(1)–Ag(1)#1	151.54(10)	O(3)–Ag(2)–O(5)	142.5(2)
O(2)–Ag(1)–O(5)#4	82.0(14)	P–O(3)–Ag(2)#5	106.7(2)
Ag(1)#1–Ag(1)–O(5)#4	70.77(9)	P–O(3)–Ag(2)#5	113.4(2)
O(1)#1–Ag(1)–Ag(2)	63.89(12)	P–O(5)–Ag(2)#4	113.5(3)
O(3)#3–Ag(1)–Ag(2)	142.35(9)		
O(3)#5–Ag(2)–O(5)#4	137.6(2)		
O(5)#4–Ag(2)–O(5)#2	78.4(2)		
O(5)#4–Ag(2)–Ag(1)	62.48(11)		
O(2)–Ag(1)–O(1)#2	125.40(14)		
O(2)–Ag(1)–O(3)#3	91.0(2)		
Ag(1)#7–O(1)–Ag(2)#7	69.20(11)		

#1 -x , -y , -z #2 x +1 , y , z #3 x +1 , y +1 , z #4 -x -1, -y -1, -z

#5 -x , -y -1, -z #6 x -1 , y -1 , z #7 x -1 , y , z

3.1.2. IR Spectra of compound (1)

A parallel study of the IR spectra of silver compounds gives some interesting information regarding the binding sites of phosphonoacetic acid ligand. The absence of strong IR bands around 1730 cm^{-1} in the spectra of silver compound implies that the carboxylic group is fully deprotonated [211–212]. The Δ values, defined by Deacon and Phillips for asymmetric and symmetric stretching vibrations of carboxylate, relieves some qualitative information which correlate the data of the infrared spectra with the coordination modes of metal carboxylates. The Δ value (ca. 112 cm^{-1}) is compatible with the presence of bridging carboxylate. For non-bridging carboxylate coordination, this Δ separation is usually greater than (ca. 350 cm^{-1}) [213–214].Deacon and Phillips have vastly investigated the FT-IR spectra of many metal carboxylate complexes with known crystal structure and they have finally come to a conclusion for the correlations between carboxylate stretching frequencies and their coordination sphere [213]. In the IR spectra of compound **(1)**, two strong bands exist at 1522 cm^{-1} and 1410 cm^{-1} which are attributed to asymmetric and symmetric stretching vibrations of a bridging acetate functionality of the phosphonoacetate ligand, respectively. The difference of 112 cm^{-1} between the asymmetric and symmetric stretching vibrations is ascribed to the syn–anti tetradentate bridging mode (μ_4-η^2:η^2) of the acetate group. In principle, the order of Δ (Δ = $\upsilon_{as(COO-)}$–$\upsilon_{s(COO-)}$) for divalent metal carboxylates is followed by Δ (bridging) < Δ (monodentate) [213–220]. The lower values of Δ (for example Δ = 112) compared to higher values strongly imply the presence of syn–anti bidentate bridging or chelating in comparison to the monodentate terminal coordination .

On the other hand, there is no peak found between 3641 cm^{-1} and 3349 cm^{-1}, which normally are assigned to υ_{O-H} of water molecules that are involved in hydrogen bonds. Hence the absence of such peaks indicates the absence of water molecules. Furthermore, the sharp peaks in the 953–1178 cm^{-1} region can be ascribed to the P–O and P=O stretching vibrations of phosphonate moieties.

3.1.3. Thermal analysis of compound (1)

The framework stability and thermal decomposition behavior of silver compound were studied by thermal gravimetric analysis (TGA) and differential scanning calorimetric (DSC) techniques under the air atmosphere in the temperature range between 25 and 800 °C.The TG/DSC curves are depicted in (Figure 3.4) and the decomposition of the organic material occurs only in two steps. The TGA curve exhibits that this compound has very high stability and it is stable upon to ca. 260 °C. The main mass loss of 12.17 % onsets at 260 °C and is completed at 300 °C, with an exothermic DSC peak at 289.1 °C.This mass loss stage can be ascribed to partial decomposition of ligand.The silver compound undergoes a second mass loss of 4.16% between 750 and 800 °C.The total mass loss of 16.33% is in agreement with the theoretical values of 15.56%.For this compound, thermal decomposition product with percentage 83.67% can be assigned to $Ag_4P_2O_7$ compound which corresponds well to calculated value 84.7%.

The new silver compound shows very high stability against the temperature rising.This material underwent the total mass loss (16.33%) by heating up around 800 °which indicates the higher thermal stability of new compound.

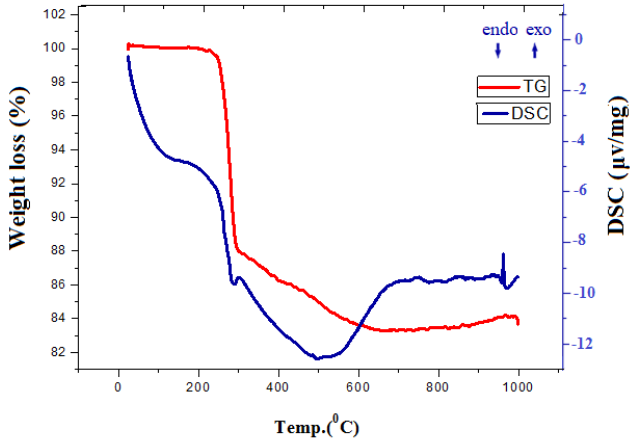

Figure 3.4: Thermal analysis curves of compound $[Ag_2(HO_3PCH_2COO)]_n$ along with Differential Scanning Calorimetric (DSC), recorded at various representative temperatures

3.2. Lanthanide coordination polymers

3.2.1. Crystal structure determination of Neodymium (2) and Samarium coordination polymers (3)

Neodymium and samarium coordination polymer were synthesized by reaction between 2,5-furan-dicarboxylic acid (H_2FDA = 2,5-furandicarboxylic acid) and samarium and neodymium nitrate in DMF as solvent.The X-ray structural analysis relieves that neodymium compound $\{[Nd_2(FDA)_3(DMF)(H_2O)_2]\cdot DMF\cdot(H_2O)_2\}_n$ and samarium compound $\{[Sm_2(FDA)_3(DMF)(H_2O)_2]\cdot DMF\cdot(H_2O)_2\}_n$ are iso-structural and feature as three-dimensional coordination polymer and crystallize in the space group $P2_1/n$.Crystallographic data and structural refinements for both compounds are listed in (Table 3.3). Since both structures of neodymium and samarium coordination compounds are identical, neodymium coordination polymer is described in detail. In compound **(2)**, each asymmetric unit contains of two crystallographically independent Nd(III) (Nd1, Nd2) ions, three FDA^{2-} ligands, three coordinated and two non-coordinated water molecules and one coordinated and one non-coordinated DMF molecules which is shown in (Figure 3.5). Nd1 ion is nine-coordinated and surrounded by six carboxylate oxygen atoms from four individual FDA^{2-} ligands and two oxygen atoms from two coordinated water molecules (O1W and O3W) and one oxygen atom from DMF molecule (O17) which adopts monocapped square antiprismatic coordination sphere with O−Nd1−O bond angles ranging from 47.8 to 154.9° in which the oxygen atoms of (O1W, O3W, O7 and O14) and (O1, O2 , O6, O7) define upper and lower tetragonal caps while the (O17) atom occupied an axial position. Nd2 ion is also nine-coordinated and the coordination environment around each Nd2 ion are eight carboxylate oxygen atoms of five individual FDA^{2-} ligands and one oxygen atom from coordinated water molecule (O2W). Therefore, each Nd2 ion exhibits the coordination environment of slightly distorted monocapped square antiprism with O−Nd2−O bond angles ranging from 49.8 to 158.3° in which an axial position is occupied by oxygen atoms (O12), although the upper and lower tetragonal caps are assigned by oxygen atoms (O4, O9W, O9) and (O3, O8 , O11, O13) respectively. Selected bond lengths and angles of compound **(2)** are given in (Table 3.4).

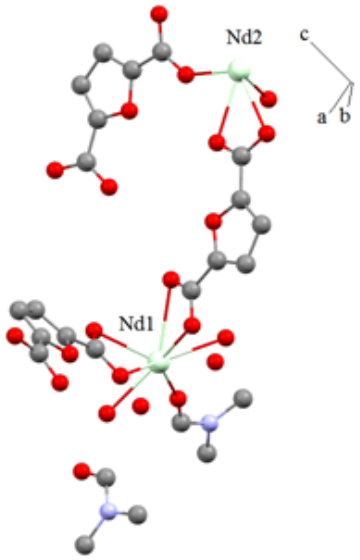

Figure 3.5 : Asymmetric unit of neodymium coordination polymer.

The two neighboring Nd1 ions are connected through the bridging behavior of oxygen atoms (O7) to generate the dinuclear unit. Furthermore there is the same for both Nd2 ions as dinuclear unit. By far, the oxygen atoms (O4) are bridging between adjacent Nd2 centres to compose a dinuclear unit (Figure 3.7). Moreover, the adjacent dinuclear units of Nd1 and Nd2 are further linked through bridging behavior of carboxylic oxygen atoms of two FDA^{2-}ligands by using coordination mode $(\kappa^2\text{-}\mu_2)\text{-}(\kappa^2)\text{-}\mu_3$ (O14, O12, O7, O8 and O9), resulting two-dimensional layer illustrated in (Figure 3.6).Then the neighboring sheets are pillared through bridging by whole FDA^{2-} ligands in μ_4-bridge mode to form three-dimensional frameworks, (Figure 3.8 and 3.9). Obviously, FDA^{2-}ligands also act as pillar of adjacent layers and coordinate to Nd(III) ions in two types coordination modes [221−223], (I) bis-bidentate chelating-bridging $(\kappa^1\text{-}\kappa^1)\text{-}(\kappa^1\text{-}\kappa^1)\text{-}\mu_4$ and (II) ligand acts as pentadentate donor $(\kappa^2\text{-}\mu_2)\text{-}(\kappa^2)\text{-}\mu_3$ which is illustrated with (Figure 3.6).

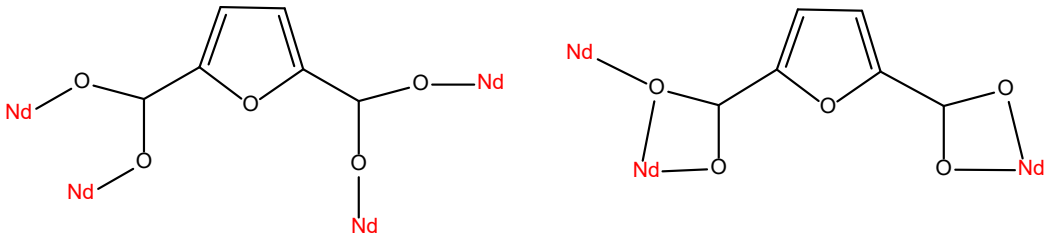

(I) (II)

Figure 3.6: Different coordination modes of ligand (2,5-Furandicarboxylic acid) in compounds **(2)** and **(3)**

The Nd1–O and Nd2–O bond lengths vary from of 2.293(4) to 2.820(3) Å and 2.391(3) to 2.685(4) Å respectively, comparable to the usual Nd–$O_{carboxylate}$ bond lengths reported in previous works [224–228]. It is worth to note that Nd1–O7 bond distance 2.820(3) Å is considerably longer than that of Nd1–O2 2.531(4) Å,which is common for a tridentate carboxylate coordination [227]. Moreover, the angles formed at the metal atom by the chelate rings are quite small [O1–Nd1–O2, 50.85(1)°; O7–Nd1–O6, 47.8(1)°], leading to a distorted polyhedron around the neodymium ions.

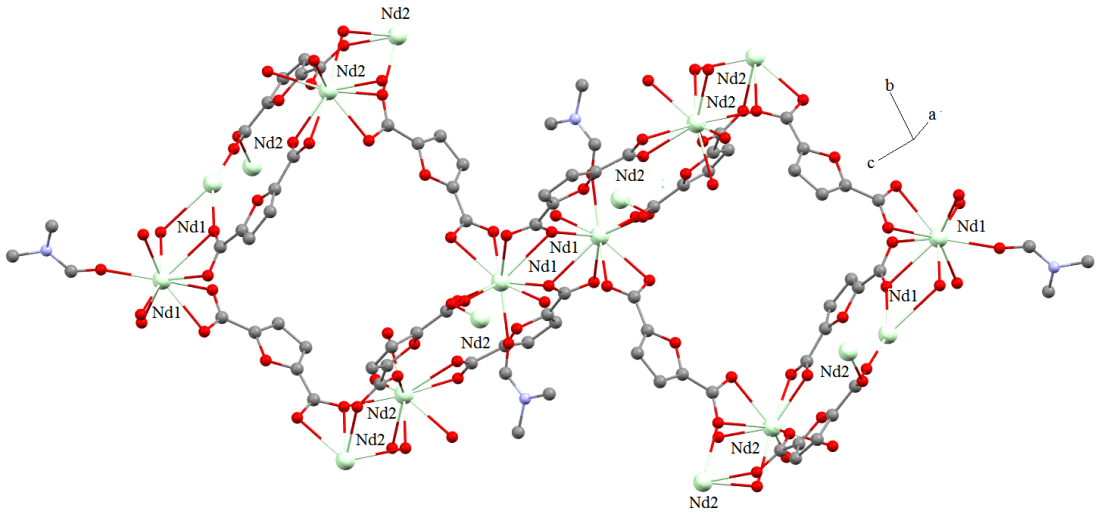

Figure 3.7: Extension of dimetallic units of Nd(III) by ligand (2,5-Furandicarboxylic acid)

Table 3.3: Crystal data and refinement details for the X-ray structure determinations of the neodymium **(2)** and samarium **(3)** compounds respectively.

	Neodymium	**Samarium**
Empirical formula	$C_{24}H_{30}N_2Nd_2O_{22}$	$C_{24}H_{30}N_2Sm_2O_{22}$
crystal system	monoclinic	monoclinic
Space group	P 2_1/n	P 2_1/n
Formula weight /g.mol^{-1}	986.98	999.20
a/ Å	10.3810(10)	10.333(10)
b/ Å	21.112(2)	21.051(2)
c/ Å	15.7160(10)	15.6280(10)
α/°	90	90
β/°	93.800(7)	93.844(8)
γ/°	90	90
Cell volume/ Å^3	3436.8(5)	3391.8(5)
Formulas in unit cell	4	4
Density (calcd.) / Mg·cm^{-3}	1.907	1.957
Wavelength / Å	0,71073	0.71073
Absorption coefficient /mm^{-1}	3.078	3.520
Numerical absorption	min./max.Transmittance	min./max.Transmittance
correction	0.35323/0.77591	0.573/0.864
Temperature/ K	293(2)	293(2)
Crystal size/mm	0.10*0.45*0.65	0.04*0.24*0.40
F (000)	1936	1952
Θ range / °	2.60 – 25.00	2.61 – 25.00
Limiting indices	$-1 \le h \le 12$	$-1 \le h \le 12$
	$-1 \le k \le 25$	$-1 \le k \le 25$
	$-18 \le l \le 18$	$-18 \le l \le 18$
Reflection collected	6967	6497
Independent reflection	5686 (R_{int} = 0.0214)	5279 (R_{int} = 0.0298)
Refinement method	Full–matrix least–squares on $\|F\|^2$	Full–matrix least–squares on $\|F\|^2$
Goodness–of–fit on $\|F\|^2$	1.233	1.233
R indices (all data)	R1= 0.0371, wR2 = 0.0816	R1= 0.0553, wR2 = 0.0730
Largest diff. Peak and hole	1.658 and –0.713 eÅ^{-3}	1.000 and –1.005 eÅ^{-3}

Table 3.4 : Selecetd bonds and angles of neodymium compound **(2)**.

Bond length (Å)			
Nd(1)–OW(1)	2.451(4)	Nd(2)–O(13)#2	2.391(3)
Nd(1)–OW(3)	2.491(4)	Nd(2)–O(11)#3	2.431(3)
Nd(1)–O(1)	2.603(3)	Nd(2)–O(4)#5	2.685(4)
Nd(1)–O(2)	2.531(4)	Nd(2)–O(3)#5	2.557(4)
Nd(1)–O(6)	2.568(4)	Nd(2)–O(12)	2.428(4)
Nd(1)–O(7)	2.820(3)	Nd(2)–O(9)	2.513(4)
Nd(1)–O(17)	2.436(4)	Nd(2)–O(8)	2.652(3)
Nd(1)–O(14)#1	2.293(4)	Nd(2)–OW(2)	2.471(4)
Nd(2) –OW2	2.471(4)		

Angles (°)			
O(14)#1–Nd(1)–O(7)#1	154.9(2)	OW1–Nd(1)–O(6)	137.82(12)
O(7)#1–Nd(1)–O(17)	77.0(2)	O(2)–Nd(1)–O(6)	84.92(13)
O(7)#1–Nd(1)–OW1	95.47(13)	O(2)–Nd(1)–O(1)	50.85(11)
O(14)#1–Nd(1)–OW3	81.1(2)	O(6)–Nd(1)–O(7)	47.81(10)
O(17)–Nd(1)–OW3	70.69(14)	O(6)–Nd(2)–O(6)	68.70(12)
O(13)#2–Nd(2)–O(8)	80.43(12)	O(17)–Nd(1)–O(1)	137.96(14)
O(17)–Nd(1)–OW1	73.50(14)	O(12)–Nd(2)–OW2	72.19(14)
O(7)#1–Nd(1)–OW3	81.95(12)	OW3–Nd(1)–O(6)	72.51(13)
OW1–Nd(1)–O(2)	75.16(14)	O(6)–Nd(1)–O(1)	68.70(12)
OW2–Nd(2)–O(9)	73.56(13)	OW3–Nd(1)–O(7)	67.58(12)
O(8)–Nd(2)–Nd(2)#3	153.63(8)	O(12)–Nd(2)–O(9)	73.01(12)
Nd(1)#1–O(7)–Nd(1)	112.65(12)	O(2)–Nd(1)–O(7)	94.31(10)
OW2–Nd(2)–O(3)#5	144.80(13)	O(17)–Nd(1)–O2	135.4(2)

#1 -x , -y, -z + 2 #2 x -1 , y, z #3 -x -1/2 , -y ,-z +3 #4 -x -1/2 , y- 1/2 ,-z +5/2 #5 x -1/2 , -y +1/2 , z +1/2

#6 x +1/2 , -y +1/2 , z -1/2 #7 -x -1/2 , y +1/2 , -z +5/2 #8 x +1 ,y ,z

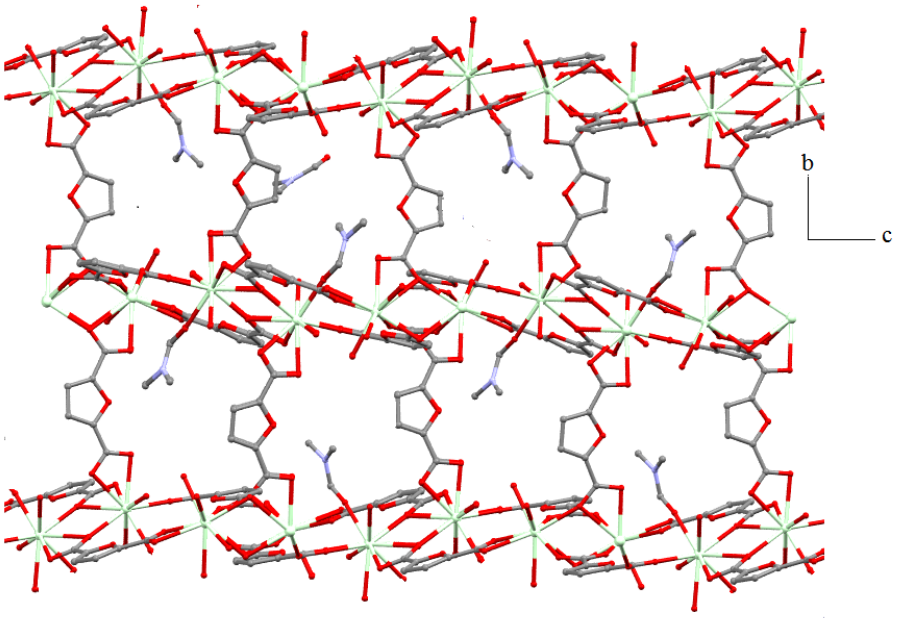

Figure 3.8 : Representation of 3D framework with pillaring ligand, when viewed along *c*-axis

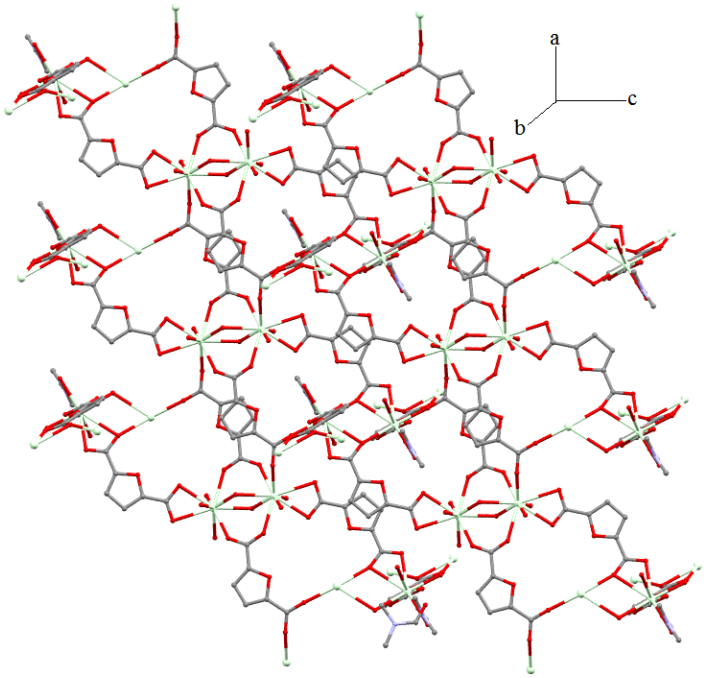

Figure 3.9: Packing arrangement of neodymium coordination polymer *a*-axis and *c*-axi

3.2.2. IR spectra of compounds (2) and (3)

FT-IR spectra of neodymium and samarium compounds were recorded in the range 400−4000 cm^{-1}. As expected, The IR spectra of both lanthanide compounds are quite similar and in good agreement with the X-ray diffraction structural analysis results. Meanwhile, in a typical spectrum of neodymium complex, the peak around 3100–3500 cm^{-1} is attributed to the characteristic peak of O—H stretching vibration of water molecules which involves both coordinated and guest water molecules (ν_{O-H}). The sharp peak appears in region 1651–1548 cm^{-1} and 1438–1366 cm^{-1} are contributed to asymmetric and symmetric stretching vibrations of carboxylic groups [213, 224–228] which indicates that the carboxylate groups expose in different coordination modes. Furthermore, the absence of strong peak in the range 1685–1740 cm^{-1} indicates that the ligands are fully deprotonated in polymeric network [227].The FT-IR of C═O peak of coordinated DMF molecules is shown at 1638 cm^{-1}, the stretching vibration of C—N bonds is at 1104 cm^{-1}.

3.2.3. Thermal analysis of compounds (2) and (3)

The Thermogravimetric (TG) and the Differential Scanning Calorimetric (DSC) curves of neodymium and samarium coordination polymers were investigated to estimate stability and pathway of thermal decomposition in temperature range from 25 to 1000 ^0C under flowing of

air atmosphere with a heating rate of 10 °C cm^{-1}, which is shown in (Figure 3.10 and 3.11). The TG and DSC curves of both compounds reveal approximately similar thermal stability and behaviors. In neodymium compound, the mass loss in the temperature range between 25 and 800 °C, occurring in one dehydration stage and four overlapped decomposition steps leading to final residue Nd_2O_3.The TG curve exposed a gradual mass loss of 7.03% from room temperature to 130 °C, accompanied by an exothermic DSC peak at 114.4 °C, can be attributed to the removal of two guest water molecules and two coordinated water molecules. Second step is an offset of decomposition of molecular skeleton, hence the decomposing of the water free coordination polymer of formula $Nd_2(L)_3.2DMF$ takes place in temperature range between 130–650 °C, including four overlapping decomposition stages with two endothermic and one exothermic peaks. Final product is assigned to Nd_2O_3 which is found 34.88%, agreed with calculated value 34.09%.

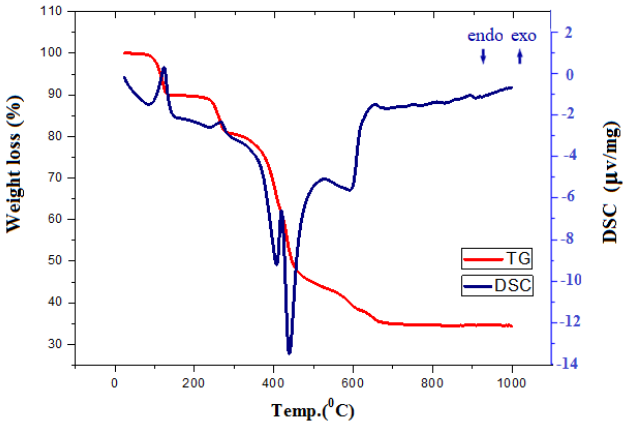

Figure 3.10: Thermal analysis curves of neodymium coordination polymer **(2)** along with Differential Scanning Calorimetric (DSC), recorded at various representative temperatures

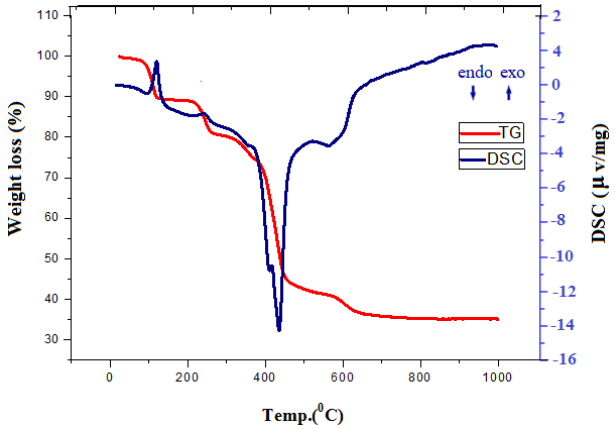

Figure 3.11: Thermal analysis curves samarium compound **(3)** along with Differential Scanning Calorimetric (DSC), recorded at various representative temperatures

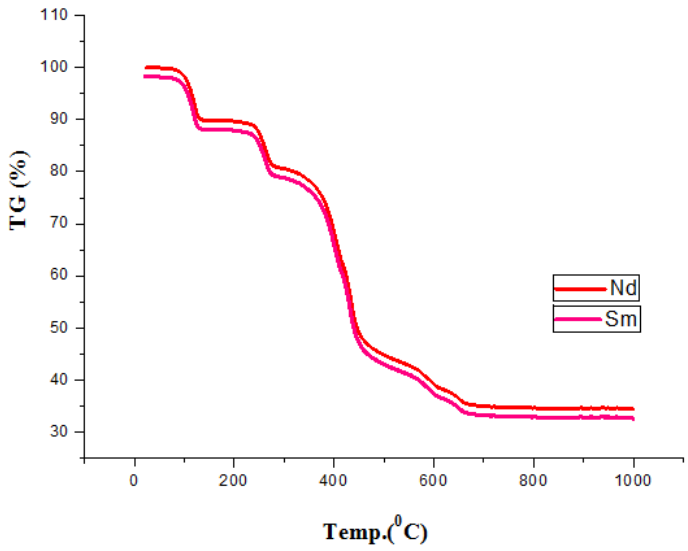

Figure 3.12: Thermal analysis curves of neodymium **(2)** and samarium **(3)** compounds

3.2.4. Crystal structure determination of cerium coordination polymer $[Ce(pdc)(DMF)_2(NO_3)]_n$ (4)

Cerium coordination polymer has been synthesized by reaction between 3,5-pyrazole-dicarboxylic acid (H_2pdc = 3,5-pyrazoledicarboxylic acid) and cerium nitrate in DMF as solvent. The X–ray crystallographic analysis reveals that cerium coordination polymer displays 2D polymeric structure, and it crystallizes in the orthorhombic system with *Pna2₁* space group {**a**= 10.308(2), **b**= 19.023 (2), **c**= 8.990 (1) Å; **α**= **γ**= **β**= 90° }.In a structure of compound **(4)**, an asymmetric unit comprises one crystallographically independent cerium ion, one completely deprotonated pdc^{2-} ligand, two coordinated DMF molecules and one coordinated nitrate anion.Ce(III) ion is nine-coordinated, exposing slightly distorted monocapped square antiprismatic coordination sphere with O–Ce–O angles vary from 71.4 to 142.6° in which an oxygen atom of DMF molecule (O9) occupies an axial position along *b*-axis while three carboxyl oxygen atoms (O1, O3, O4) as well as DMF oxygen atom (O8) lie in the upper tetragonal caps and also one carboxyl oxygen atom (O2), two oxygen atoms from nitrate anions (O5 , O6) and one nitrogen atom of pdc^{2-} ligand (N1) are attributed lower tetragonal caps respectively.The Ce–N bond length is 2.671 (6) Å while the Ce–O bond lengths range from 2.464 (6) Å to 2.612(6) Å.These distances are comparable to the usual Ce–$O_{carboxylate}$ bond lengths reported in previous works [231–234]. As it is observed in (Figure 3.14), in compound **(4)**, each pdc^{2-} ligand acts as heteroatomic chelating ligand and adopts a μ_5-η^2N,O, η^1,O′, η^1O″, η^1O‴ coordination mode to link four Ce(III) ions [235].Furthermore, the nitrate anion acts as chelating ligand and linked to Ce(III) ions through both oxygen atoms

(O5 and O6), occupying an axial position along *b*-axis. Moreover, both DMF molecules act as mondentate ligand and also are coordinated to Ce(III) ion through their oxygen atoms (O9 , O8), lying on *b*-axis position, however they show *trans* configuration to nitrate anions around metal ion.Also, it is worth mentioning that each nitrate anion is located on trans position to DMF moieties of adjacent complex in polymeric network (Figure 3.13).

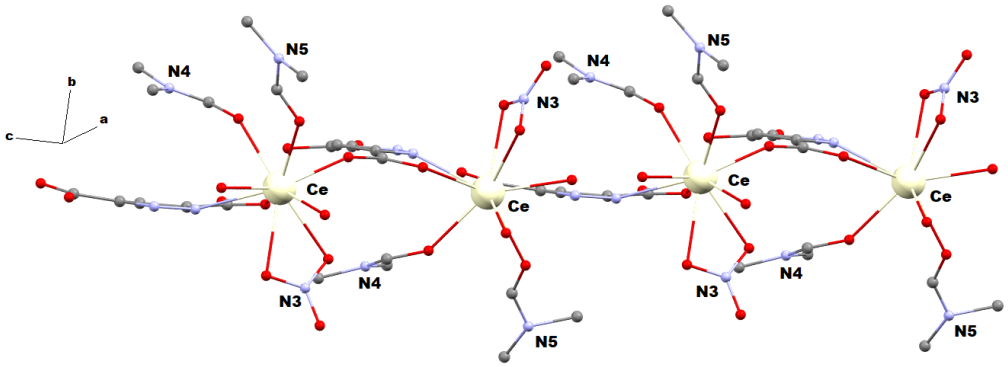

Figure 3.13: The coordination environment around cerium ions

As it is observed in (Figure 3.14), each pdc^{2-} ligand is coordinated to four Ce(III) atoms through four carboxylate oxygen atoms (O1, O2, O3 and O4) and one nitrogen atom Ce–N and also two neighboring Ce(III) ions are further linked to each other by chelating carboxylate oxygen atoms in fashions Ce–(O1)–(C1)–(O2)–Ce and Ce–(O3)–(C5)–(O4)–Ce, constructing rather square tetranuclear unit in which each Ce(III) atom is placed on corner. Interestingly, in each unit, the pdc^{2-} ligand is coordinated to metal atoms in different direction in comparison with adjacent units. For example, the pdc^{2-} ligand is coordinated to metal ions along *a*-axis direction while this ligand is bridged to metal atoms in *c*-axis direction in neighboring units. Finally, adjacent units are extended in two dimensions by edge sharing, generating a layer framework, as depicted in (Figure 3.14 and 3.15).

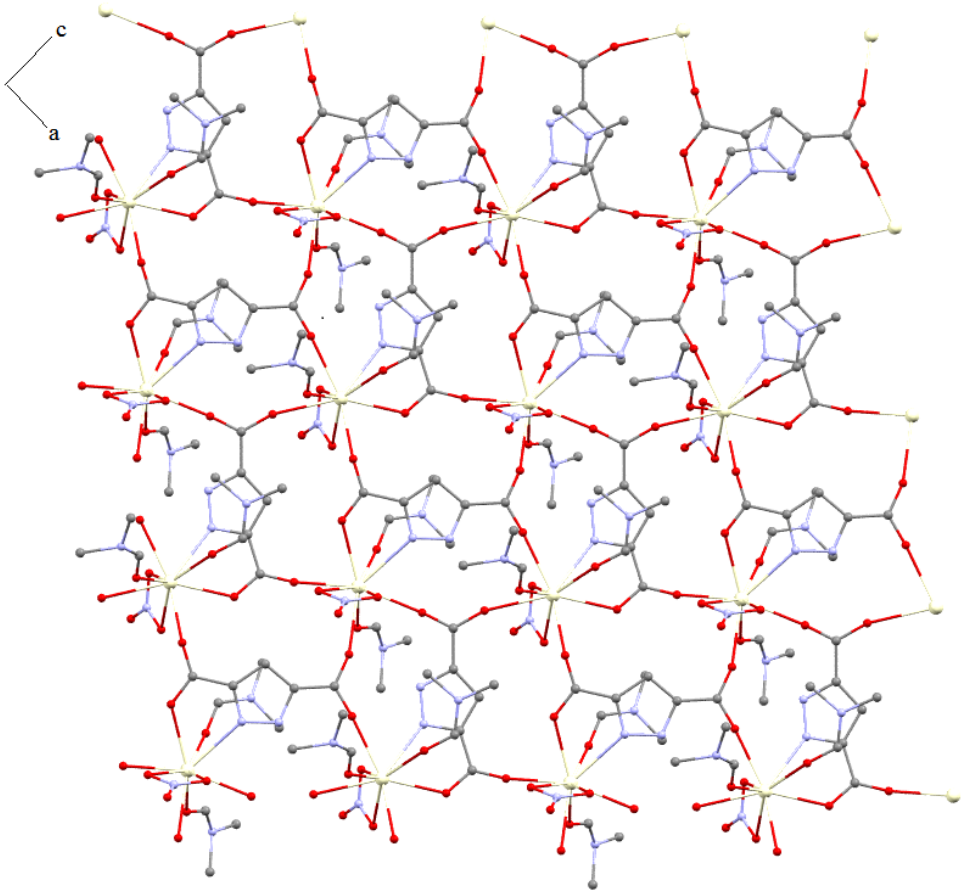

Figure 3.14 : The view of 2D cerium coordination polymer from *b*-axis

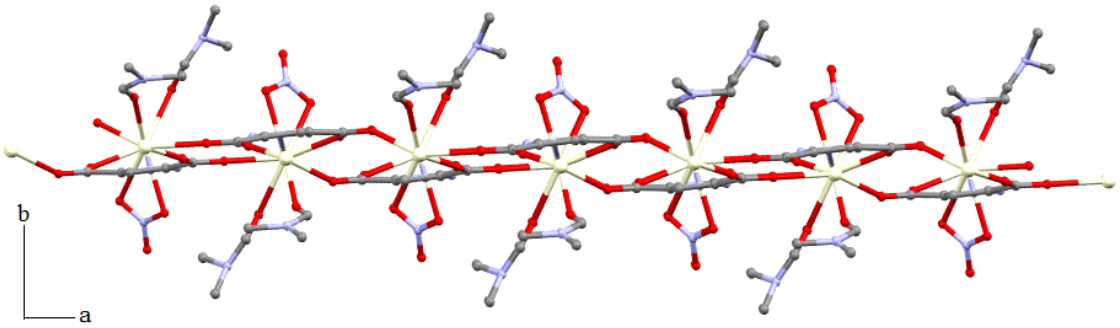

Figure 3.15 : The view of 2D cerium coordination polymer from *c*-axis

Table 3.5: Crystal data and refinement details for the X-ray structure determinations of the cerium compound **(4)**

Empirical formula	$C_{11}H_{16}CeN_5O_9$
crystal system	orthrombic
Space group	$Pna2_1$
Formula weight /g.mol^{-1}	502.41
a/ Å	10.308(2)
b/ Å	19.023(2)
c/ Å	8.9900 (10)
α/°	90
β/°	90
γ/°	90
Cell volume/ Å^3	1762.8 (4)
Formulas in unit cell	4
Density (calcd.) / Mg·cm^{-3}	1.893
Wavelength / Å	0.71073
Absorption coefficient /mm^{-1}	2.638
Numerical absorption	min./max.Transmittance
correction	0.75153/0.96853
Temperature/ K	293(2)
Crystal size/mm	0.08*0.18*0.24
F (000)	988
Θ range / °	2.51 – 24.99
Limiting indices	$-12 \le h \le 12$
	$-22 \le k \le 22$
	$-10 \le l \le 10$
Reflection collected	3055
Independent reflection	2864 (R_{int} = 0.0242)
Refinement method	Full–matrix least–squares on $\|F\|^2$
Goodness–of–fit on $\|F\|^2$	1.224
R indices (all data)	R1= 0.0521 , wR2 = 0.0715
Largest diff. Peak and hole	0.386 and –0.405 eÅ^{-3}

Table 3.6 : Selected bond lenghts and angles of compound **(4)**.

Bond length (Å)			
Ce–O(1)#1	2.417(5)	Ce–N(1)	2.672(6)
Ce–O(2)	2.527(5)	O(3)–Ce#5	2.468(5)
Ce–O(3)#2	2.468(5)	O(4)–Ce#6	2.520(5)
Ce–O(4)#3	2.520(5)	Ce–N(1)	3.013(8)
Ce–O(5)	2.612(6)	O(1)–Ce#4	1.417(5)
Ce–O(6)	2.595(6)		
Ce–O(8)	2.464(6)		
Ce–O(9)	2.540(7)		

Angles (°)			
O(2)–Ce–N(1)	59.8(2)	O(3)#2–Ce–N(1)	66.5(2)
O(4)#3–Ce–O(6)	70.2(2)	O(6)–Ce–N(1)	103.7(2)
O(9)–Ce–O(6)	129.5(2)	O(6)–Ce–N(3)	24.2(8)
O(8)–Ce–O(5)	140.7(2)	N(1)–Ce–N(3)	89.9(8)
O(4)#3–Ce–O(5)	70.1(2)	O(2)–Ce–N(3)	81.3(7)
O(1)#1–Ce–O(2)	78.7(2)	O(1)#1–Ce–O(3)#2	150.6(2)
O(3)#2–Ce–O(2)	126.3(2)	O(1)#1–Ce–O(4)#3	90.6(2)
O(1)#1–Ce–O(8)	88.5(2)	O(3)#2–Ce–O(4)#3	77.5(2)
O(8)–Ce–O(3)#2	83.3(2)	O(8)–Ce–O(2)	77.6(2)
O(8)–Ce–O(4)#3	138.4(2)	O(4)#3–Ce–O(2)	142.6(2)
O(1)#1–Ce–O(9)	77.2(2)	O(1)#1–Ce–O(6)	75.0(2)
O(3)#2–Ce–O(9)	73.4(2)	O(2)–Ce–O(6)	72.4(2)
O(6)–Ce–N(1)	103.7(2)	O(3)#2–Ce–O(5)	78.2(2)
O(1)#1–Ce–N(3)	100.2(2)	O(2)–Ce–O(5)	85.9(2)
O(9)–Ce–N(1)	125,4(2)	O(6)–Ce–O(5)	48.3(2)
O(5)–Ce–N(1)	71.4(2)	O(8)–Ce–N(3)	69.4(2)
O(8)–Ce–N(3)	155.9(2)	O(4)#3–Ce–N(1)	131.4(2)
O(9)–Ce–N(3)	133.5(2)	N(2)–N(1)–Ce	132.1(4)
O(5)–Ce–N(3)	24.5(2)	O(6)–N(3)–Ce	58.8(5)
O(4)#3–Ce–N(3)	64.9(2)	N(3)–O(5)–Ce	95.9(5)
N(3)–O(6)–Ce	97.0(6)	O(7)–N(3)–Ce	167.3(8)

#1 -x +1, -y +1, z- 1/2	#2 -x , -y +1, z- 1/2	#3 x , y , z- 1
#4 -x +1, -y +1, z+ 1/2	#5 –x , -y +1, z+ 1/2	#3 x , y , z+ 1

3.2.5. IR analysis of compound (4)

The IR spectra of cerium compound emerges the absence of free carboxylate groups by characteristic of no peak and absorption around 1700 cm^{-1} [211–212].The strong absorptions peaks in region 1674–1556 cm^{-1} and 1489–1444 cm^{-1} are assigned to anti-symmetric and symmetrical stretching vibrations of the coordinated carboxylate groups, respectively.The

difference between the anti-symmetric and symmetric carboxylate groups stretchings, Δ (Δ=$\upsilon_{as}-\upsilon_{s}$), clarifies that the carboxylate groups in Ce (III) compound are coordinated as bridging multidentate ligand [213].These observations are in accordance with the X-ray diffraction structural analysis. Moreover, the weak $\upsilon(NO_3^-)$ out-of-plane bending vibration is observed at 853−770 cm^{-1}[236–237].

3.2.6. Thermal analysis of compound (4)

In order to investigate the thermal stability of cerium coordination polymer**,** thermal gravimetric analyses and Differential Scanning Calorimetric (DSC) were carried out by heating range from 25 to 1000 °C under air atmosphere with a heating rate of 10 °C/min, as shown in (Figure 3.16).The TGA curve presents three stages of decompositions, accompanied with three distinctive exothermic peaks and also two endothermic effects. The large mass loss of 31.95% takes place with temperature range of 250–290 °C with moderate exothermic peak at 251 °C can be ascribed to collapse or oxidation of the coordination framework and the formation of decomposition intermediate species before the formation of final residue [238–239]. The temperature was increased from 290 to 425 °C, while the weight loss continued with two consecutive stages, combined with one moderate and one sharp endothermic peak. Further temperature rising between 370–425 leads total mass loss of 67.34% can be assigned to complete decomposition and removal of organic part. The last decomposition step occurs between 425 and 1000 °C which indicate the formation of Ce_2O_3 residue with total mass loss of 67.34% which is comparable with the expected value of 68.01%.

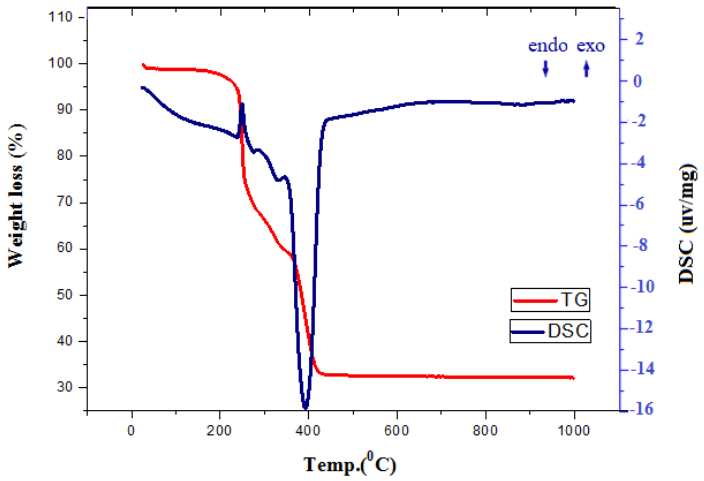

Figure 3.16: TGA-DTA curves of cerium compound **(4)**

3.3. Copper coordination polymers

3.3.1. Structure determination of [Cu((μN,N′-4-MeO-ba)2bn)Br]n (5)

Self-assembly reaction of L1, [N,N′-bis(4-methyl-benzylidene)butane-1,4-diamine] with CuBr gave a one-dimensional coordination polymer with formula **[Cu((μN,N′-4-MeO-ba)2bn)Br]n**, as depicted in (Figure 3.18).Compound **(5)** exhibits a polymeric chain and crystallizes in the monoclinic space group *C2/c* and the asymmetric unit consists of a copper(I) ion, one bromide anion and one half of L1 (N,N′-MeO-ba)2bn ligand.Each copper (I) ion is coordinated by one bromide anion (Br) and two imino nitrogen atoms of two neighboring ligand molecules (Figure 3.17), thus the coordination environment around the metal ion can be described as slightly distorted trigonal planar with the N–Cu–N and N–Cu–Br angles which are 126.9° and 116.6° respectively.

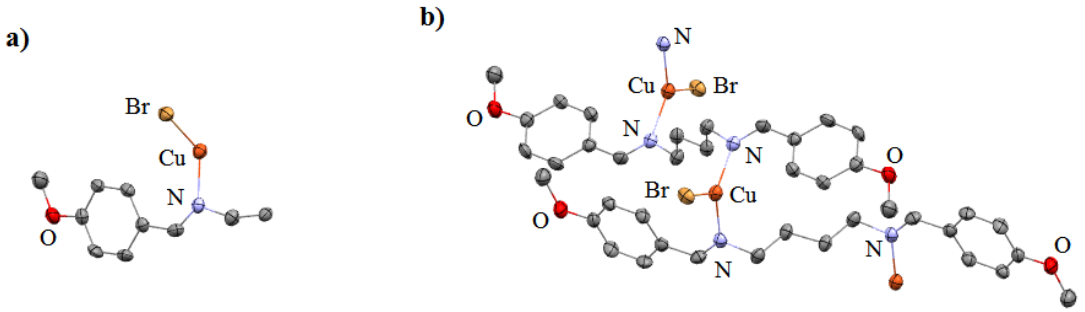

Figure 3.17: a) asymmetric unit of compound **(5)**; b) The view of molecule of copper compound **(5)** and planar CuN_2Br motif

In this compound, the ligand L1 acts as bis-monodentate bridging ligand through its imine nitrogen atoms, leading to polymeric chain of copper (I) complex (Figure 3.17 and 3.18).The both Cu–N bond lengths are equal (1.976 Å and 1.976 Å), hence it indicates the strong coordination of the ligands to the metal ion.Nevertheless, both bond lengths are within the normal range and correspondent to other copper (I) complexes that have been previously reported [240–250]. Crystallographic data are given in (Table 3.7).

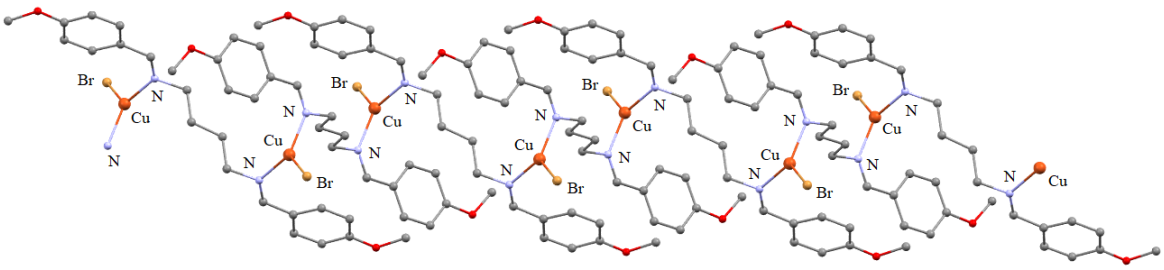

Figure 3.18: One-dimensional copper compound **(5)** along *b*-axis

In compound **(5)**, the large distances between two copper(I) ions (7.768 and 9.521 Å) prevents that bromide anion can connect them, however the shorter distances are found in some previous works in which halide anion can link two copper ions [242].

Table 3.7: Crystal data and refinement details for the X-ray structure determinations of the compounds **(5)**, **(6)** and **L_2** ligand .

	Compound (5)	**Compound (6)**	**L_1**
Empirical formula	$C_{20}H_{24}BrCuN_2O_2$	$C_{20}H_{24}ICuN_2O_2$	$C_{10}H_{12}NO$
crystal system	monoclinic	monoclinic	monoclinic
Space group	C2/c	C2/c	C2/c
Formula weight /g.mol^{-1}	467.45	514.45	162.21
a/ Å	23.739(3)	17.965(1)	8.0380(10)
b/ Å	8.840(1)	7.671(1)	8.0980(10)
c/ Å	11.389(1)	15.317(2)	13.4730(10)
α/°	90	90	90
β/°	111.423(8)	90.770(7)	90.542(8)
γ/°	90	90	90
Cell volume/ Å^3	2023.5(4)	2110.6(4)	909.4(2)
Formulas in unit cell	4	4	4
Density (calcd.) / Mg·cm^{-3}	1.536	1.620	1.185
Wavelength / Å	0.71073	0.71073	0.71073
Absorption coefficient /mm^{-1}	3.070	2.513	0.077
Numerical absorption correction	min./max.Transmittance 0.5822/0.7203	min./max.Transmittance 0.7677/0.8253	min./max.Transmittance 0.9560/0.9729
Temperature/ K	293(2)	293(2)	293(2)
Crystal size/mm	0.14*0.14*0.24	0.08*0.10*0.80	0.40*0.64*0.74
F (000)	952	1024	348
Θ range / °	2.70–25.00	2.70–25.00	2.86–26.99
Limiting indices	$-1 \le h \le 28$ $-1 \le k \le 9$ $-13 \le l \le 12$	$-1 \le h \le 21$ $-1 \le k \le 9$ $-18 \le l \le 18$	$-1 \le h \le 10$ $-1 \le k \le 10$ $-17 \le l \le 17$
Reflection collected	2227	2398	2724
Independent reflections	1786 (R_{int} = 0.0550)	1865 (R_{int} = 0.0249)	1974 (R_{int} = 0.0433)
Refinement method	Full–matrix least–squares on $\|F\|^2$	Full–matrix least–squares on $\|F\|^2$	Full–matrix least–squares on $\|F\|^2$
Goodness–of–fit on $\|F\|^2$	1.158	1.510	1.234
R indices (all data)	R1= 0.1254 , wR2 = 0.0865	R1= 0.0544 , wR2 = 0.0583	R1= 0.0520 , wR2 = 0.0689
Largest diff. Peak and hole	0.399 and –0.404 eÅ^{-3}	0.380 and –0.356 eÅ^{-3}	0.137 and –0.109 eÅ^{-3}

Table 3.8 : Selected bonds length for compounds $[Cu((\mu_{N,N'}\text{-4-MeO-ba})_2bn)Br]_n$ **(5)**, $[Cu_2((\mu\text{-Me}_2\text{N-ba})_2bn)I]_n$**(6)**

Bond length (Å) (Compound **(5)**)		Bond length (Å) (Compound **(6)**)	
Cu–N	1.976(5)	Cu–N	2.010(4)
Br–Cu	2.347(2)	I–Cu	2.4792(9)
N–C(8)	1.477(7)	N–C8	1.463(5)
N–C7	1.267(7)	N–C7	1.274(6)
Cu–N#1	1.976(5)	Cu–N#1	2.010(4)

Table 3.9 : Selected angles for compounds $[Cu((\mu_{N,N'}\text{-4-MeO-ba})_2bn)Br]_n$ **(5)**, $[Cu_2((\mu\text{-Me}_2\text{N-ba})_2bn)I]_n$**(6)**

Angles**(°)** (Compound **(5)**)		Angles(°) (Compound **(6)**)	
N#1–Cu–N	126.8(3)	N–Cu–N#1	101.0(2)
N#1–Cu–Br	116.58(14)	N#1–Cu–I	129.52(10)
C(7)–N–Cu	132.0(5)	C(8)–N–Cu	111.1(3)
C(8)–N–Cu	110.2(4)	C(8)–N–C(7)	117.1(4)
C(7)–N–C(8)	117.5(4)	N–Cu–I	129.52(10)
		C(7)–N–Cu	131.1(3)

#1 –x , y ,-z + 3/2 #1 –x , y ,-z + 1/2

#2 –x, -y, -z +1 #2 –x, -y-1 , -z

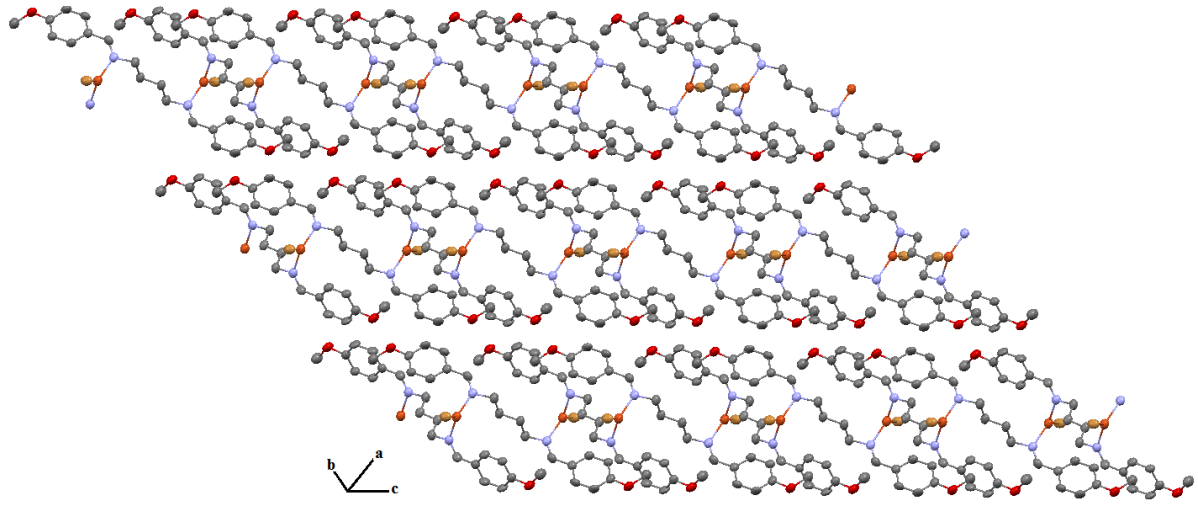

Figure 3.19: The coordination polymer chains of compound **(5)**, extended along *c*-axis

3.3.2. Structure determination of $[Cu((\mu_{N,N'}\text{-4-MeO-ba})_2bn)I]_n$ (6)

The reaction between L_1[N,N′-bis(4-methyl-benzylidene)butane-1,4-diamine] and CuI yielded a one-dimensional copper coordination polymer of formula **$[Cu((\mu_{N,N'}\text{-4-MeO-ba})_2bn)I]_n$** shown in (Figure 3.20 and 3.21).The X-ray structural study shows that this compound crystallizes in monoclinic system with space group **C2/c**, and an asymmetric unit contains one copper (I) ion, one iodide anion, and one half of L_1 (N,N′-4-MeO-ba)$_2$bn ligand.The coordination sphere around each copper(I) ion consists of a coordinated iodine anion and two coordinated nitrogen atoms of imine groups from two symmetrically related schiff-base ligands (Figure 3.20). Hence, the copper (I) adopts the slightly distorted trigonal planar coordination sphere.

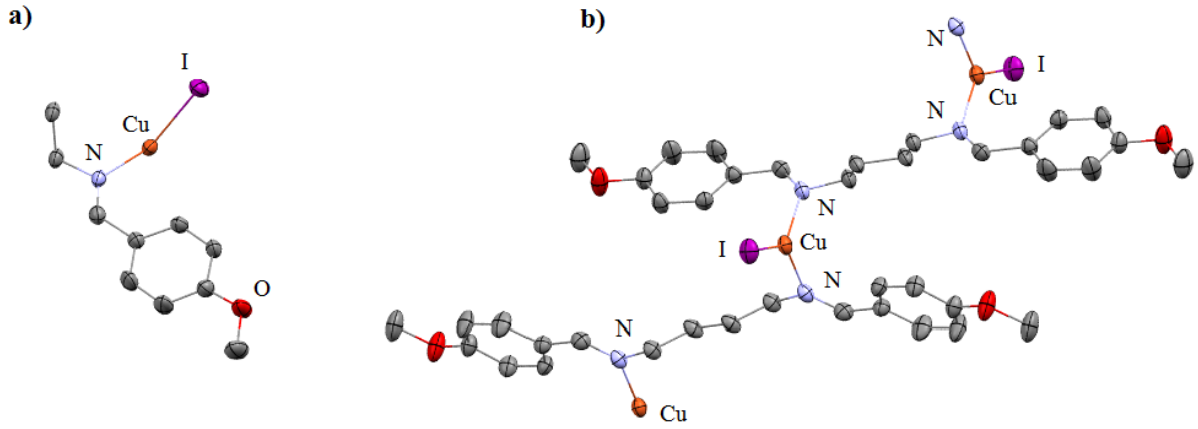

Figure 3.20 : a) asymmetric unit of compound $[Cu((\mu_{N,N'}\text{-4-MeO-ba})_2bn)I]_n$ **(6)**; b) The view of molecule of copper compound and planar CuN_2I moietiy

Similar to compound $[Cu((\mu_{N,N'}\text{-4-MeO-ba})_2bn)Br]_n$, the ligand L_1 also appears as bis-monodentate bridging ligand by using two nitrogen atoms of azomethine groups, constructing one-dimensional copper coordination polymer. In compound **(6)**, the both Cu–N bond lengths are also identical (2.010 Å and 2.010 Å), although they are a little longer in comparison with Cu–N bonds in compound $[Cu((\mu_{N,N'}\text{-4-MeO-ba})_2bn)Br]_n$.However, they are in normal range and are comparable to these bonds in the other reported copper (I) coordination compounds [240–256]. In compound $[Cu((\mu_{N,N'}\text{-4-MeO-ba})_2bn)I]_n$, copper (I) ion also adopts slightly distorted trigonal planar coordination environment and ∠N–Cu–N and ∠N–Cu–I angles are 129.5° and 101.0° respectively (Figure 3.20 and 3.21). Crystallographic data and selected bond lengths and angles are given in (Table 3.7, 3.8 and 3.9).

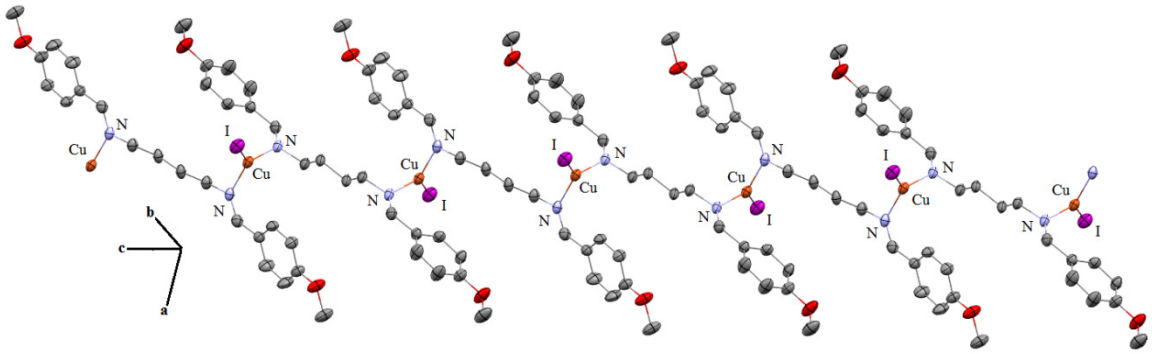

Figure 3.21: Polymeric structure of copper complex $[Cu((\mu_{N,N'}\text{-4-MeO-ba})_2bn)I]_n$ **(6)** along *c*-axis

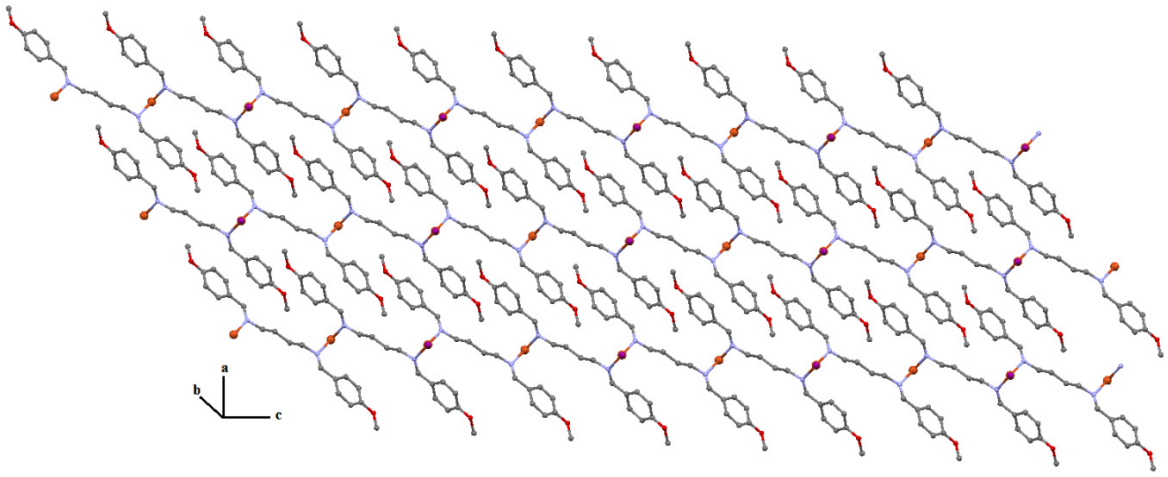

Figure 3.22: The coordination polymer chains of compound $[Cu((\mu_{N,N'}\text{-4-MeO-ba})_2bn)I]_n$, extended along *c*-axis

In compound **(6)**, the distance between two copper(I) ions (7.817 Å) is large to prevents that iodine atom can be bridge between them, however the shorter distance is found in some previous works in which the iodine anion acts as bridging ligand and links two copper ions [242].

3.3.3. Structure determination of $[Cu((\mu_{N,N'}\text{-4-Cl-ba})_2bn)I]_n$ (7)

The reaction between L_2[N,N′-bis(4-chloro-benzylidene)butane-1,4-diamine] and CuI in mixture of acetonitrile and dichloromethane provided a crystalline material with formula **$[Cu((\mu_{N,N'}\text{-4-Cl-ba})_2bn)I]_n$** shown in (Figure 3.23 and 3.24).The X-ray structural analysis confirmed the formation of a one-dimensional polymeric structure of this compound through copper(I)–nitrogen coordination bonds.This compound crystallizes in the monoclinic system

with space group **C2/c** and a copper(I) ion, one iodide ion and one half of L_2 ligand are observed overall in the asymmetric unit (Figure 3.23).

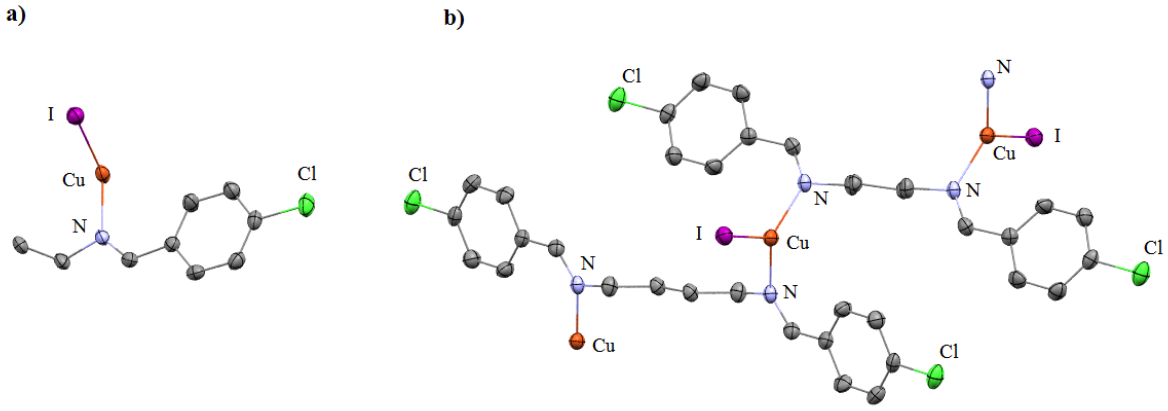

Figure 3.23 : a) asymmetric unit of compound $[Cu((\mu_{N,N'}\text{-4-Cl-ba})_2bn)I]_n$ **(7)**; b) The view of molecule of copper compound **(7)** and planar CuN_2I moiety

Compound **(7)** displays same coordination environment through two nitrogen atoms of two neighboring ligand molecules and iodine atom to Cu(I) ions, corresponding with compounds $[Cu((\mu_{N,N'}\text{-4-MeO-ba})_2bn)I]_n$ and $[Cu((\mu_{N,N'}\text{-4-MeO-ba})_2bn)Br]_n$. Also L_2 ligand behaves similar to L_1 ligand as bis-monodentate bridging ligand through its azomethine nitrogen atoms to form chain structure of copper complex.The Cu–N bond length is 1.978 Å and N–Cu–N and N–Cu–I angles are 125.7° and 117.1° respectively.Crystallographic data and selected bond lengths and angles are presented in (Table 3.10 and 3.11).Moreover, this is worth to note that the Cu···Cu distances are (7.950 and 7.950 Å**)** which is considerably much more than an iodine anion can connect them [242]

Table 3.10: Crystal data and refinement details for the X-ray structure determinations of the compound $[Cu((\mu_{N,N'}\text{-4-Cl-ba})_2bn)I]_n$ **(7)**

Compound	**(7)**
Empirical formula	$C_{18}H_{18}Cl_2CuIN_2$
crystal system	monoclinic
Space group	C 2/c
Formula weight /g.mol^{-1}	523.68
a/ Å	17.247(2)
b/ Å	7.0520(10)
c/ Å	15.853(2)
α/°	90
β/°	99.467(7)
γ/°	90
Cell volume/ Å^3	1901.9(4)
Formulas in unit cell	4
Density (calcd.) / Mg·cm^{-3}	1.829
Wavelength / Å	0.71073
Absorption coefficient /mm^{-1}	3.055
Numerical absorption	min./max.Transmittance
correction	0.3684/0.4371
Temperature/ K	293(2)
Crystal size/mm	0.38*0.40*0.40
F (000)	1024
Θ range / °	2.39–26.99
Limiting indices	$-1 \le h \le 22$
	$-1 \le k \le 8$
	$-20 \le l \le 19$
Reflection collected	2637
Independent reflections	2058 (R_{int} = 0.0270)
Refinement method	Full–matrix least–squares on $\|F\|^2$
Goodness–of–fit on $\|F\|^2$	1.679
R indices (all data)	R1= 0.0390 , wR2 = 0.0720
Largest diff. Peak and hole	1.352 and –0.954 eÅ^{-3}

Table 3.11: Selected bond lenghts and angles of compound $[Cu((\mu_{N,N'}\text{-4-Cl-ba})_2bn)I]_n$ **(7)** .

Bond length (Å)		Angles (°)	
Cu–N	1.978(3)	N–Cu–N#1	125.7(2)
Cu–I	2.5382(11)	N#1–Cu–I	117.14(10)
N–C(8)	1.469(5)	C(7)–N–Cu	131.5(3)
N–C(7)	1.282(5)	C(7)–N–C(8)	116.1(4)
Cu–N#1	1.978(3)	N–Cu–I	117.14(10)

#1 –x , y ,-z + 1/2 #2 –x, -y +1 , -z

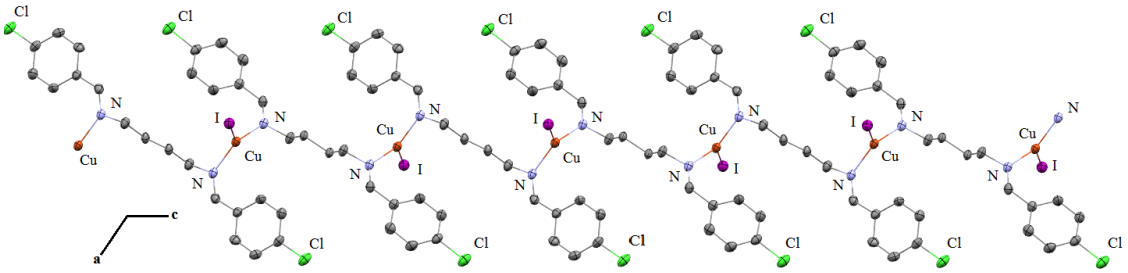

Figure 3.24: The polymeric structure of copper compound $[Cu((\mu_{N,N'}\text{-4-Cl-ba})_2bn)I]_n$ **(7)** along *c*-axis

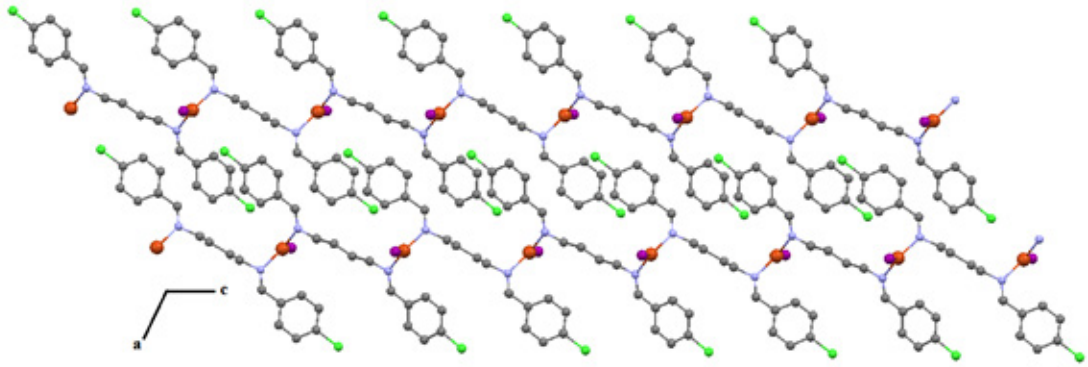

Figure 3.25: The coordination polymer chains of compound $[Cu((\mu_{N,N'}\text{-4-Cl-ba})_2bn)I]_n$ **(7)**, extended along *c*-axis

3.3.4. IR spectra analysis of copper compounds (5), (6) and (7)

The IR spectra of the three copper coordination compounds have been investigated. In the FT-IR spectra of copper coordination polymers, the significant spectrum is relevant to stretching vibration of azomethine group and it shifted to lower frequencies in copper(I) compounds because of coordination to metal ions in comparison with free ligands. The stretching vibration spectrum of imin group $\upsilon_{C=N}$ appears at 1644 cm^{-1} and 1646 cm^{-1} for free ligands, L_1 = {**(N,N´-MeO-ba)$_2$bn**} and L_2 = {**(N,N´-4-Cl-ba)$_2$bn**} respectively. $\upsilon_{C=N}$ of L_1 was observed at 1620 cm^{-1} in compound $[Cu((\mu_{N,N'}\text{-4-MeO-ba})_2bn)Br]_n$ **(5)** and at 1625 cm^{-1} in compound $[Cu((\mu_{N,N'}\text{-4-MeO-ba})_2bn)I]_n$ **(6)** respectively.This shift is attributed to the coordinated nitrogen atom of imin group to copper(I) ions in both compounds $[Cu((\mu_{N,N'}\text{-4-MeO-ba})_2bn)I]_n$ and $[Cu((\mu_{N,N'}\text{-4-MeO-ba})_2bn)Br]_n$. In compound $[Cu((\mu_{N,N'}\text{-4-Cl-ba})_2bn)I]_n$ **(7)** This band was observed at 1624 cm^{-1} that has been shifted to a lower frequency relative to the free ligand L_2 (1646 cm^{-1}), due to the coordination of the imine nitrogen atom to the metal ion.

3.3.5. Thermal analysis of compounds $[Cu((\mu_{N,N'}\text{-}4\text{-MeO-ba})_2bn)Br]_n$ (5) and $[Cu((\mu_{N,N'}\text{-}4\text{-MeO-ba})_2bn)I]_n$ (6)

To determine the thermal stability of compounds **(5)** and **(6)**, their thermal stability were carried out under a nitrogen atmosphere in the temperature range from 25 to 1000 °C.The goal is to investigate the thermal behavior of these coordination polymers since they were synthesized by similar ligand and under same reaction conditions.From TG curve of compound **(5)** (Figure 3.26), it can be observed that compound **(5)** remains stable upon to 220 °C. In the range between 225 and 290 °C, the structure starts to collapse, with a weight loss of 19.63% which is assigned to the first step decomposition of the organic ligand. Due to further increasing of the temperature, the combustion of the remaining organic ligand raised. The second weight loss of 33.49 % occurs in range of 290–450 °C. In this stage, the mass loss is attributed to further decomposition of organic structure.Finally, the last step of decomposition occurs in range 450–800 °C, leading to mass loss of 17.06 (calculated, 18,61%) and generation CuBr as the final residue with mass percentage of 29.89% which indicates that whole molecule framework collapsed and is good agreeable with calculated value 30.68%.

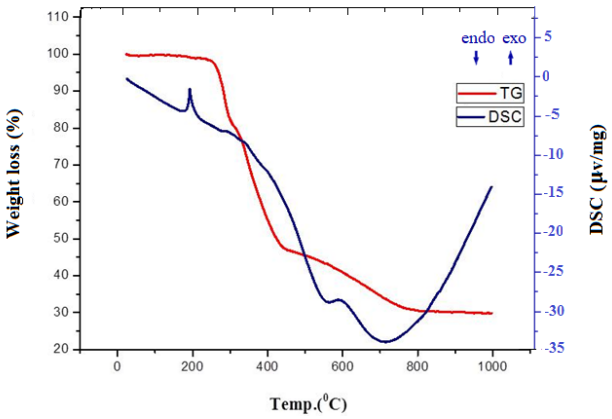

Figure 3.26: Thermogravimetric analysis (TGA) curves of compound **(5)**, accompanyied with Differential Scanning Calorimetric (DSC)

The TG curve of compound **(6)** indicates that it is stable up to 225 °C at which temperature it started to decompose (Figure 3.27).Removal of the ligand takes place with three decomposion stages in the range between 260 and 800 °C. The first weight loss of 28.72 % from 225 °C to 300 °C and second weight loss turns out in the range of 300–475 °C which is contributed to partial decomposion of organic part.Due to increasing temperature, the last decomposition stage occurred with mass loss of 28.98% which is assigned to total removal of remained

organic part which was observed in temperature range 450–800 °C, corresponding with calculated value 27.64%.The final product may be C_2Cu with mass percentage of 17.98%, which is in good agreement with the calculated value of 18.02 %.

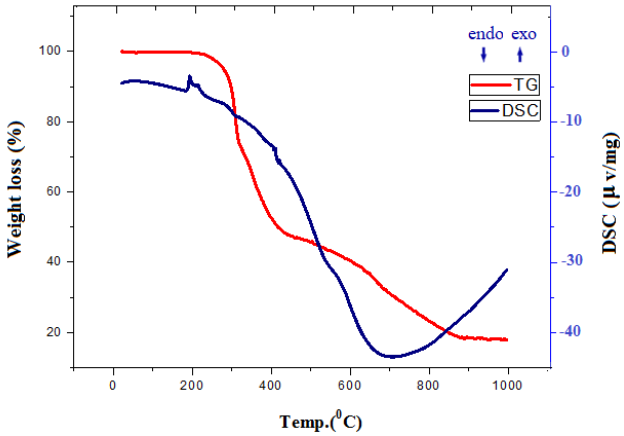

Figure 3.27: Thermogravimetric analysis (TGA) and Differential Scanning Calorimetric (DSC) curves of compound **(6)**

3.3.6. Thermal analysis of compound $[Cu((\mu_{N,N'}\text{-4-Cl-ba})_2bn)I]_n$ (7)

To investigate thermal stability of compounds **(7)** thermogravimetric analysis (TGA) was performed in the temperature range of 25–1000 °C under nitrogen gas. The TGA curve for this compound is illustrated with (Figure 3.28).This compound was stable up to 225 °C and then started to decompose upon rising temperature. The initial weight loss of 13.56 % occurs at 225–325 °C. The second continuous weight loss of 22.55% happened in the temperature range between 325 and 475 °C, which can be assigned to decomposition partially of ligand. The major weight loss of 28.09 % occurred at last stage of decomposition.This is assigned to remove completely the remained organic part which is comparable to calculated 30.05 %). The final residue can be $CuCl_2$ with mass percentage of 27.15 % (calculated 25.67%).

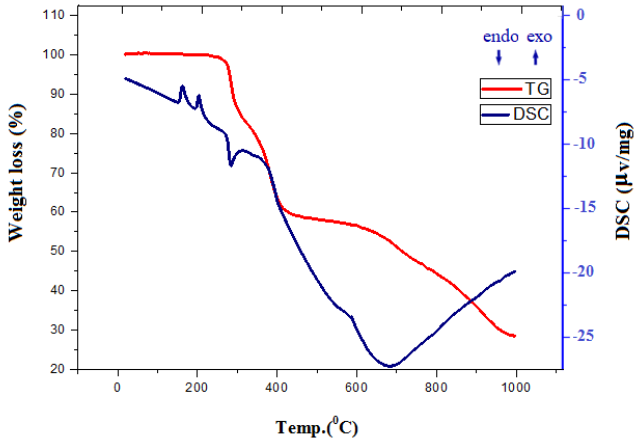

Figure 3.28: Thermogravimetric analysis (TGA) and Differential Scanning Calorimetric (DSC) curves of compound **(7)**

3.4. Lead coordination polymer

3.4.1. Crystal structure determination of compound $[Pb_3(CH_3COO)_2(N_3)_4]_n$ (8)

Crystalline material of compound $[Pb_3(CH_3COO)_2(N_3)_4]_n$ was produced by reaction of $Pb(CH_3COO)_2$ and sodium azide salt in ligand / metal ratio 2:1 in acetonitrile as solvent. Compound **(8)** is a 3D coordination polymer and crystallizes in orthorhombic space group Pccn. The asymmetric unit consists two crystallographically independent lead ions (Pb1 and Pb2), two azide ions and one acetate anion. Pb1 ion displays near pentagonal bipyramid coordination sphere with four nitrogen atoms from four different azide ions and three oxygen atoms from two acetate groups. The Pb2 ions show a square antiprismatic coordination environment arising from six nitrogen atoms from six individual azide ions and two oxygen atoms from two different acetate groups. In this compound, azide ions display coordination modes μ_4-1,1,3,3 and μ_3-1,1,3. The acetate group is also coordinated to metal ions in coordination mode μ_3-η^2:η^2 [257]. As it is shown in (Figure 3.29b and 3.30), two Pb1 ions are linked by bridging of two oxygen atoms (O1) from two different acetate groups, forming four-membered dinuclear ring in which acetate groups are placed in *trans* configuration. Furthermore, Pb2 ions are interconnected between oxygen atoms (O2) from two neighboring acetate groups along *a*-axis (Figure 3.29b and 3.30). On the other hand, adjacent Pb2 ions are connected through chelating behavior of nitrogen atoms (N3) from two azide ligands along *c*-axis. The Pb2 and Pb1 ions are further linked to each other by the bridging behavior of azide ions to generate a 3D coordination network, (Figure 3.30 and 3.31). As it is mentioned above, the azide ion adopts two different coordination modes in this structure. For example, the azide

ion exposing coordination mode μ4-1,1,3,3 connects two Pb2 ions via the nitrogen atom (N3) along *c*-axis while the nitrogen atom (N1) links two neighboring Pb1 ions along *b*-axis.The other azide ion with coordination mode μ3-1,1,3 links two adjacent Pb1 ions via nitrogen atoms (N4), although the nitrogen atom (N6) coordinates to Pb2 ions. As matter of fact, the azide ions with high binding modes play a role for the formation of a 3D network since they link several metal ions in this structure. Crystallographic data and selected bond lengths and bond angles are presented in (Table 12, 13 and 14). In compound **(8)**, the Pb–O bond lengths range from 2.545(4) to 2.687(4) Å for Pb1 and 2.687(4) Å for Pb2. Additionally, Pb1–N and Pb2–N bond lengths vary from 2.543(4) to 2.716(4) Å and 2.657(5) to 2.704(5) Å respectively, corresponding to the usual Pb–O and Pb–N bond lengths in the previous works [258–266].

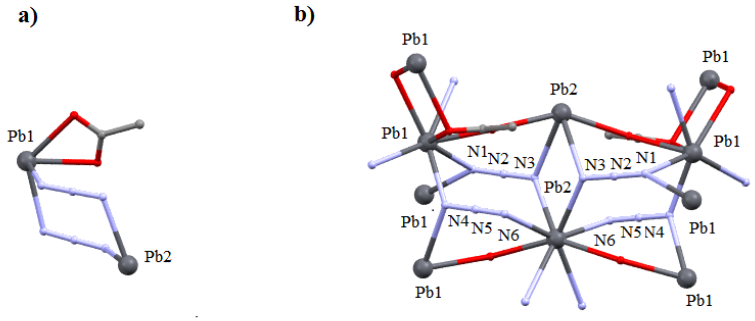

Figure 3.29: a) asymmetric unit; b) molecular structure of compound $[Pb_3(CH_3COO)_2(N_3)_4]_n$ **(8)**

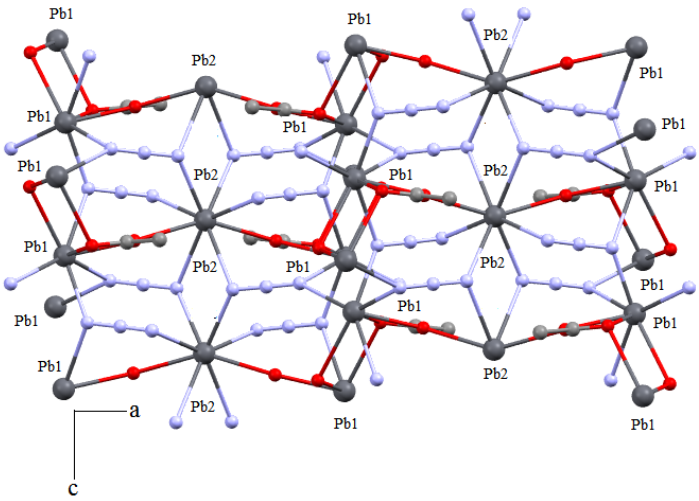

Figure 3.30: Coordination environment around Pb1 and Pb2 atoms in compound **(8)**

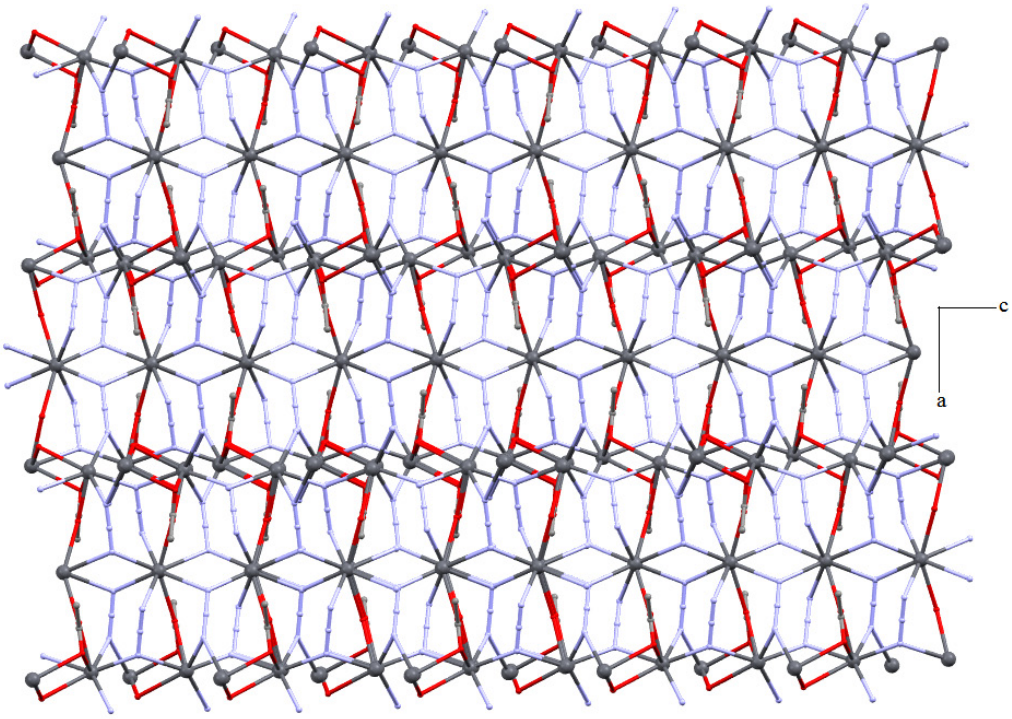

Figure 3.31: 3D coordination network of compound **(8)**

Table 12: Crystal data and refinement details for the X-ray structure determinations of the compounds $[Pb_3(CH_3COO)_2(N_3)_4]_n$ **(8)** and $[Na_2Pb_2(CH_3COO)_6]_n$ **(9) .**

	$[Pb_3(CH_3COO)_2(N_3)_4]_n$	$[Na_2Pb_2(CH_3COO)_6]_n$
Empirical formula	$C_4H_6N_{12}O_4Pb_3$	$C_{12}H_{18}Na_2O_{12}pb_2$
crystal system	orthorhombic	orthorhombic
Space group	*Pccn*	$P2_12_12_1$
Formula weight /g.mol^{-1}	907.78	814.62
a/ Å	19.692 (2)	11.0940 (10)
b/ Å	7.9661 (5)	12.979 (3)
c/ Å	9.0885 (7)	14.401 (4)
α/°	90	90
β/°	90	90
γ/°	90	90
Cell volume/ Å^3	1425.7 (2)	2073.6 (8)
Formulas in unit cell	4	4
Density (calcd.) / Mg·cm^{-3}	4.229	2.478
Wavelength / Å	0.56085	0.71073
Absorption coefficient /mm^{-1}	19.344	16.314
Numerical absorption correction	min./max.Transmittance 0.0507/0.5685	min./max.Transmittance 0.01577/0.05098
Temperature/ K	293(2)	293(2)
Crystal size/mm	0.38*0.30*0.40	0.48*0.40*0.36
F (000)	1568	1488
Θ range / °	6.29–30.47	2.11–25.00
Limiting indices	$-35 \le h \le 35$ $-14 \le k \le 14$ $-16 \le l \le 16$	$-13 \le h \le 4$ $-1 \le k \le 15$ $-1 \le l \le 17$
Reflection collected	34084	3427
Independent reflections	4334 (R_{int} = 0.0528)	2997 (R_{int} = 0.0615)
Refinement method	Full–matrix least–squares on $\|F\|^2$	Full–matrix least–squares on $\|F\|^2$
Goodness–of–fit on $\|F\|^2$	1.090	1.256
R indices (all data)	R1= 0640, wR2 = 0.1384	R1= 0.0652 , wR2 = 0.0834
Largest diff. Peak and hole	2.723 and –1.818 eÅ^{-3}	1.515 and –1.300 eÅ^{-3}

Table 3.13 : Selected bands of compound $[Pb_3(CH_3COO)_2(N_3)_4]_n$ **(8)** and $[Na_2Pb_2(CH_3COO)_6]_n$ **(9)** .

Bond length (Å) Compound **(8)**		(Bond length (Å) Compound **(9)**	
Pb(1)–N(1)	2.649(5)	Pb(1)–O(1)	2.543(13)
Pb(1)–N(4)	2.543(4)	Pb(1)–O(5)	2.578(13)
Pb(1)–O(1)	2.595(5)	Pb(1)–O(3)	2.43(2)
Pb(1)–O(2)	2.545(4)	Pb(1)–O(4)	2.676(12)
Pb(2)–N(3)	2.704(5)	O(12)–Na(1)#6	2.70(2)
Pb(2)–N(6) #2	2.657(5)	Pb(1)–O(7)	2.569(13)
Pb(2)–O(2) #3	2.687(4)	Pb(1)–Na(1)	3.626(6)
N(4)–Pb(1)#4	2.716(4)	Pb(1)–Na(2)	3.737(7)
Pb(2)–N(3)	2.704	Pb(2)–O(6)#2	2.460(12)
Pb(2)–O(2)#4	2.687(4)	Pb(2)–O(10)	2.459(12)
Bond($[Na_2Pb_2(CHCOO)_6]_n$)	Bond length (Å)	Pb(2)–Na(2)	3.477(7)
Na(2)–O(8)	2.371(12)	Pb(2)–Na(1)#2	3.928(7)
Na(2)–O(9)	2.53(2)	Na(2)–Na(1)#2	3.778(10)
Na(2)–O(11)	2.33(2)	Na(2)–Pb(2)#1	3.603(7)
Na(2)–O(6)#2	2.383(13)	Pb(2)–O(11)	2.422(13)
Na(2)–O(10)#1	2.29(1)	Pb(2)–O(3) #3	2.674(14)
Na(2)–O(12)#1	2.44(2)	Pb(1)–O(12) #1	2.738(13)
Na(1)–O(2)#4	2.29(2)		

Table 3.14 : Selected angles of compound **(8)**

Angles (°)			
N(1)–Pb(1)–N(4)#1	76.3(2)	N(4)–Pb(1)–O(1)	73.3(1)
N(6)#2–Pb(2)–N(6)	145.5(2)	O(1)–Pb(1)–N(1)	121.77(13)
N(4)–Pb(1)–O(1)	73.3(2)	N(6)–Pb(2)–N(6)	140.6
N(4)–Pb(1)–N(1)	77.1(2)	N(6)–Pb(2)–N(3)	73.7
N(6)#2–Pb(2)–O(2)#3	73.33(14)	N(6)–Pb(2)–O(2)	116.3
N(4)–Pb(1)–N(4)#1	144.2(2)	N(1)–N(2)–N(3)	178.7(5)
Pb(1)–O(2)–Pb(2)#1	141.7(2)	N(4)–N(5)–N(6)	178.7(5)
Pb(1)–N(4)–Pb(1)#4	120.3(2)	N(2)–N(1)–Pb(1)	116.3(4)
N(3)–Pb(2)–N(3)#2	71.0(2)	N(2)–N(3)–Pb(2)	121.3(4)
#1 x , -y +1/2 , z - 1/2	#2 -x +3/2 , -y +1/2 , z	#3 -x +3/2 , y, z +1/2	#4 x , -y +1/2 , z +1/2

Table 3.15 : Selected angles of compound **(9)**

Angles (°)			
O(3)–Pb(1)–O(1)	82.7(5)	O(3)–Pb(1)–O(5)	119.5(5)
O(1)–Pb(1)–O(7)	139.4(4)	O(7)–Pb(1)–O(5)	73.5(4)
O(1)–Pb(1)–O(5)	80.9(5)	O(1)–Pb(1)–O(4)	70.7(4)
O(3)–Pb(1)–O(4)	49.9(4)	O(3)–Pb(1)–Na(1)	87.2(3)
Na(1)–Pb(1)–Na(1)#2	157.37(3)	O(11)–Pb(2)–O(10)	75.3(4)
O(3)–Pb(1)–O(12)#1	118.1(5)	O(3)–Pb(1)–O(7)	83.2(5)
O(4)–Pb(1)–O(12)#1	120.5(4)	Na(7)–Pb(1)–Na(2)	124.5(2)
O(1)–Pb(1)–Na(1)	100.3(3)	O(7)–Pb(1)–O(4)	71.1(5)
O(3)–Pb(1)–Na(2)	86.6(3)	O(1)–Pb(1)–Na(2)	133.3(3)
O(7)–Pb(1)–Na(2)	83.4(3)	O(5)–Pb(1)–Na(2)	141.7(4)
O(7)–Pb(1)–Na(1)#2	136.7(4)	O(3)–Pb(1)–Na(2)	86.6(3)
O(3)–Pb(1)–Na(1)#2	115.4(3)	O(8)–Na(2)–Pb(1)	51.1(3)
O(1)–Pb(1)–O(12)#1	93.1(5)	Pb(2)–Na(2)–Pb(1)	112.4(2)
O(4)–Na(1)–Na(2)#4	97.9(3)	O(8)–Na(2)–Pb(2)	137.6(4)
O(4)–Na(1)–O(12)#5	136.9(5)	O(10)–Pb(2)–Na(2)	83.9(3)
Pb(2)–Na(2)–Na(1)#2	65.4(2)	O(5)–Na(1)–O(7)	80.8(5)
Pb(1)–Na(2)–Na(1)#2	59.60(14)	O(11)–Na(2)–O(8)	107.7(5)

#1 x -1/2 ,-y +3/2 , -z + 1 #2 -x +1/2 ,-y +1 , z + 1/2 #3 x +1/2 ,-y +3/2 , -z + 1

#4 -x +1/2 ,-y +1 , z -1/2 #5 -x +1 ,y - 1/2 , -z + 1/2 #6 -x +1 ,y + 1/2 , -z + 1/2

3.4.2. Crystal structure determination of compound $[Na_2Pb_2(CH_3COO)_6]_n$ (9)

A new lead coordination polymer was synthesized by reaction of $Pb(CH_3COO)_2$ and sodium azide salt in ligand and metal ratio 1:1 in acetonitrile. This compound is a 3D coordination polymer and crystallizes in the orthorhombic system with space group $P2_12_12_1$.An asymmetric unit of this compound contains two crystallographically independent lead ions (Pb1 and Pb2), two crystallographically independent sodium ions (Na1 and Na2) and six acetate anions. As it is shown in (Figure 3.33 and 3.34), the both sodium ions (Na1 and Na2) are hexa-coordinated; however the coordination environment around each sodium ion is different. Na1 ions adopt distorted trigonal prismatic coordination environment while Na2 owns the configuration close to octahedral. Contrary to sodium ions, Pb ions (Pb1 and Pb2) show higher coordination numbers. The coordination sphere around the Pb2 atom by coordination of seven oxygen atoms of six anionic acetate ligands is defined as a distorted capped trigonal prism while Pb1 is eight-coordinated with O–Pb–O angles in range of 46.9 to 165.8° and exhibits hemidirected coordination environment in which the bonds to ligand atoms are directed throughout only part of the coordination sphere and there is an attributable void (or gap) in the distribution of bonds to the ligands (Figure 3.32) [263–265]. In this structure, the acetate anion acts as

chelating, bridging ligand and is coordinated to metal ions through coordination modes μ_4-η^2:η^3. As it can be seen in (Figure 3.32 and 3.33), the acetate groups bridge between the metal ions such as Pb1–O–Na1, Pb2–O–Na2, Na1–O–Na2 and Pb2–O–Na1 and because of high bridging mode and chelating behavior of acetate, the 3D coordination framework is constructed. In this compound, the Pb1–O and Pb2–O bond lengths range from of 2.43(2) to 2.738(13) Å and 2.422(13) to 2.674(14) Å respectively, comparable to the usual Pb–O bond lengths reported in previous works [258–265].

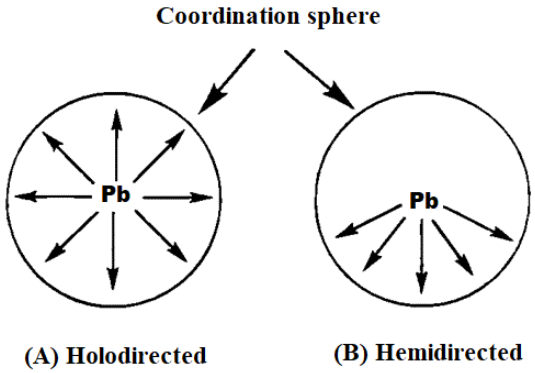

Figure 3.32: (A) Holodirected and (B) Hemidirected Coordination sphere [263–265]

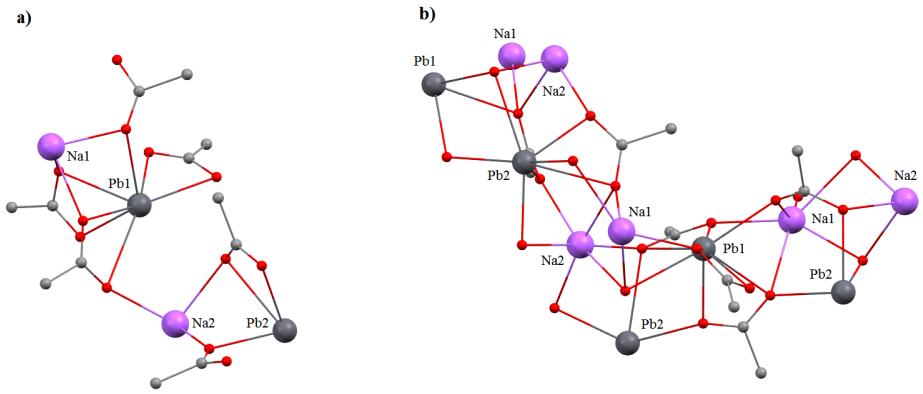

Figure 3.33: a) asymmetric unit; b) molecular structure of compound $[Na_2Pb_2(CH_3COO)_6]_n$ **(9)**

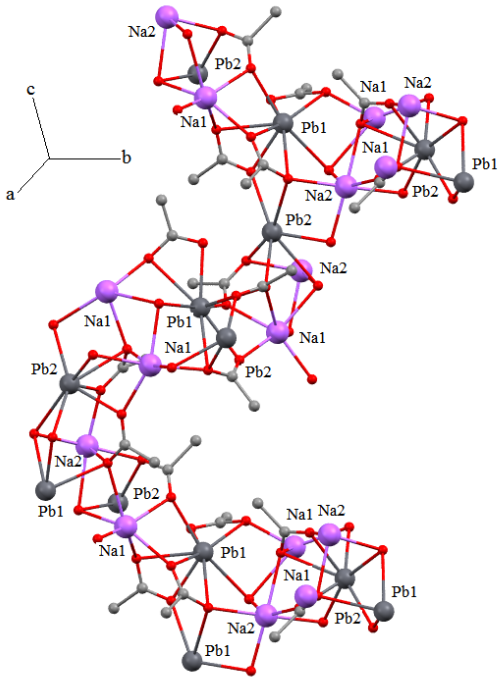

Figure 3.34: The structure of compound $[Na_2Pb_2(CH_3COO)_6]_n$ **(9)**

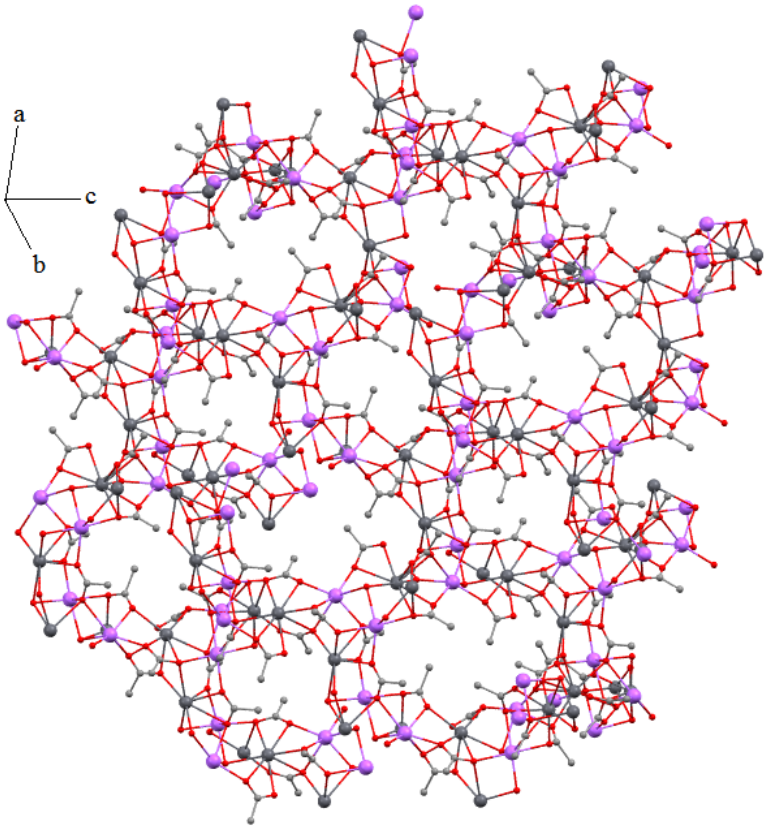

Figure 3.35: View of three-dimensional coordination polymer of compound $[Na_2Pb_2(CH_3COO)_6]_n$ **(9)** from *b*-axis

3.4.3. IR analysis of compounds (8) and (9)

In compound $[Pb_3(CH_3COO)_2(N_3)_4]_n$, the FT-IR spectrum shows two peaks at 1485 cm^{-1} and 1395 cm^{-1}, can be assigned to symmetric and asymmetric stretching of the carboxylate groups in this complex respectively.A correlation of the carboxylate coordination modes to metal ions was studied by examining the difference $\Delta\nu(COO) = \nu_{as}(COO) - \nu_s(COO)$ of compound **(8)**.The difference is 90, which implies that the carboxylic group of acetate ligands coordinated to Pb(II) ions in bridging mode and it is comparable with the X-ray single crystal structural analysis.The appearance of very strong absorption peak at 2019 cm^{-1} in this compound is due to the asymmetric stretching frequencies, $\nu_{as}(N_3)$ of the bridged azide ligands in coordination modes μ_4-1,1,3,3 and μ_3-1,1,3.The strong intensity peak at 1334 cm^{-1} and weak peak at 1147 cm^{-1} can be attributed to symmetrical stretching vibrations, $\nu_s(N_3)$ [266−268]. It is worth to notice, the highest frequency peak of $\nu_{as}(N_3)$ is assigned to *end-on* binding (*i.e.*, μ-1,1) and the lowest frequency peak is due to the *end-to-end* binding of the azide ligand (*i.e.*, μ-1,3) which have been reported in previous coordination compounds [269−274].

In lead compound $[Na_2Pb_2(CH_3COO)_6]_n$, two very strong peaks are at 1528 cm^{-1} and 1391 cm^{-1} are due to symmetric and asymmetric stretching of the carboxylate of acetate groups in the network. The difference $\Delta\nu(COO) = \nu_{as}(COO) - \nu_s(COO)$ of this compound is 137 which indicates the acetate groups are coordinated to lead ions by bridging mode [213].

3.4.4. Thermal analysis of compound (9)

In order to examine the thermal stability of lead compound **(9)**, thermal gravimetric (TG) and differential thermal analyses (DTA) were carried out in the temperature range between 25 and 800 °C in the static atmosphere of air (Figure 3.36). The TG curve of this compound indicates that this compound is stable up to 230 °C at which temperature the structure begins to collapse. The TG curve indicates the release of ligand molecules from 230 up to 520 °C with several short decomposition steps and two exothermic effects at 176.7 and 300.8 °C and one distinct endothermic effect at 494, (Figure 3.36). The solid residue formed at around 500 °C is suggested to be Na_2O and PbO.

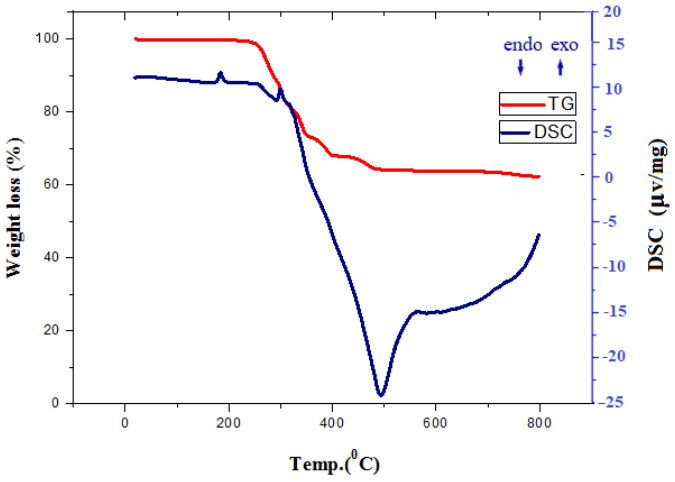

Figure 3.36: TG and DSC curves of lead compound $[Na_2Pb_2(CH_3COO)_6]_n$ **(9)**

3.4.5. Structure determination of compound $[Pb(DHBDA)]_n$ (10)

The reaction between $Pb(NO_3)_2$ and (H_2-DHBDA = 2,5-Dihydroxy-1,4-benzenediacetic acid), yielded a new lead coordination polymer of formula $[Pb(DHBDA)]_n$.This compound represents a 3D coordination polymer in solid state and crystallizes in the monoclinic space group ***C*2/*c***. The asymmetric unit of compound **(10)** comprises one lead (II) ion and one half of ligand 2,5-Dihydroxy-1,4-benzenediacetic acid. Each lead (II) ion owns coordination number six and shows hemidirected coordination sphere in which the O–Pb–O angles vary from 167.1 to 51.5 ° and Pb–O bond lengths are in range between 2.469 and 2.738 Å [263–265]. The ligand 2,5-Dihydroxy-1,4-benzenediacetic acid behaves as chelating, bridging ligand and is coordinated to lead (II) ions through its carboxylate oxygen atoms (O1 and O2) in coordination mode (μ_3-η^1:η^2).Both carboxylate groups of the ligand are linked to metal ions in the same coordination fashion and they are oriented in polymeric network as *trans* configuration, while the oxygen atoms of hydroxyl groups remain uncoordinated (Figure 3.37).As it is observed in (Figure 3.38 and 3.39), the Pb ions are bridged to each other by chelatig behavior of ligand to make a three-dimensional coordination network.

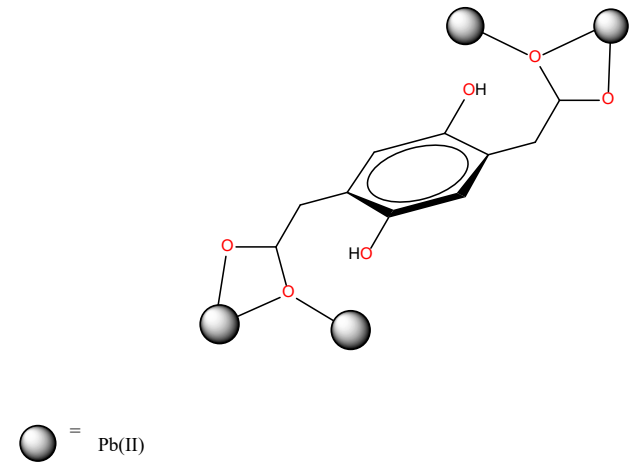

Figure 3.37: 2,5-Dihydroxy-1,4-benzenediacetate coordination modes in compound $[Pb(DHBDA)]_n$ **(10)**

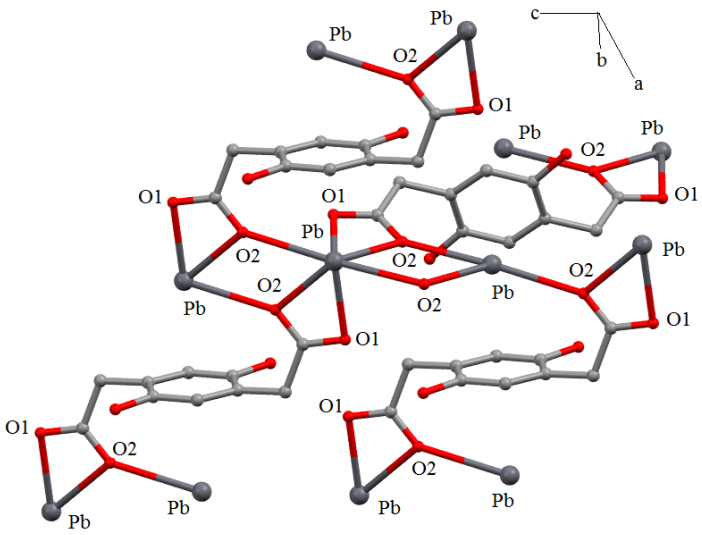

Figure 3.38: The coordination environment of Pb(II) ions in compound $[Pb(DHBDA)]_n$ **(10)**

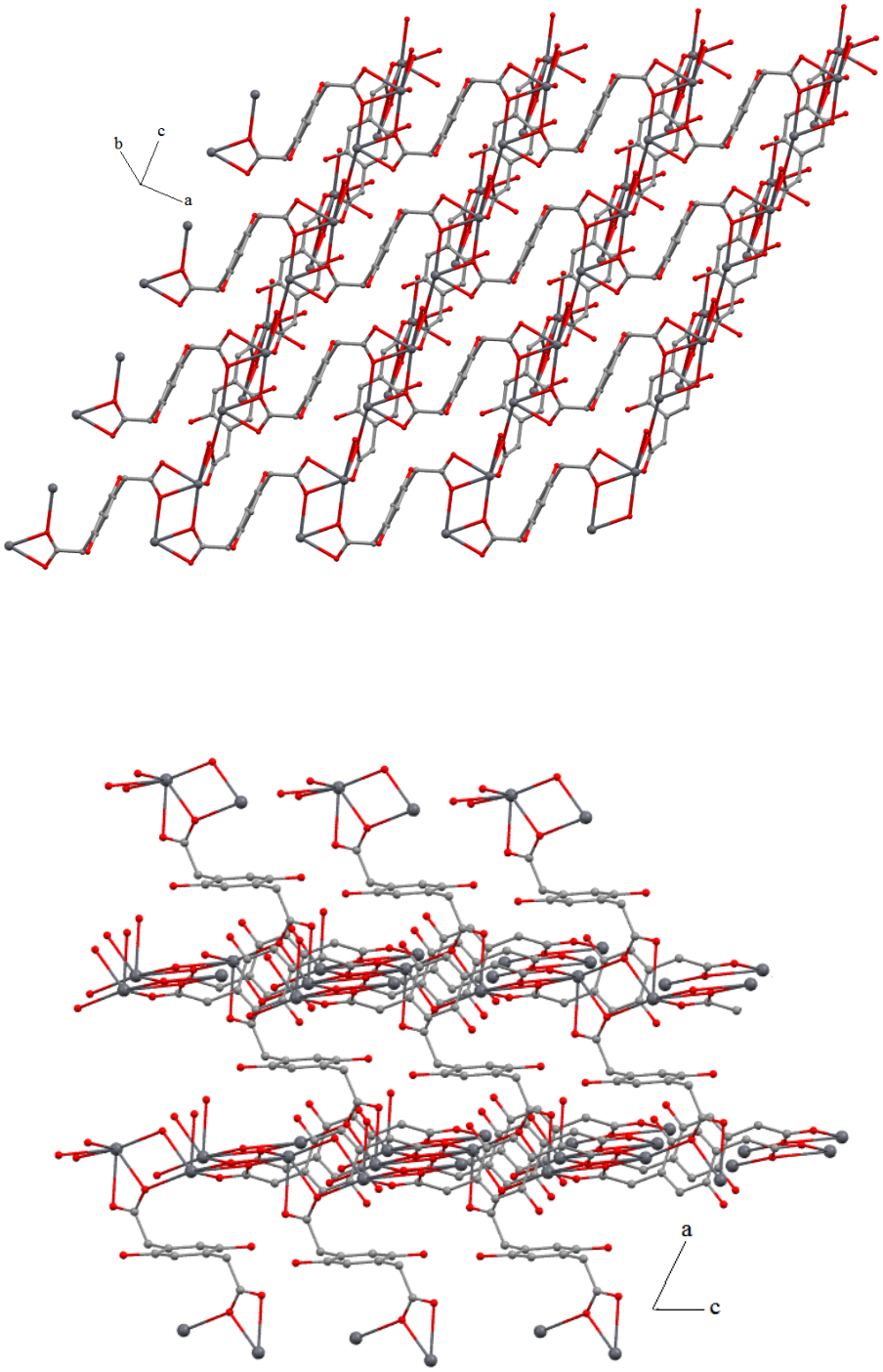

Figure 3.39: Perspective view of lead compound $[Pb(DHBDA)]_n$ **(10)** from *c*-axis

Table 16: Crystal data and refinement details for the X-ray structure determinations of lead compound $[Pb(DHBDA)]_n$ **(10)**

Empirical formula	$C_{10}H_8O_6Pb$
crystal system	monoclinic
Space group	*C2/c*
Formula weight /g.mol^{-1}	431.35
a/ Å	13.016(2)
b/ Å	11.9680(10)
c/ Å	8.8000 (10)
α/°	90
β/°	131.840(10)
γ/°	90
Cell volume/ Å^3	1021.3 (2)
Formulas in unit cell	4
Density (calcd.) / Mg·cm^{-3}	2.805
Wavelength / Å	0.71073
Absorption coefficient /mm^{-1}	16.534
Numerical absorption correction	min./max.Transmittance 0.66132/0.76364
Temperature/ K	293(2)
Crystal size/mm	0.2*0.1*0.15
F (000)	792
Θ range / °	2.70–25.98
Limiting indices	$-16 \le h \le 16$ $-14 \le k \le 14$ $-10 \le l \le 10$
Reflection collected	2076
Independent reflections	999 (R_{int} = 0.0283)
Refinement method	Full–matrix least–squares on $\|F\|^2$
Goodness–of–fit on $\|F\|^2$	1.421
R indices (all data)	R1= 0.0301 , wR2 = 0.0491
Largest diff. Peak and hole	1.038 and –0.737 eÅ^{-3}

Table 3.17 : Selected bond lenghts and angles of lead compound $[Pb(DHBDA)]_n$ **(10)**

Bond length (Å)			
Pb–O(1)	2.469(5)	Pb–C(1)	2.874(6)
Pb–O(2)	2.527(4)	Pb–C(1)#1	2.874(6)
Pb–O(2)#2	2.738(4)	O(2)–Pb#3	2.738(4)
Pb–O(1)#1	2.469(5)		
Pb–O(2)#1	2.527(4)		
Pb–O(2)#3	2.738(4)		

Angles (°)			
O(1)–Pb–O(1)#1	98.0(2)	O(1)–Pb–O(2)	51.49(14)
O(1)#1–Pb–O(2)	81.6(2)	O(1)–Pb–O(2)#1	81.6(2)
O(1)#1–Pb–O(2)#1	59.49(14)	O(2)–Pb–O(2)#1	108.3(2)
O(1)–Pb–O(2)#2	77.4(2)	O(2)#1–Pb–O(2)#3	128.8(2)(8)
O(2)–Pb–O(2)#2	128.8(2)	O(1)–Pb–C(1)	25.8(2)
O(1)–Pb–O(2)#3	111.46(14)	O(2)–Pb–C(1)	25.9(2)
O(2)–Pb–C(2)#3	60.3(2)	Pb–O(2)–Pb#3	119.7(2)
O(1)#1–Pb–C(1)	92.2(2)	C(1)–O(1)–Pb	95.4 (4)
O(2)#1–Pb–C(1)	97.5(2)	C(1)–O(2)–Pb#3	145.2(4)
C(1)–O(2)–Pb	92.7(4)		

#1 -x , y , -z + 1/2 #2 x , -y +2, z + 1/2 #3 -x , -y +2 , - z

#4 -x -1/2, -y +3/2, -z -1

3.4.6. **IR Spectra analysis of compound (10)**

The symmetric and asymmetric vibrations of the carboxylate group are observed as strong peaks at 1524 cm^{-1}, 1498 cm^{-1}, 1426 cm^{-1} and 1397 cm^{-1} respectively.The various $\Delta(\upsilon_{as}-\upsilon_{s})$ values indicate that the carboxylate anions coordinate to the Pb(II) ions in bridging mode [213].Furthermore, the absence of a strong bond at 1700 cm^{-1} corresponds to fully deprotonated carboxylate groups of the ligand.The relatively weak peak around 3010–3035 cm^{-1} are due to C–H vibration involving the aromatic ring hydrogen atoms.

Summary

The present work deals with the preparation and characterization of ten new coordination polymers prepared from different metal ions and ligands by different synthetic methods. In addition to the structural characterization of these compounds by means of X-ray single-crystal diffraction data, the focus is on the consideration of thermal and spectroscopic properties.

The new silver coordination polymer exhibits very unique, robust and interesting polymeric structure with high thermal stability.Two new lanthanide coordination polymers (neodymium and samarium) have been synthesized with H_2FDA = 2,5-furandicarboxylic acid in DMF as solvent via capped tube method. The compounds are iso-structural and exhibit three-dimensional coordination polymers.The goal of using DMF as the pure solvent instead of a mixture of water and other solvents was to synthesize new coordination polymer which might show a very intensive luminescence effect.The investigation has turned out that these compounds emerge no significant luminescence effect.As it has been reported in previous works in which the H_2FDA = 2,5-furandicarboxylic acid was used for construction of lanthanide coordination polymers in water as solvent, however the compounds have exposed very interesting luminescence properties [229–230]. A new cerium coordination polymer has been produced with ligand (H_2pdc = 3,5-pyrazoledicarboxylic acid) under solvothermal condition in DMF as solvent. Indeed, ligand (H_2pdc = 3,5-pyrazoledicarboxylic acid) is very versatile to construct coordination network by various coordination modes. Three copper (I) coordination polymers have been successfully synthesized via solvent diffusion technique in test tube. The compounds all display 1D polymeric structure with rather similar coordination environment around metal ions.Moreover, they are very stable against temperature rising. The compounds $[Pb_3(CH_3COO)_2(N_3)_4]_n$ and $[Na_2Pb_2(CH_3COO)_6]_n$ were synthesized under same synthesis conditions and starting materials but with different metal salt and ligand ratios. Interestingly, the both products show three-dimensional frameworks, however, they expose different coordination structures.Actually, the investigation shows that the changing metal salt and ligand ratio can result in the formation different structures of coordination networks, although they have been produced under the same reaction conditions.Compound $[Pb(DHBDA)]_n$ has been made with ligand 2,5-Dihydroxy-1,4-benzenediacetic acid.This ligand molecule has been reported in very few works for constructing coordination compounds.

Zusammenfassung

Die hier vorliegende Arbeit behandelt die Darstellung und Charakterisierung von zehn neuen Koordinationspolymeren, die aus unterschiedlichen Metallionen und Liganden durch unterschiedliche Synthesemethoden hergestellt wurden. Neben der strukturellen Charakterisierung dieser Verbindungen anhand von Röntgen Einkristall Beugungsdaten steht die Betrachtung der thermischen und spektroskopischen Eigenschaften im Fokus. Das neue Silber-Koordinationspolymer weist einen einzigartigen, robusten und interessanten Aufbau mit hoher thermischer Stabilität auf. Zwei neue Lanthanoid-Koordinationspolymere $\{[Ln_2(FDA)_3(DMF)(H_2O)_2]\cdot DMF\cdot(H_2O)_2\}_n$(Ln = Sm, Nd) wurden mit H_2FDA = 2,5-Furandicarbonsäure in DMF als Lösungsmittel mit verschlossenem Glasreaktor im Maßstab Technik synthetisiert. Die Verbindungen sind Iso-strukturell und zeigen drei-dimensionale Koordinationspolymere. Das Ziel der Verwendung von DMF als reines Lösungsmittel anstelle einer Mischung aus dem Wasser und anderen Lösungsmitteln war die Synthese eines neuen Koordinationspolymers, das einen sehr intensiven Lumineszenzeffekt zeigen könnte. Die Untersuchung hat ergeben, dass diese Verbindungen keinen signifikanten Lumineszenzeffekt aufweisen. Wie in früheren Arbeiten berichtet wurde, in denen die H_2 FDA = 2,5-Furandicarbonsäure für den Aufbau von Lanthanoid-Koordinationspolymeren in Wasser als Lösungsmittel verwendet wurde, haben die Verbindungen sehr interessante Lumineszenzeigenschaften gezeigt [229–230]. Ein neues Ce-Koordinationspolymer wurde mit einem Liganden (H2pdc = 3,5-Pyrazoledicarbonsäure) unter Solvothermen Bedingungen in DMF als Lösungsmittel hergestellt.In der Tat ist Ligand (H2pdc = 3,5-Pyrazoledicarbonsäure) sehr vielseitig, um ein Koordinationsnetzwerke durch verschiedene Koordinationsmodi aufzubauen. Drei Kupfer (I) -Koordinationspolymere wurden erfolgreich mit der Lösungsmitteldiffusionstechnik im Reagenzglas synthetisiert. Die Verbindungen zeigen alle eine 1D-Polymerstruktur mit einem annähernden Koordinationsumfeld um die Metallionen herum. Darüber hinaus sind sie sehr stabil gegen den Temperaturanstieg. Die Verbindungen $[Pb_3(CH_3COO)_2(N_3)_4]_n$ und $[Na_2Pb_2(CH_3COO)_6]_n$ wurden unter den gleichen Synthesebedingungen und mit den gleichen Ausgangsstoffen synthetisiert, jedoch mit unterschiedlichen Metallsalz und Liganden Verhältnissen. Interessanterweise zeigen beide Produkte drei-dimensionale Gerüste, die jedoch unterschiedliche Koordinationsstrukturen aufweisen. Tatsächlich zeigt die Untersuchung, dass das sich ändernde Metallsalz- und Ligand-Verhältnis zur Bildung unterschiedlicher Strukturen von Koordinationsnetzwerken führen kann, obwohl sie unter den gleichen Reaktionsbedingungen hergestellt wurden. Die

Verbindung $(Pb(DHBDA)]_n$ wurde mit Ligand 2,5-Dihydroxy-1,4-benzoldiessigsäure hergestellt. Nur in sehr wenigen Arbeiten zur Herstellung von Koordinationspolymeren wurde dieser Ligand verwendet.

References

[1] J.C. Bailar, Jr. Prep, *Inorg. React*.**1964**,1, 1

[2] J.L. Atwood, J.W. Steed (Eds.), *Encyclopedia of Supramolecular Chemistry, Taylor & Francis*.London, 2004

[3] C.B. Aakeröy, N.R. Champness, C. Janiak, *CrystEngComm*. **2010**, 12, 22

[4] J.J. Perry IV, J.A. Perman, M.J. Zaworotko, *Chem. Soc. Rev*. **2009**, 38, 1400

[5] S. Qiu, G. Zhu, Coord. *Chem. Rev*. **2009**, 253, 2891

[6] M.J. Zaworotko, *Cryst. Growth Des*. **2007**, 7, 4

[7] S. Kitagawa, K. Uemura, *Chem. Soc. Rev*.**2005**, 34, 109

[8] C.N.R. Rao, S. Natarajan, R. Vaidhyanathan, Angew.*Chem.Int. Ed*. **2004**, 43, 1466

[9] S. Kitagawa, R. Kitaura, S. Noro, *Angew. Chem. Int. Ed*. **2004**, 43, 2334

[10] C. Janiak, *Dalton Trans*. **2003**, 2781

[11] S.L. James, *Chem. Soc. Rev*. **2003**, 32, 276

[12] (a) R.D. Joyner, M.E. Kenney, Inorg. Chem. **1962**,1, 717; (b) P.M. Kuznesof, K.J. Wynne, R.S. Nohr, M.E. Kenny, J. Chem. Sot. Chem. Commun. **1980**,121; (c) R.S. Nohr, P.M. Kuznesof, K.J. Wynne, M.E. Kenny, P.G. Siebenman, J. Am. Chem.Sot. **1981**,103, 4371; (d) R.S. Nohr, K.J. Wynne, J. Chem. Sot. Chem. Commun. **1981**, 1210; (e) K.J. Wynne and R.S. Nohr, Mol. Cryst. Liq. Cryst. **1982**, 81, 243; (f) P. Brant, R.S. Nohr, K.J. Wynne, DC. Weber, Mol. Cryst. Liq. Cryst. **1982**, 81, 255

[13] A.Y. Robin, K.M. Fromm, Coord. Chem. Rev. **2006**, 250, 2127

[14] L. Ma,O. R. Evans, B. M. Foxman, W. Lin, *Inorg. Chem.*,**1999**, *38* (25), 5837–5840

[15] Zh. Xie, L. Ma, K. E. deKrafft, A. Jin, W. Lin, *J. Am. Chem. Soc.* **2010**, *132* (3), 922–923

[16] S. Zang,Y. Su,Y. Li, Zh. Ni, Q. Meng, *Inorg. Chem.* **2006***, 45* (1), 174–180

[17] H. Hou, X. Meng, Y. Song, Y. Fan,Y. Zhu, H. Lu, C. Du, W. Shao, *Inorg. Chem.* **2002**, 41 (15), 4068–4075

[18] W. B. Lin, Z. Y. Wang, L . Ma, *J. Am. Chem. Soc.* **1999**, *121*, 11249

[19] Lin, W. B.; Evans, O. R.; Xiong, R. G.; Wang, Z. Y, *J. Am. Chem. Soc.* **1998**, 120, 13272

[20] H. W.Hou, Y. L. Song, Y. T. Fan, L. P.Zhang, C. X. Du, Y. Zhu, *Inorg. Chim. Acta.* **2001**, 316, 140

[21] M. Burak Coban, A. Amjad, M. Aygun, H. Kara, *Inorg.Chim. acta*. **2017**, 455, 25–33

[22] U. Erkarslan, G. Oylumluoglu, M.B. Coban, E. Öztürk, H. Kara, Inorg. Chim. Acta. **2016**, 445, 57–61

[23] Y. Yahsi, H. Ozbek, M. Aygun, H. Kara, Acta Crystallogr., Sect. C: Struct. Chem. **2016**, 72, 426–431

[24] Y.-X. Ren, S.-S. Xiao, X.-J. Zheng, L.-C. Li, L.-P. Jin, Dalton Trans. **2012**, 41, 2639–2647

[25] K. Liu, B. Ma, X. Guo, D. Ma, L. Meng, G. Zeng, F. Yang, G. Li, Z. Shi, S. Feng, CrystEngComm. **2015**, 17, 5054–5065

[26] W. Gao, P. Li, F. Liu, X.-M. Zhang, J.-P. Liu, CrystEngComm. **2016**, 18 ,1523–1531

[27] C. Hopa, I. Cokay, Acta Crystallogr., Sect. C: Struct. Chem. **2016**, 72

[28] Y. Yahsi, Acta Crystallogr., Sect. C: Struct. Chem. **2016**, 72, 585–592

[29] G. Cucinotta, M. Perfetti, J. Luzon, M. Etienne, P.E. Car, A. Caneschi, G. Calvez, K. Bernot, R. Sessoli, Angew. Chem. Int. Ed. **2012**, 51, 1606–1610

[30] M.-E. Boulon, G. Cucinotta, J. Luzon, C. Degl'Innocenti, M. Perfetti, K. Bernot, G. Calvez, A. Caneschi, R. Sessoli, Angew. Chem. Int. Ed. **2013**, 52, 350–354

[31] R. Sessoli, A.K. Powell, Coord. Chem. Rev. **2009**, 253, 2328–2341

[32] C. Coulon, R. Clérac, W. Wernsdorfer, T. Colin, H. Miyasaka, Phys. Rev. Lett. **2009**, 102 , 167204

[33] M. Kariem, M. Yawer, M. Kumar, H. N. Sheikh, P. Sood, S. S. Kolekar, *J. Solid State Chem*. **2017**, 255, 61–69

[34] L.E. Kreno, K. Leong, O.K. Farha, M. Allendorf, R.P. Van Duyne, J.T. Hupp, Chem. Rev. **2012**, 112 , 1105–1125

[35] J.R. Li, R.J. Kuppler, H.C. Zhou, Chem. Soc. Rev. **2009**, 38, 1477–1504

[36]Q. Meng, W. Zhang, M. Hu, J.-S. Jiang., Chem. Commun. **2016**, 52, 1957

[37] Y.Zhao, K. Li, J.Li, *Z.Naturforsch*. **2010**, 65b, 976–998.

[38] S. A. Barnett, N. R. Champness, *Coord. Chem. Rev*. **2003**, 246, 145

[39] Feature article: M. J. Zaworotko, *Chem. Commun.* **2001**, 1

[40] M. Munakata, L. P. Wu, T. Kuroda-Sowa, *Adv. Inorg. Chem.* **1999**, 46, 173

[41] Recent example: A. J. Blake, P. Hubberstey, U. Suksangpanya and C. L. Wilson, *J.Chem. Soc., Dalton Trans.* **2000**, 3873; L. Brammer,J. C. Mareque Rivas, R. Atencio, S. Fang and F. C. Pigge, *J. Chem.Soc., Dalton Trans.*, **2000**, 3855; A. L. Gillon, G. R. Lewis, A.

[42] Examples with complementary hydrogen bonding: A. D. Burrows,R. W. Harrington, M. F. Mahon and C. E. Price, *J. Chem. Soc.,Dalton Trans.* **2000**, 3845; C. B. Aakeröy, A. M. Beatty andK. R. Lorimer, *J. Chem. Soc., Dalton Trans.***2000**, 3869; C. B. Aakeröy, A. M. Beatty, D. S. Leinen and K. R. Lorimer, *Chem.Commun.* **2000**, 935

[43] Reviews on hydrogen-bonded assemblies: S. Subramanian andM. J. Zaworotko. *Coord. Chem. Rev.* **1994**, 137, 357; C. B. Aakeröyand A. M. Beatty, *Aust. J. Chem.* **2001**, 54, 409

[44] S. Leininger, B. Olenyuk and P. J. Stang, *Chem. Rev.* **2000**, 100, 853; B. Olenyuk, A. Fechtenkötter and P. J. Stang, *J. Chem. Soc., DaltonTrans.* **1998**, 1707; P. J. Stang and B. Olenyuk, *Acc. Chem. Res.* **1997**, 30, 502

[45] M. Fujita, *Chem. Soc. Rev.***1998**, 27, 417

[46] R.-D. Schnebeck, E. Freisinger and B. Lippert, *Eur. J. Inorg. Chem.* **2000**, 1193

[47] M. Fujita, *Acc. Chem. Res.* **1999**, 32, 53; M. Fujita, in *MolecularCatenanes, Rotaxanes and Knots*, ed. J.-P. Sauvage and C. Dietrich-Buchecker. Wiley-VCH, Weinheim, **1999** ,57–76

[48] D. L. Caulder and K. N. Raymond, *J. Chem. Soc., Dalton Trans.***1999**, 1185; D. L. Caulder and K. N. Raymond. *Acc. Chem. Res.***1999**, 32, 975

[49] See the special feature on supramolecular chemistry and selfassembly in *Proc. Natl. Acad. Sci. USA*. **2002**, 99, 4762

[50] T. Steiner, *Angew. Chem. Ed. Engl*. **2002**, 41, 48

[51] A. Nangia, *Cryst. Eng. Commun*. **2002**, 4, 93

[52] G. Aullon, D. Bellamy, A.G. Orpen, L. Brammer, E.A. Bruton, *Chem. Comm*. **1998**, 653.

[53] G.R. Desiraju, *Acc. Chem. Res*. **1996**, 29, 441

[54] N. S. Oxtoby, A. J. Blake, N. R. Champness and C. Wilson, *Proc.Natl. Acad. Sci. USA*. **2002**, 99, 4905

[55] M. Eddaoudi, J. Kim, D. Vodak, A. Sudik, J. Wachter, M. O'Keeffeand O. M. Yaghi, *Proc. Natl. Acad. Sci. USA*. **2002**, 99, 4900

[56] C. Janiak, *J. Chem. Soc. Dalton Trans*. **2000**, 3885

[57] S.Sengupta, A.Goswami, S.Ganguly, S.Bala, M.K. Bhunia , R. Mondal, *Cryst. Eng.Commun*. **2011**, 13, 6136

[58] E. Semitut, T. Sukhikh, E. Filatov, A. Ryadun, A. Potapov, Crystals. **2017**, 7, 354

[59] C.-Y. Sun**,** C. Qin, X.-L. Wang**,** G.-S. Yang**,** K.-Z. Shao**,** Y.-Q. Lan**,** Z.-M. Su**,** P. Huang**,** C.-G. Wang, E.-B. Wang, Dalton Trans. **2012**, 41, 6906–6909

[60] P. Horcajada, R. Gref, T. Baati, P. K. Allan, G. Maurin, P. Couvreur, G. Férey, R. E. Morris, C. Serre., *Chem. Rev.* **2012**, 112 (2), 1232–1268

[61] L. E. Kreno, K. Leong, O. K. Farha, M. Allendorf, R. P. Van Duyne, J. T. Hupp, *Chem. Rev.* **2012**, 112 (2), 1105–1125

[62] P. Horcajada, T. Chalati, C. Serre, B. Gillet, C. Sebrie, T. Baati, J. F. Eubank, D. Heurtaux, P. Clayette, C. Kreuz, J.-S. Chang, Y. Kyu Hwang, V. Marsaud, P.-N. Bories, L. Cynober, S. Gil, G. Férey , P. Couvreur, R. Gref, Nature Material. **2010**, 9, 172–178

[63] C.-D. Wu, A. Hu, L. Zhang, W. Lin, *J. Am. Chem. Soc.* **2005**, 127 (25), 8940–8941

[64] C. Janiak, *Dalton Trans.* **2003**, 2781–2804

[65] M. Gu,Y. Ren,Y. Hu, M.Tang, Z. Kong, B.Yue, H. He, Eur. J. Inorg. Chem. **2015**, 488–493

[66] A.-X. Tian, J. Ying, J. Peng, J.-Q. Sha, H.-J. Pang, P.-P. Zhang, Y. Chen, M. Zhu, Z.-M. Su, *Inorg. Chem.* **2009**, 48 (1), 100–110

[67] A.-X. Tian, J. Ying, J. Peng, J.-Q. Sha, H.-J. Pang, P.-P. Zhang, Y. Chen, M. Zhu, Z.-M. Su, *Cryst. Growth Des.* **2008**, 8 (10), 3717–3724

[68] H.-Y. An, E.-B. Wang, D.-R. Xiao, Y.-G. Li, Z.-M. Su, L. Xu, Angew. Chem. **2006**, 118, 918 –922

[69] F.A. Mautner, R. Cortés, L. Lezama and T. Rojo, *Angew. Chem. Int. Ed. Engl*. **1996**, 35, 78–81

[70] H. S. Yoo, J. I. Kim, N. Yang, E. K. Koh, J.-G. Park,C. S. Hong, Inorg. Chem. **2007**, 46 (22), 9054–9056

[71] Y.-Q. Wang, Y.-F. Gao, Q.-H. Tan, Z.-L. Liu, E.-Q. Gao, Inorg.Chem.Commun. **2014**, 45, 101–104

[72] T. C. Stamatatos, J.C. Vlahopoulou, V. Tangoulis, C. P. Raptopoulou, A. Terzis, G. S. Papaefstathiou, S. P. Perlepes, Polyhedron. **2009**, 28, 1656–1663

[73] Y. Zeng, S.-J. Liu, C.-M. Liu,Y.-R. Xie, Z.-Y. Du, New J. Chem. **2017**, 41, 1212–1218

[74] C. J. Adams, M. C. Muñoz, R. E. Waddington, J. Antonio Real, *Inorg. Chem.* **2011**, 50 (21), 10633–10642

[75] X. Y. Wang, B. L. Li, X. Zhu and S. Gao, *Eur. J. Inorg. Chem*. **2005**, 3277–3286

[76] P. M. Secondo, J. M. Land, R. G. Baughman, H. L. Collier, Inorg.Chim.Acta. **2000**, 309 (1–2), 13–22

[77] A.O.Legendre, A.E.Mauro, J.G.Ferreira, S.R.Ananias, R.H.A.Santos, Adelino V.G.Netto, *Inorg. Chem.Commun*. **2007**, 10, 815–820

[78] S. Wöhlert, U. Ruschewitz, C. Näther, *Cryst. Growth Des.* **2012**, 12 (6), 2715–2718

[79] N. de la Pinta, G.Madariaga, T. Ezpeleta, M.Luz Fidalgo, L. Lezama, R. Cortés, Polyhedron. **2013**, 52, 1256–1261

[80] W.-Y. Yan, R.-T. He, M. Dai, Z.-G. Ren, H.-X. Li, J.-P. Lang, Inorg. Chem. Comm. 2013, 36, 51–55

[81] G.-C. Xu, Y.-J. Ding, T.-A. Okamura,Y.-Q. Huang, Z.-S. Bai, Q. Hua, G.-X. Liu, W.-Y. Sun, N. Ueyama, *Cryst. Growth Des.* **2009**, 9 (1), 395–403

[82] P. Amo-Ochoa, O. Castillo, F. Zamoraa, *Dalton Trans*. **2013**, 42, 13453

[83] G. Mahmoudi, A. Morsali, L.-G. Zhu, Polyhedron. **2007**, 21(26), 2885

[84] M. M. Dîrtu, Y. Boland, D. Gillard, B. Tinant, K. Robeyns, D. A. Safin, E. Devlin, Y. Sanakis ,Y. Garcia, *Int. J. Mol. Sci.* **2013**, 14(12), 23597–23613

[85] N. Zhao , Y.-E. Deng , P. Liu, C.-X. An, T.-X. Wang , Z.-X. Lian, *Transition Met Chem* . **2015**, 40, 11–19

[86] G. M. Sequeira **,** W. Y. Tan and E. G. Moore, Dalton Trans. **2015**, 44, 13378–13383

[87] H. Guo **,** Y. Yan **,** X. Guo **,** H. Zou **,** Y. Qi, C. Liu, Cryst. Eng. Commun. **2014,** 16, 10245–10254

[88] R. R. Ozer, J. P. Hinestroza, RSC Adv. **2015**, 5, 15198–15204

[89] S.-I. Noro, S. Kitagawa , T. Akutagawa, T.Nakamura, Prog. Poly. Sci. 2009, 34(3), 240–279

[90] (a) G. Minguez Espallargas, E. Coronado, Chem. Soc. Rev. **2018**, 47, 533–557.(b) P.Z. Li, X.J. Wang, Y. Li, Q. Zhang, R.H.D. Tan, W.Q. Lim, R. Ganguly, Y. Zhao, Microporous Mesoporous Master. **2013**, 176, 194–198

[91] L.Chen, H.Y. Jia, X.J. Hong, D.H. Chen, Z.P. Zheng, H.G. Jin, Z.G. Gu, Y.P. Cai, *Inorg. Chem. Commun*. **2013**, 27, 22–25

[92] Y.X. Sun, W. Y. Sun, Chin. Chem. Lett. **2014**, 25(6), 823–828

[93] D.Kim, X.Song, J.H. Yoon, M.S. Lah, Cryst. Growth Den. **2012**, 12 (8), 4186–4193

[94] P. Mahata, M. Parbu, S. Natarajan, Inorg. Chem. **2008**, 47(19), 8451–8463

[95] X.Q. Lü, J.J. Jiang, C.L. Chen, B.S. Kang, C.Y. Su, *Inorg. Chem*. **2005**, 44(13), 4515–4512

[96] S.A. Bourne, L.J.Moitsheki, *Cryst.Eng.Comm*. **2005**, 7 (112), 674–681

[97] S.C. McKellar, A.J. Graham, D.R. Allan, M.I.H. Mohideen, R.E. Morris, S.A. Moggach, *Nanoscale*. **2014**, 6 (8) , 4163–4173

[98] R.Seetharaj, P.V.Vandana, P.Arya, S.Mathew, *Arabian Journal of Chemistry*. **2016**, 19–21

[99**]** Y. yang Dang, D. xing Ju, L. Wang, X. Tao, CrystEngComm. **2016**, 18, 4476–4484

[100] G.H. Wang, Z.G. Li, H.Q. Jia, N.H. Hu, J.W. Xu ,*CrystEngComm*. **2009**, 11 (2), 292–297

[101] P. Li, Y. He, J. Guang, L. Weng, J.C.-G. Zhao, S. Xiang, B.Chen, *J. Am. Chem. Soc*. **2014**, 136 (2), 547–549

[102] S. Zhang, X. Liu, Q. Yang, Q. Wei, G. Xie, S.Chen, *Cryst. Eng. Comm*. **2015**, 17 (17), 3312–3324

[103] Introduction to crystal growth, Prof. V. Krishnakumar. **2014**, 1–18

[104] (a) S. Miller, *Tips and Tricks for the Lab: Growing Crystals Part 3*, Chem.Pub.Soc. **2016**, 1. (b) R.Q. Zou, L. Jiang, H. Senoh, N. Takeichi, Q. Xu, *Chem.Commun*. **2005**, 28, 3526–3528

[105] A. Y. Robin **,** J. L. Sagué, K. M. Fromm, CrystEngComm. **2006**, 8, 403–416

[106] Alexander J. Blake ,Crystal Growth, Evaluation and Handling

[107] S. Miller, *Tips and Tricks for the Lab: Growing Crystals Part 3*, Wiley-VCH Verlag, **2012**, 1

[108] S. K. Arora, V. Patel, A. Kothari, B. Amin, *Cryst. Growth Des*. **2004**, 4(2), 343

[109] C. Barta, Z. Zemelicka and V. Rene, *J. Cryst. Growth*. **1971**, 10, 158

[110] M. Ohta, M. Tsutsumi, *J. Cryst. Growth* . **1979**, 47, 135

[111] C. K.Chauhan, Mihir. J. Joshi, *J. Cryst. Growth*. **2013**, 362, 330–337

[112] G. Mahmoudi, A. Morsali, CrystEngComm. **2009**, 11, 1868–1879

[113] H. Sadeghzadeh, A. Morsali, CrystEngComm. **2010**, 12, 370–372

[114] A. Aslani, A. Morsali, M. Zeller, Solid State Sciences. **2008**, 10, 1591–1597

[115] M. J. Soltanian, Fard-Jahromi, A. Morsali, Ultrasonics Sonochemistry. **2010**, 17, 435–440

[116] (a) G. Mahmoudi**,** A. Morsali, A. D. Hunter, M. Zeller,CrystEngComm. **2007**, 9, 704–714 (b) H. Shirdel, F. Marandi, A. Jalilzadeh, S. Pourbeyram, S.Huber, A. Pfitzner, Main Group Chemistry. **2015**, 14, 105

[117] K. Byrappa, T. Adschiri, Progress in Crystal Growth and Characterization of Materials. **2007** , 53, 117–166

[118] J. A. Darr, J. Zhang, N. M. Makwana, X. Weng, *Chem. Rev.* **2017**, 117 (17), 11125–11238

[119] Q.B. Bo, J.J. Pang, H.Y. Wang, C.H. Fan, Z.W. Zhang, *Inorg. Chim. Acta*. **2015**, 428, 170–175

[120] A.Y. Robin, K.M. Fromm, *Coordination Chemistry Reviews*. **2006**, 250 , 2127–2157

[121] Teflon Lined Hydrothermal Synthesis Autoclave Acid Digestion Reactor and PTFE lined and PPL lined are available and Benefits of PTFE chamber of teflon lined hydrothermal synthesis autoclave reactor produced by toption company

[122] V.P. Balema, J.W. Wiench, M. Pruski, V.K. Pecharsky, Chem Commun. **2002**, 1606–1607

[123] A. Orita, L. Jiang, T. Nakano, N. Ma, J. Otera , *Chem Commun*. **2002**, 1362–1363

[124] M. Tsuchimoto, G. Hoshina, N. Yoshioka, H. Inoue, K. Nakajima, M. Kamishima, *et al., J Solid State Chem*. **2000**, 153, 9–15

[125] P.J. Nichols, C.L. Raston, J.W. Steed., Chem Commun., **2001**, 1062–1063

[126] W.J. Belcher, C.A. Longstaff, M.R. Neckening, J.W. Steed, *Chem Commun*. **2002**, 1602–1603

[127] D. Braga, M. Curzi, F. Grepioni, M. Polito, *CrystEngComm*. **2004**, 6, 459–463

[128] D. Braga, M. Curzi, F. Grepioni, M. Polito, *Chem Commun*. **2005**, 2915–2917

[129] A. Pichon, A. Lazuen-Garay, S.L. James, CrystEngComm. **2006**, 8, 211–214

[130] G. Zhan, H. C. Zeng, Chem. Commun. **2017**, 53, 72–81

[131] M. Du, C.-P. Li, C.-S. Liu, S.-M. Fang, Coord.Chem.Rev. **2013**, 257(7–8), 1282–1305

[132] S. Jung, M. Oh ,*Angew. Chem. Int. Ed. Engl*. 2008, 47, 2049–2051

[133] M. Gustafsson, X. Zou, *J. Porous Mater*. **2013**, 20, 55–63

[134] P. Horcajada, C. Serre, D. Grosso, C. Boissiere, S. Perruchas, C. Sanchez, G. Ferey, *Adv. Mater*. **2009**, 21, 1931–1935

[135] L.S. Long, *Cryst.Eng.Comm*. **2010**, 12, 1354–1365

[136] B. Seoane, S. Castellanos, A. Dikhtiarenko, F. Kapteijn, J.Gascon, Coord. Chem. Rev. 2016, 307, 147–187

[137] S. Jung, M. Oh, *Angew. Chem. Int. Ed. Engl*. **2008**, 47, 2049–2051

[138] H.J. Lee, W. Cho, M. Oh, *CrystEngComm*. **2010**, 12, 3959–3963

[139] S. Noro, R. Kitaura, M. Kondo, S. Kitagawa, T. Ishii, H. Matsuzaka, *et al. J. Am. Chem Soc*., **2002**, 124 , 2568–2583

[140] S. Das, S. Sen, P. K. Bharadwaj, *Inorg. Chim. Acta*. **2011**, 372, 425–428

[141] R. C. Leif, L. M. Vallarino, M. C. Becker, S. Yang,Cytometry Part A. **2006**, 69A, 767–778

[142] Y. Hasegawa, T. Nakanishi, *RSC Adv*. **2015** , 5, 338–353

[143] A. Thirumurugan, S. K. Pati, M. A. Greenc, S. Natarajan, *J. Mater. Chem.* **2003**, 13, 2937

[144] C. Daiguebonne, N. Kerbellec, O. Guillou, J.-C. G. Büzli, F. Gumy, L. Catala, T. Mallah, N. Audebrand, Y. Geraut, K. Bernot, G. Calvez, *Inorg. Chem.* **2008** , 47, 3700

[145] K. Binnemans, *Chem. Rev.* **2009** , 109, 4283

[146] C. Marchal, Y. Filinchuk, X.-Y. Chen, D. Imbert, M. Mazzanti, *Chem. Eur. J.* **2009**, 15, 5273

[147] T. M. Reineke, M. Eddaoudi, M. Fehr, D. Kelley, O. M. Yaghi, *J. Am. Chem. Soc.* **1999**, 121, 1651–1657

[148] J. Rocha, L. D. Carlos, F. A. A. Paza, D. Ananias, *Chem. Soc. Rev.* **2011**, 40, 926–940

[149] Y.-Q. Sun, J. Zhanga, G.-Y. Yang, *Chem. Commun.* **2006**, 4700–4702

[150] Z.-H. Zhang, T. Okamura, Y. Hasegawa, H. Kawaguchi, L.-Y. Kong, W.-Y. Sun, N. Ueyama, *Inorg. Chem.* **2005**, 44, 6219–6227

[151] D. T. Lill, A. Bettencourt-Dias, C. L. Cahill, *Inorg. Chem.* **2007**, 46, 3960–3965

[152] K. A. White, D. A. Chengelis, K. A. Gogick, J. Stehman, N. L. Rosi, S. Petoud, *J. Am. Chem. Soc.* **2009**, 131, 18069

[153] P. Mahata and S. Natarajan, *Inorg. Chem.* **2007**, 46, 1250–1258

[154] X. Feng, J. Zhao, B. Liu, L. Wang, S. Ng, G. Zhang, J. Wang, X. Shi, Y. Liu, *Cryst. Growth Des.* **2010**, 10, 1399–1408

[155] Z. He, C. He, E.-Q. Gao, Z.-M. Wang, X.-F. Yang, C.-S. Liao, C.-H. Yan, *Inorg. Chem.* **2003**, 42, 2206–2208

[156] C. Serre, F. Pelle, N. Gardant and G. Ferey, *Chem. Mater.* **2004**, 16, 1177–1182

[157] Y. Su, J. Yu, Y. Li, S. F. Zeng Phua, G. Liu, W. Qi Lim, X. Yang, R. Ganguly, C. Dang, C. Yang, Y. Zhao, *Communications Chemistry*. **2018**, 1–12

[158] B. D. Chandler, J. O. Yu, D. T. Cramb, G. K. H. Shimizu, *Chem. Mater.* **2007**, 19, 4467–4473

[159] W. Liu, T. Jiao, Y. Li, Q. Liu, M. Tan, H. Wang, L. Wang, *J. Am. Chem. Soc.* **2004**, 126, 2280–2281

[160] L. Pan, K. M. Adams, H. E. Hernandez, X. Wang, C. Zheng, Y. Hattori, K. Kaneko, *J. Am. Chem. Soc.* **2003**, 125, 3062–3067

[161] J. Rocha, L. D. Carlos, F. A. A. Paza, D. Ananias, *Chem. Soc. Rev.* **2011**, 40, 926–940

[162] J. W. Verhoeven, Pure Appl. Chem. 1996, 68, 2223–2286

[163] J. Heine, K. Müller-Buschbaum, *Chem. Soc. Rev*. **2013**, 42, 9232

[164] S. V. Eliseevaa, J.-C. G. Bünzli, *Chem. Sci*. **2013**, 4, 1939–1949

[165] S. V. Eliseeva, J.-C. G. Bünzli, *Chem. Soc. Rev*. **2010**, 39, 189–227

[166] A. Vogler, H. Kunkely, *Inorg. Chim. Acta.* **2006**, 359, 4130–4138

[167] J. Rocha, L. D. Carlos, F. A. Almeida Paz, D. Ananias, *Chem. Soc*., Rev. **2011**, 40, 926–940

[168] M. D. Allendorf, C. A. Bauer, R. K. Bhaktaa, R. J. T. Houka, *Chem. Soc. Rev*. **2009**, 38, 1330–1352

[169] N. V. Sidgwick, H. M. Powell, *Proc. R. Soc. (London).* **1940**, 176, 153– 180

[170] F. H. Allen, *Acta Crystallogr. Sect. B.* **2002**, 58, 380– 388

[171] R. J. Gillespie, R. S. Nyholm, *Q. Rev. London* 1957, 11, 339− 380; R. J. Gillespie, I. Hargittai, *The VSEPR Model of Molecular Geometry*; Allyn and Bacon: Boston, MA, **1991**

[172] M. Imran,A. Mix, B. Neumann,H.-G. Stammler,U. Monkowius, P. Gründling, N. W. Mitzel, Dalton Trans. **2015**, 44, 924–937

[173] A.-V. Mudring, F. Rieger, *Inorg. Chem.* **2005**, 44, 6240– 6243

[174] A. Walsh, G. W. Watson, *J. Solid State Chem.* **2005**, 178, 1422– 1428

[175] A.-V. Mudring, *Eur. J. Inorg. Chem.* **2007**, 882– 890

[176] L. Shimoni-Livny, J. P. Glusker, C. W. Bock, *Inorg. Chem.* **1998**, 37, 1853– 1867

[177] I. Persson, K. Lyczko, D. Lundberg, L. Eriksson, A. Płaczek, *Inorg. Chem.* **2011**, 50 (3), ,1058–1072

[178] A. Mos-Hummel, M. Ströbele, H.-Jürgen Meyer, Dalton Trans. **2017**, 46, 7743–7749

[179] M.-L. Hu, A. Morsali, L. Aboutorabi, Coord.Chem.Rev. **2011**, 255(23–24), 2821–2859

[180] A. Aslani, A. Morsali, Inorg. Chim. Acta, **2009**, 362, 5012

[181] A. Aslani, A. Morsali, V.T. Yilmaz, C. Kazak, J. Mol. Struct. **2009**, 929,187

[182] N. Noshiranzadeh, A. Ramazani, A. Morsali, A.D. Hunter, M. Zeller, Inorg. Chem. Commun. **2007**, 10, 738

[183] A. Aslani, A. Morsali, M. Zeller, Solid State Sci. **2008**, 10, 854

[184] F. Marandi, A.A. Soudi, A. Morsali, R. Kempe, J. Coord. Chem. **2005**, 58, 1233

[185] S.-M. Fang, M. Hu, Q. Zhang, M. Du, C.-S. Liu, *Dalton Trans*. **2011**, 40, 4527

[186] M.-L. Tong, X.-M. Chen, S.W. Ng, *Inorg. Chem. Commun*. **2000**, 3(8), 436–441

[187] A.J. Blake, G. Baum, N.R. Champness, S.S.M. Chung, P.A. Cooke, D. Fenske, A.N. Khlobystov, D.A. Lemenovskii, W.-S. Li, M. Schröder, *Dalton Trans*. **2000**, 4285 –4291

[188] Q. Chu, D.C. Swenson, L.R. MacGillivray, *Angew. Chem., Int. Ed*. **2005**, 44(23), 3569

[189] R. Santra, K. Biradha, *Cryst. Growth Des*. **2010**, 10(8), 3315–3320

[190] M. Nagarathinam, J.J. Vittal, *Angew. Chem., Int. Ed*. **2006**, 45(26), 4337

[191] S. Roy, H. M. Titi, B. Kumar Tripuramallu, N. Bhunia, R. Verma, I. Goldberg, *Cryst. Growth Des.* **2016**, 16 (5), 2814–2825

[192] Z.-J. Zhang, H.-Y. Liu, S.-Y. Zhang, W. Shi, P.Cheng, Inorg.Chem.Commun. **2009**, 12(3), 223–226

[193] Rodney P. Feazell, Cody E. Carson, Kevin K. Klausmeyer, *Inorg. Chem.* **2005**, 44 (4), 996–1005

[194] Z.P. Deng, Z.B. Zhu, S. Gao, L.H. Huo, H. Zhao, S. Weng Ng., *Dalton Trans*., **2009**, 33,6552–6561

[195] Y. Song, R.Q. Fan, S. Gao, X.M. Wang, P. Wang, Y.L. Yang, Y.L. Wang, *Inorg. Chem. Commun.* **2015**, 53, 34

[196] A.P. Cote, M.J. Ferguson, K.A. Khan, G.D. Enright, A.D. Kulynych, S.A. Dalrymple, G.K.H. Shimizu, *Inorg. Chem*. **2002**, 41, 287

[197] S.-S. Shen, X. Wang, H.-M. Hu , F.Yuan, F.-X. Dong,G. Xue, *Polyhedron*. **2015**, 91, 52–58

[198] O. Kristiansson, *Inorganic Chemistry*. **2001**, 40(20), 5058–5059

[199] M.L. Tong, X.M. Chen, B.H. Ye, S.W. Ng, *Inorganic Chemistry*, **1998**, 37(20), 5278–5281

[200] B.L. Fei, W.Y. Sun, T.A. Okamura, W.X. Tang, N. Ueyama. *New J. Chem*., **2001**, 25, 210–212

[201] S. Dawn, S. R. Salpage, M. D. Smith, S. K. Sharma, L. S. Shimizu, *Inorg. Chem. Common*. **2012**, 15, 88–92

[202] D. Mal, R. Sen, P. Brandao, F. Shi, R. A.S. Ferreira, Z. Lin. *Inorg. Chem. Common*. **2014**, 40, 92–96

[203] Y.-Z. Zheng, Z. Zheng, X.-M. Chen, *Coordin. Chem. Rev*. **2014**, 258–259, 1–15

[204] S.-J. Liu **,** L. Xue **,** T.-L. Hu, X.-H. Bu , *Dalton, Trans.* **2012**, 41, 6813–6819

[205] G. Guerrero **,** J. G. Alauzun **,** M. Granier **,** D. Laurencin, P. H. Mutin, *Dalton,Trans.* **2013**, 42, 12569–12585

[206] K. Su, F. Jiang, J. Qian, J. Pan, J. Pang, X. Wan, F. Hu, M. Hong, *RSC Adv.* **2015**, 5, 33579–33585

[207] J. Zhu, X. Bu, P. Feng, G. D. Stucky, *J. Am. Chem. Soc.* **2000**, 46, 11563–11564

[208] J.-J. Hou, X.-M. Zhang, *Cryst. Growth Des*. **2006**, 6(6), 1445–1452

[209] M. Sanselme, M. Riou-Cavellec , J.-M. Grenèche, G. Férey, *J. Solid State Chemistry*. **2002**, 164(2), 354–360

[210] S. Lodhia, A. Turner, M. Papadaki, K. D. Demadis, G. B. Hix, *Cryst. Growth Des*. **2009**, 9(4), 1811–1822

[211] L.-L. Lv, L.-J. Zhang, H. Zhao, B.-L. Wu, *Polyhedron*. **2016**, 155, 204–211

[212] G.-Q. Zhong, D. Li, Z.-P. Zhang, *Polyhedron*. **2016**, 111, 11–15

[213] G. B. Deacon and R. J. Philllips, Coord. Chem. Rev., **1980**, 33, 227

[214] A. Patra, T. K. Sen, R. Bhattacharyya, S. K. Mandal, M. Bera, *RSC Adv.* **2012**, 2, 1774–1777.

[215] T. Ishioka, Y. Shibata, M. Takahaski, I. Kanesaka, Y. Kitagawa and K. T. Nakamura, Spectrochim, *Acta, Part A.* **1998**, 54, 1827

[216] V. Zelenak, I. Cisarova and P. Lewellyn, *Inorg. Chem. Commun*. **2007**, 10, 27

[217] V. Zelenak, M. Sabo, W. Massa and P. Llewellyn, *Inorg. Chim. Acta.* **2004**, 357, 2049

[218] K. Nakamoto, Infrared and Raman Spectra of Inorganic and Coordination Compounds, John Wiley & Sons, New York, **1997**

[219] B. S. Manhas and A. K. Trikha, *J. Indian Chem. Soc*. **1982**, 59, 315

[220] D. Martini, M. Pellei, C. Pettinari, B. W. Skelton and A. H. White, *Inorg. Chim. Acta.* **2002**, 333, 72

[221] J.-Q. Liu , J. Wu , Y.-Y. Wang , J.-T. Lin, H. Sakiyama, *CrystEngComm.* **2014**, 16, 3103–3112

[222] Y.-Z. Zheng, Z. Zheng, X.-M. Chen, *Coord.Chem.Rev*. **2014**, 258–259, 1–15

[223] L. Wu, D. Chigan, L. Yan, H. Chen, RSC Adv. **2017**, 7, 5541–5548

[224] N. Scales, Y. Zhang, M. Bhadbhade, I. Karatchevtseva, Linggen Kong, *Polyhedron*. **2015**, 102,130–136

[225] D. Pizon, N. Henry, T. Loiseau , P. Roussel, F. Abraham, *J. Solid State. Chem.* **2010**, 183, 1943–1948

[226] N.E. Brese, M. O'Keeffe, Acta Crystallogr.B. **1991**, 47, 192

[227] Z.Wang, C.-M. Jin, T. Shao, Y.-Z. Li, K.-L. Zhang, H.-T. Zhang, X.-Z. You , *Inorg Chem Commun*. **2002**, 5 (9), 642–648

[228] L.-P. Zhang , Y.-H. Wan , L.-P. Jin, *Polyhedron*. **2003**, 22, 981–987

[229] H. Wang, S.-J. Liu, D. Tian, J.-M. Jia, and T.-L. Hu, *Cryst. Growth Des.* **2012**, 12, 3263–3270

[230] H.-H. Li, W. Shi, N. Xu, Z.-J. Zhang, Z. Niu, T. Han, P. Cheng, *Cryst. Growth Des.* **2012**, 12 (5), 2602–2612

[231] L. Yang, L. Wu, H. Zhang, S. Song, L. Liu, M. Li, Dyea and Pigments. **2013**, 99(2), 257–267

[232] Iurie L. Malaestean, M. Kutluca-Alıcı, A. Ellern, J. van Leusen, H. Schilder, M. Speldrich, Svetlana G. Baca, P. Kögerler, *Cryst. Growth Des.* **2012**, 12 (3),1593–1602

[233] P. Gohari Derakhshandeh, J. Soleimannejad, J. Janczak, Ultra.Sonochemistry., **2015**, 26, 273–280

[234] R. Mohammadinasab, M. Tabatabaee , B.-M. Kukovec, H. Aghaie, Inorg Chim Acta. **2013**, 405, 368–373

[235] T.-H. Yang, A. Rosa Silvaa , F.-N. Shi, Dalton trans, **2013**, 42, 13997

[236] Q. Wang, X. Yan, H. Zhang, W. Liu, Y. Tang, M. Tan, J Solid State Chem. **2011**, 184, 164–170

[237] Y. Su, L. Yang, Y. Xu, Z. Wang, S. Weng, C. Yan, D. Wang, J. Wu, Inorg. Chem. **2007**, 46, 5508–5517

[238] W. D. G. Nunes, J. A. Teixeira, A. L. C. S. do Nascimento, F. J. Caires, E. Y. Ionashiro, M. Ionashiro, J Therm Anal Calorim. **2016**, 125, 397–405

[239] R. Hammami, H. Batis, *Arabian J.Chem*. **2017**, 1–11

[240] A. Dehno Khalaji, K. Jafari , B. Bahramian, K. Fejfarova, M. Dusek, *Monatsh Chem*. **2013**,144

[241] A. Dehno Khalaji, J. Rohlicek, P. Machek, D. Das, *J. Clust Sci*. **2014**, 25, 1425–1434

[242] A. Dehno Khalaji, S. J. Peyghoun, A. Akbari, N. Feizi, M. Dusek, V. Eigner, *Polyhedron*. **2016**, 119, 429–433

[243] A. Dehno Khalaji, S. J. Peyghoun, A. Akbari, N. Feizi, M. Dusek, V. Eigner, *J. Molecular structure* . **2017**, 1127, 511–514

[244] X. H. Zhou,T. Wu, D. Li ,Inorg Chim Acta. **2006**, 359–1442

[245] K. Matjani, M. Mousavi,E. Ahmadi, D. L.Hughes, Inorg Chim Acta. **2011**, 376–408

[246] A. D. Khalaji, H. Stoeckli Evans,D. Das, Monatsh Chem. **2012**, 143–595

[247] A. D. Khalaji, S. Triki, D. Das ,J Therm Anal Calorim. **2011**,103–779

[248] M. Morshedi , M. Amirnasr, S.Triki, A. D. Khalaji, Inorg Chim Acta. **2009**, 362–1637

[249] A. D. Khalaji, H. Hadadzadeh, M. Daryanavard, Inorg Chim Acta. **2009**, 362–4837

[250] K. Gotoh, H. Ishida, Acta Cryst E. **2009**, 65, 70

[251] Jahangir Mondal, Anindita Mukherjee, Goutam K. Patra, Inorg Chim Acta. **2017**, 463, 44–53

[252] T.-H. Huang , H. Yang, G. Yang, S.-L. Zhu, C.-L. Zhang, Inorg Chim Acta. **2017**, 455, 1–8

[253] L.-R. Lu, M. Shao, Z.-X. Wang, X. He, M.-X. Li, Inorg. Chem. Commun. **2017**, 79, 25–28

[254] A. Beheshti , V. Nobakht, L. Carlucci, D. M. Proserpio, C. Abrahams, *J. Molecular structure*. **2013**, 1037, 236–241

[255] M. Hakimi , K. Moeini, Z. Mardani, F Mohr, *Polyhedron*. **2014**, 70, 92–100

[256] M. Maekawa, A. Minamino, K. Sugimoto, T. Okubo, T. K. Sowa, M. Munakata, Inorg Chim Acta. **2014**, 114, 257–263

[257] M.-L. Hu , A. Morsali, L. Aboutorabi, Coord Chem Rev. **2011**, 255, 2821–2859

[258] L. Shimoni-Livny, J.P. Glusker, C.W. Bock, Inorg. Chem. **1998**, 37, 1853

[259] A. Aslani, A. Morsali, Inorg. Chim. Acta. **2009**, 362, 5012

[260] A. Aslani, A. Morsali, V.T. Yilmaz, C. Kazak, J. Mol. Struct. **2009**, 929,187

[261] N. Noshiranzadeh, A. Ramazani, A. Morsali, A.D. Hunter, M. Zeller, Inorg. Chem. Commun. **2007**, 10, 738

[262] A. Aslani, A. Morsali, M. Zeller, Solid State Sci. **2008**, 10, 854

[263] A. Morsali, Z. Naturforsch. **2005**, 60b, 149

[264] Shimoni-Livny, L., Glusker, J. P., Bock, C. W, Inorg. Chem. **1998**, 37, 1853–1867

[265] H. Keypour, M. Rezaeivala, L. Valencia, P. Pérez-Lourido, Polyhedron. **2009**, 28(18), 4096–4100

[266] (a) A. Rana, M. Bera, D. S. Chowdhuri, B. Bag, R. J. Butcher, S. Dalai, J. Molecular Structure. **2011**, 990(1–3), 102–109; (b) H.-J. Shin, B.-K. Min, J Inorg Organomet Polym. **2013**, 23, 1305–1312; (c) B. Mirtamizdoust, S. Ali-Asgari, S. W. Joo, E. Maskani, Y. Hanifehpour, T. H. Oh, J Inorg Organomet Polym. **2013**, 23, 751–757

[267] S.S. Massoud, F.R. Louka, Y.K. Obaid, R. Vicente, J. Ribas, R.C. Fischer, F.A. Mautner, Dalton Trans. **2013**, 24, 3968 azide ions

[268] F.A. Mautner, F.R. Louka, J. Hofer, M. Spell, A. Lefèvre, A.E. Guilbeau, S.S. Massoud, Cryst. Growth Des. **2013**, 13, 4518

[269] A.S. Goher, F.A. Mautner, B. Sodin, B. Bitschnau, J. Mol. Struct. **2008**, 879(1–3), 96

[270] J. Carranza, J. Sletten, F. Lloret, M. Julve, J. Mol. Struct. **2008**, 890(1–3), 31–40

[271] M.A.S. Goher, Acta Chim. Hung. **1990**, 127, 213

[272] I. Agrell, Acta Chem. Scand. **1971**, 25, 2965

[273] D. Forster, W.D. Horrocks, Inorg. Chem. **1966**, 5, 1510

[274] (a) W. Beck, W.P. Fehlhammer, P. Pöllmann, E. Schuierer, K. Feldl, Chem. Ber. **1967**, 100, 2335.(b) W. Beck, W.P. Fehlhammer, P. Pöllmann, E. Schuierer, K. Feldl, Angew. Chem. **1965**, 77, 458

Appendix

A.1. The TG and DSC curves of new coordination polymers

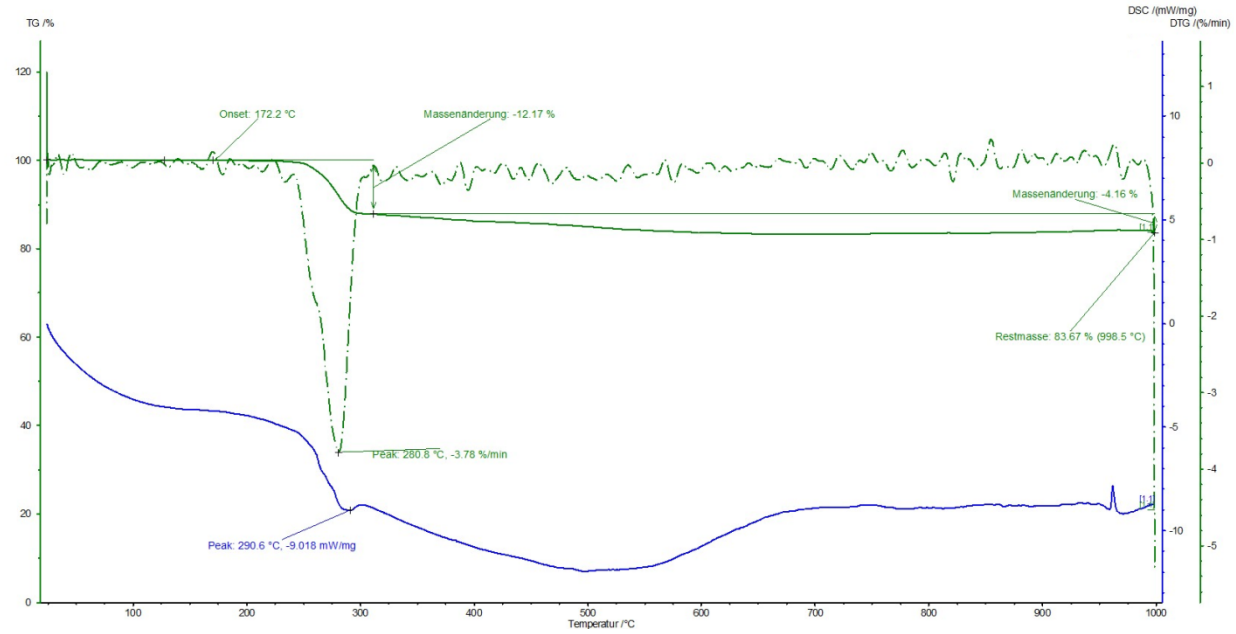

Figure A.1.1. TG/DSC curves of silver coordination polymer, $[Ag_2(HO_3PCH_2COO)]_n$ **(1)**

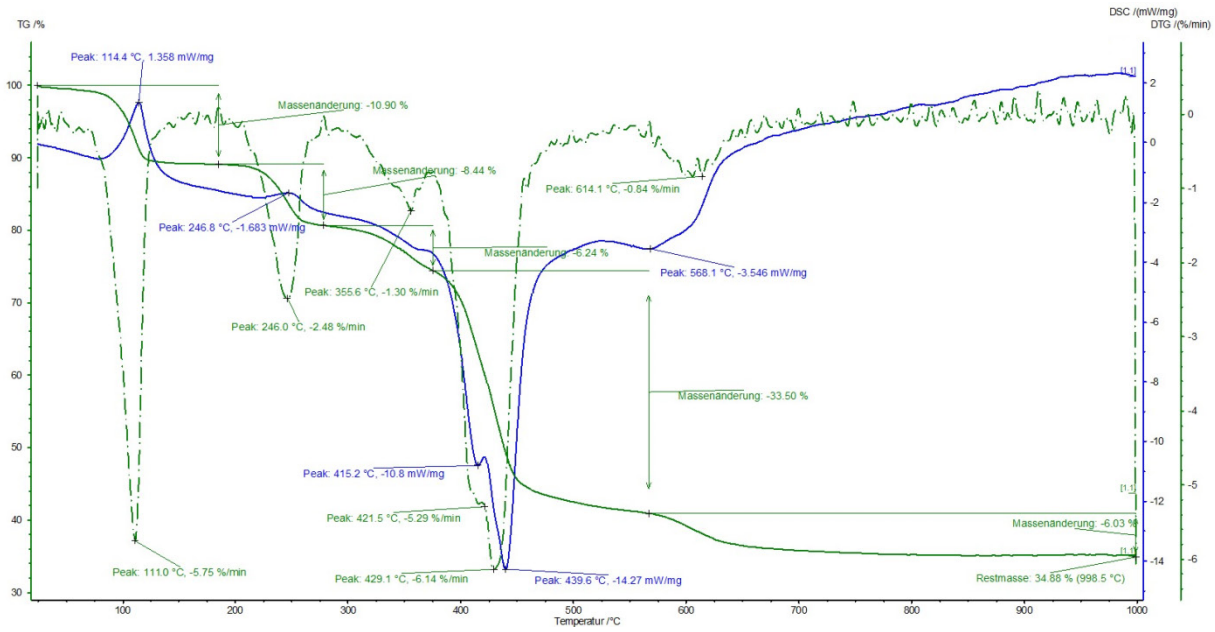

Figure A.1.2. TG/DSC curves of coordination polymer, $\{[Nd_2(FDA)_3(DMF)(H_2O)_2]\cdot DMF\cdot(H_2O)_2\}_n$ **(2)**

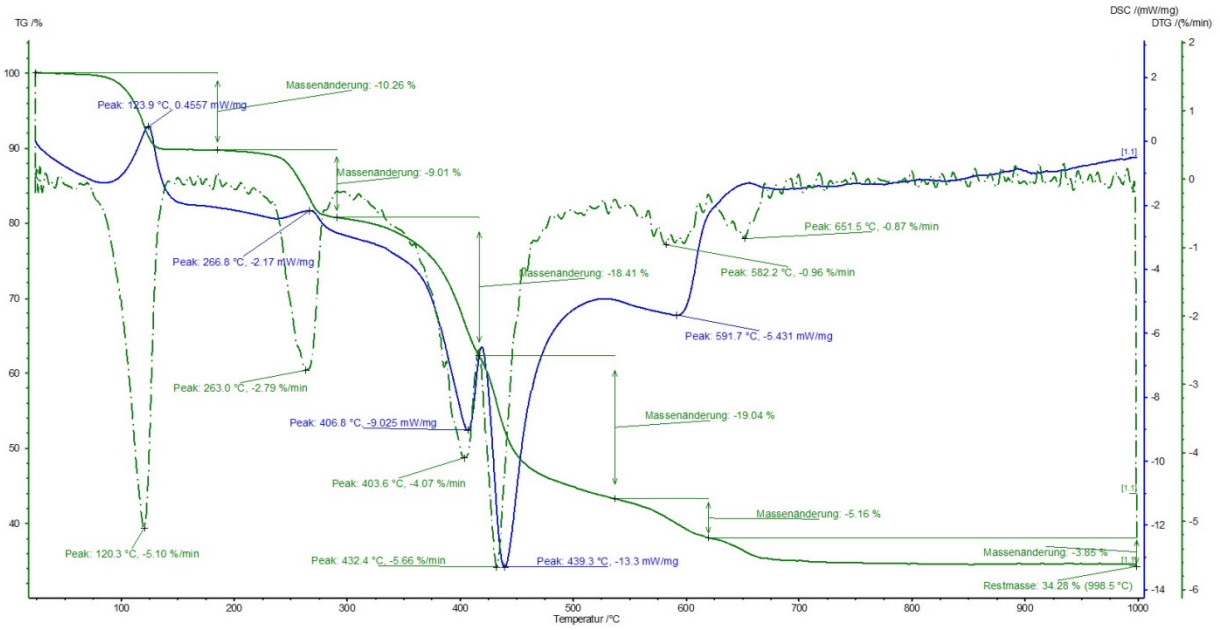

Figure A.1.3. TG/DSC curves of coordination polymer, $\{[Sm_2(FDA)_3(DMF)(H_2O)_2]\cdot DMF\cdot(H_2O)_2\}_n$ **(3)**

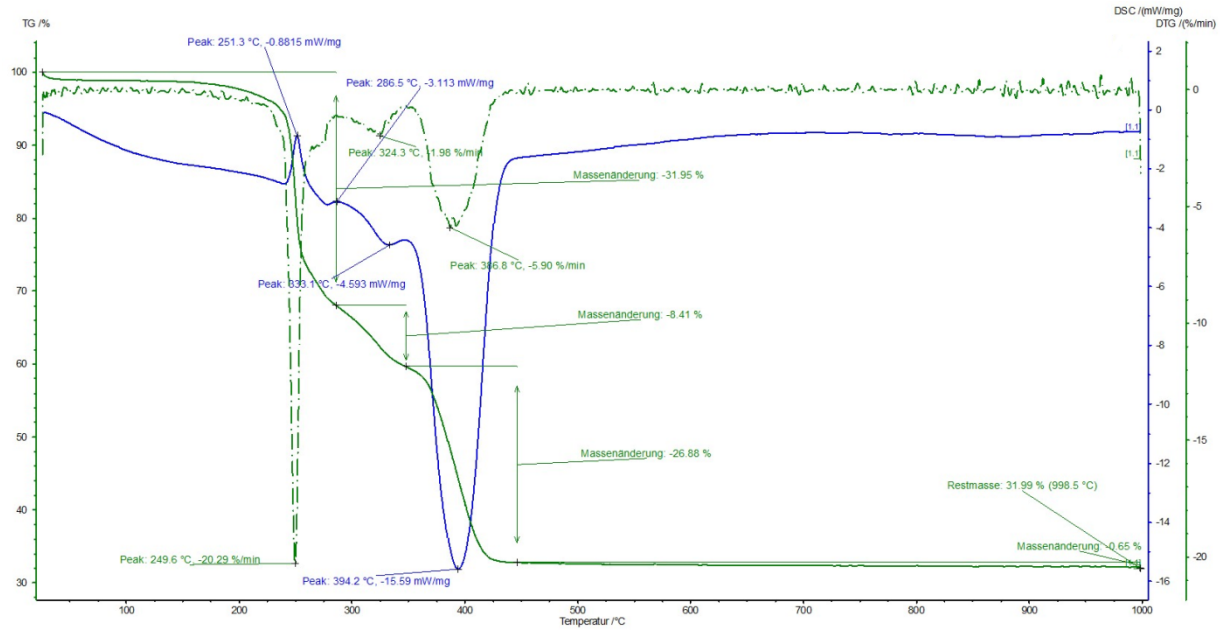

Figure A.1.4. TG/DSC curves of cerium coordination polymer, $[Ce(pdc)(DMF)_2(NO_3)]_n$ **(4)**

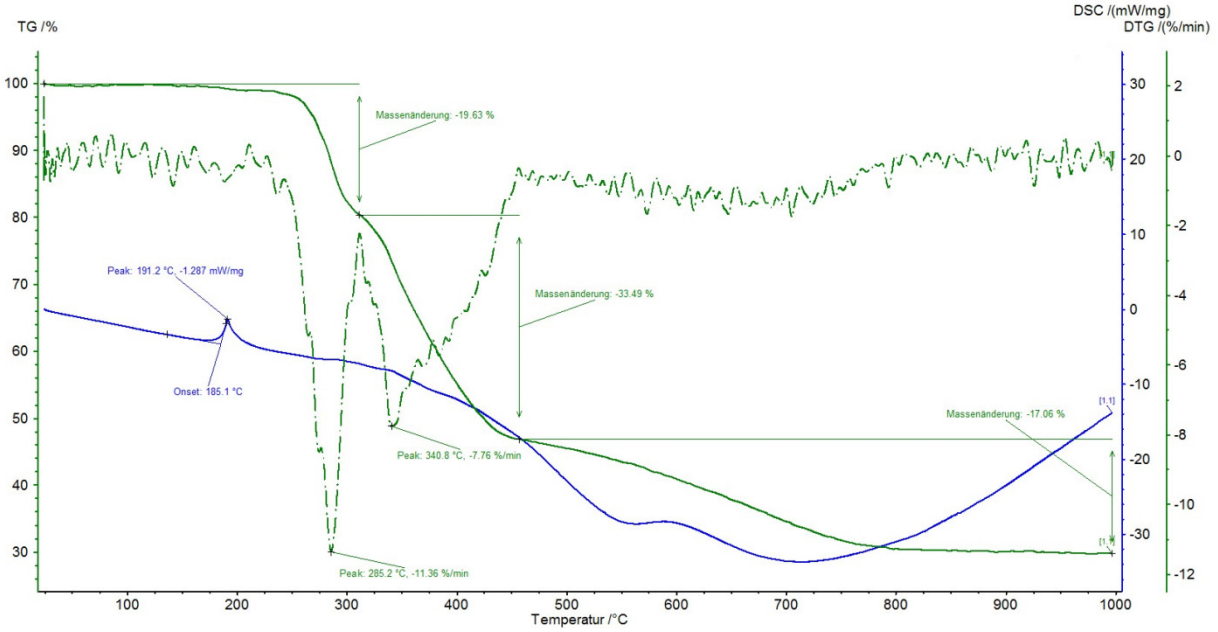

Figure A.1.5. TG/DSC curves of copper coordination polymer, $[Cu((\mu_{N,N'}\text{-4-MeO-ba})_2bn)Br]_n$ **(5)**

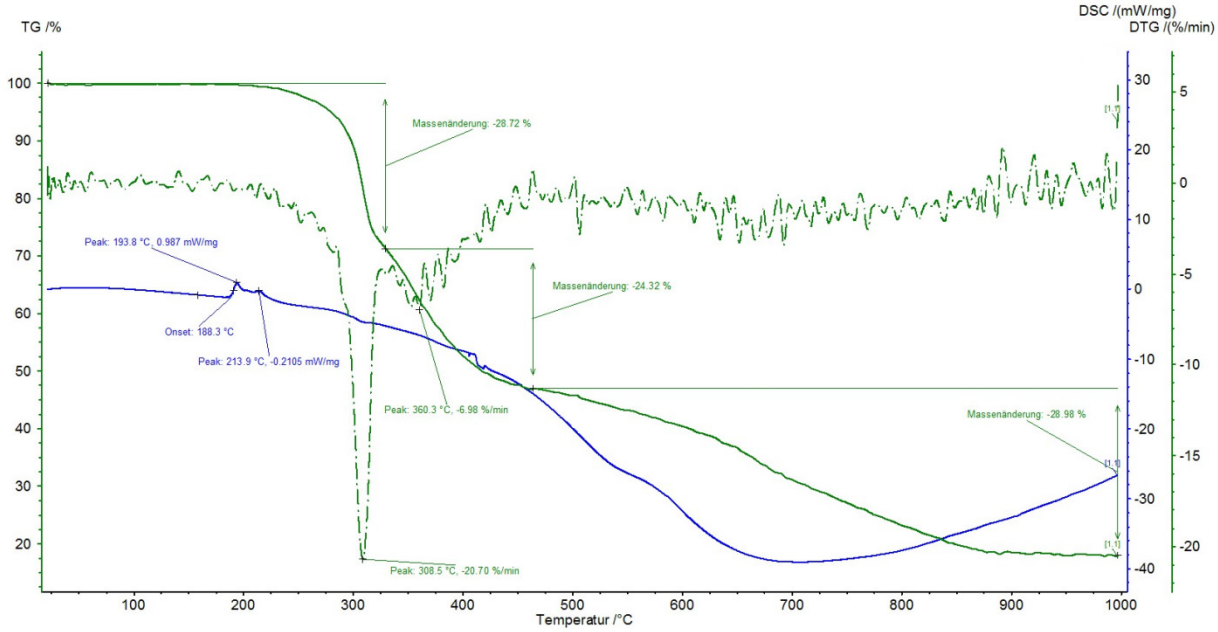

Figure A.1.6. TG/DSC curves of copper coordination polymer, $[Cu((\mu_{N,N'}\text{-4-MeO-ba})_2bn)I]_n$ **(6)**

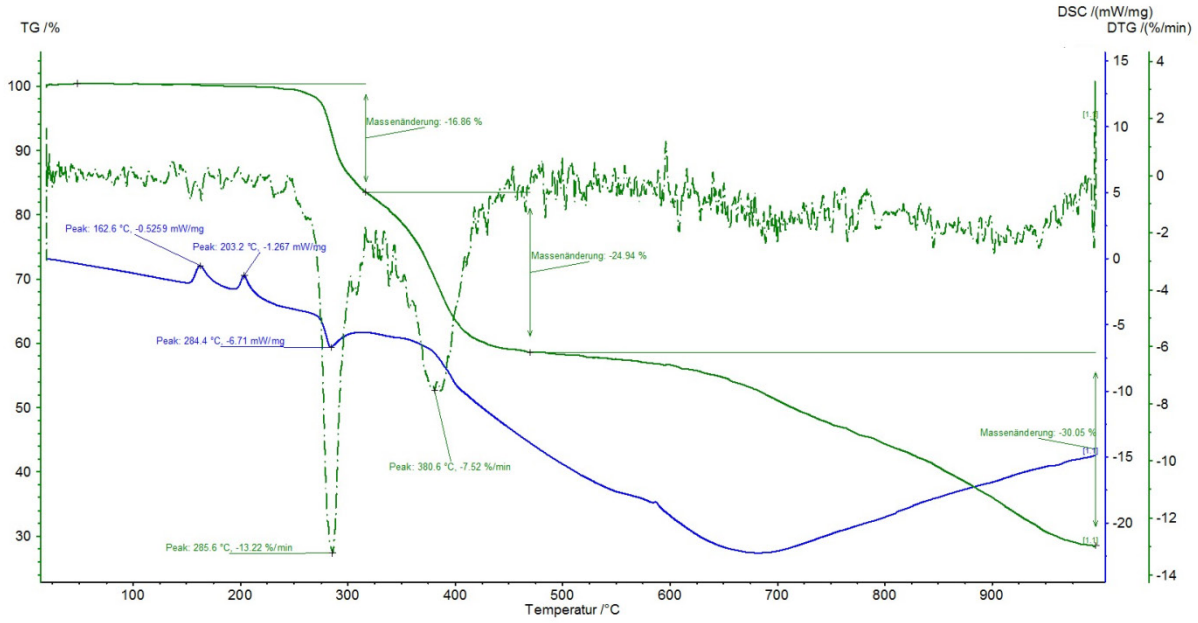

Figure A.1.7. TG/DSC curves of copper coordination polymer, $[Cu((\mu_{N,N'}\text{-4-Cl-ba})_2bn)I]_n$ **(7)**

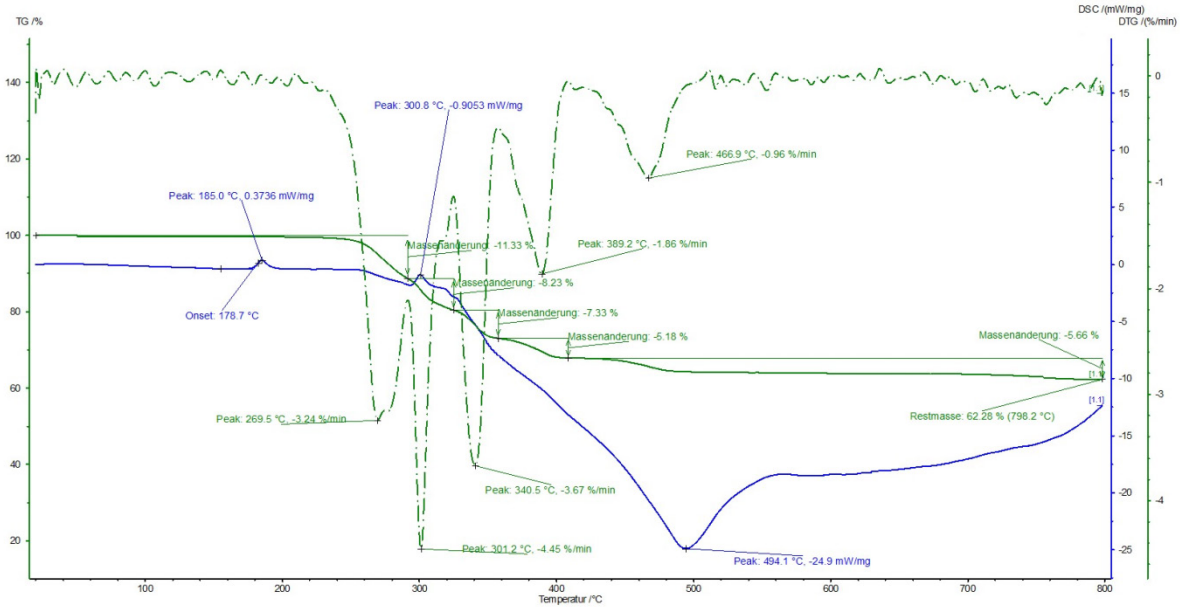

Figure A.1.8. TG/DSC curves of lead coordination polymer, $[Na_2Pb_2(CH_3COO)_6]_n$ **(9)**

A.2. (XRD) Simulated and experimental patterns

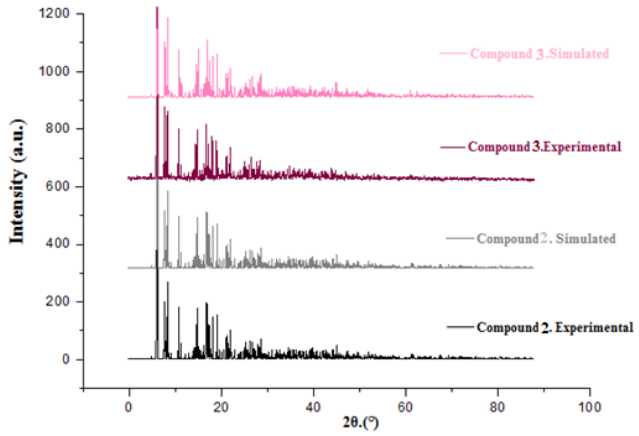

Figure A.2.1. Experimental and Simulated powder X-ray diffraction patterns for compound **(2)** (neodymium coordination polymer) and **(3)** (samarium coordination polymer)

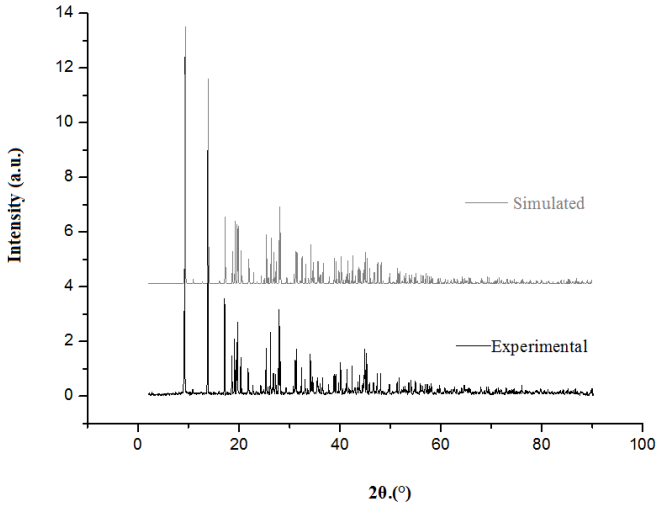

Figure A.2.2. XRD patterns: (gray) simulated pattern based on single crystal data of cerium compound **(4)** and (black) experimental pattern

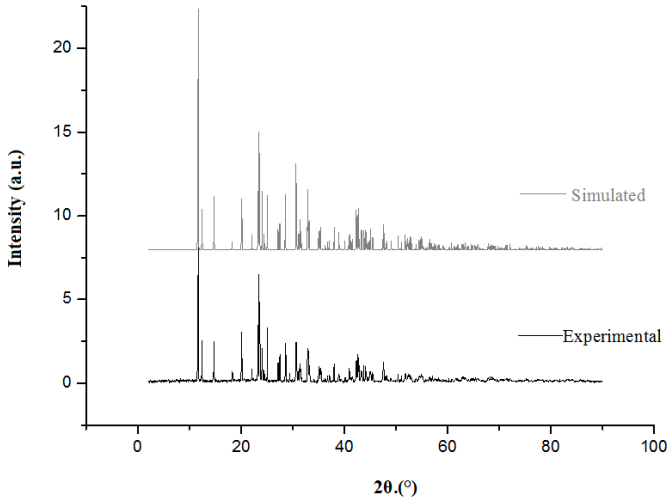

Figure A.2.3. (XRD) Simulated and experimental patterns of compound $[Pb(DHBDA)]_n$ **(10)**

Symbols and Abbreviations

CP	Coordination polymer
MOF	Metal organic framework
SBU	Second building unit
NLO	Non linear optic
SMM	Single-molecule magnets
SCM	Single-chain magnets
POM	Polyoxometalate
EE	End-to-end
EO	End-on
MO	Molecular orbital
1D	One-Dimension
2D	Two-Dimension
3D	Three-Dimension
∠	Angles

Materials

bmdt	*N*,*N*′-bis(4-methoxybenzyl)diethylenetriamine
py	pyridine
dca	dicyanamide
tem	tricyanomethanide
TBC	1,3,5-tricyanobenzene
TEB	1,3,5-tris(4-ethynylbenzonitrile)benzene
TEBB	1,3,5-tris(3-ethynylbenzonitrile)benzene
BPCN	4,4′-biphenyldicarbonitrile
tcnb	1,2,4,5-tetracyanobenzene
pyz	pyrazine
HBz	Benzoic acid
Pym	Pyrimidine
pydz	Pyridazine
4,4′-bipy	4,4′-bipyridine
2,2′-bipy	2,2′-bipyridine
H_2pzdc	2,3-pyrazinedicarboxylic

tpt	2,4,6-tris(4-pyridyl)-1,3,5-triazine
tpb	1,3,5-tri(4-pyridyle)-benzene
tri	triazine
NH_2trz	4-amino-4*H*-1,2,4-triazole
H_4BTA	biphenyl-3,3′,4,4′-tetracarboxylic acid
bib	1,2-bis(imidazole-l-yl methyl)benzene
titbm	1,3,5-tris(imidazole-l-ylmethyl)-2,4,6-trimethylbenzene
bimp	bis(4-imidazolphenoxy)methane
H_2bdc	1,4-benzenedicarboxylic acid
btc	benzene-1,3,5-tricarboxylic acid
2-pyc	pyrazine-2-carboxylate
ppca	4-(pyridine-4-yl)pyridine-2-carboxylic acid
Phen	1,10-Phenanthrolin
Bpe	(1,2-di(4-pyridyle)ethylene)
Bpa	(1,2-di(4-pyridyle)ethane)
Bpp	(1,3-di(4-pyridyle)propane)
HAT	1,4,5,8,9,12-hexaazatriphenylene
tpyt	5,10,15,20-Tetra(4-pyridyl)-prophine
H_2btm	Bis(tetrazolyl)methane
H_4adip	5,5′-(anthracene-9,10-diyl)diisphthalate
bpydb	4,4′-(4,4′-bipyridine-2,6-diyl)dibenzoate
addi	5,5′-(acridine-2,7-diyl)diisophthalate
azpy	4,4′-azopyridine
NNO	Nicotinate N-Oxide
H_2FDA	2,5-furandicarboxylic acid
H_2pdc	3,5-pyrazoledicarboxylic acid
(N,N′-MeO-ba)$_2$bn	N,N′- bis (4-methyl-benzylidene)butane-1,4-diamine
(N,N′-4-Cl-ba)$_2$bn	N,N′- bis (4-chloro-benzylidene)butane-1,4-diamine
H_2-DHBDA	2,5-Dihydroxy-1,4-benzenediacetic acid

Solvents

DMF	Dimethylformamid
DMSO	Dimethylsulfoxide
EtOH	Ethanol
MeOH	Methanol
DME	Dimethoxyethane
S_1	Solvent 1
S_2	Solvent 2

Thermal analysis

TGA	Thermal gravimetric analysis
DSC	Differential scanning calorimetric
Exo	Exothermic
Endo	Endothermic
Temp	Temperature

IR Spectroscopy

Δ	Δ values, Deacon and Phillips
$\upsilon_{as(COO-)}$	Asymmetric stretching vibration of carboxyl group
$\upsilon_{s(COO-)}$	Symmetric stretching vibration of carboxyl group
S	Strong
VS	Very strong
M	Medium
W	Weak

Lebenslauf (CV)

Mona Feizbakhsh Bazargani

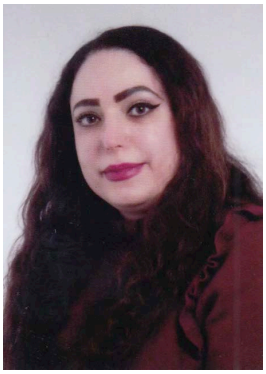

Persönliche Daten:

Name: Mona Feizbakhsh Bazargani

Geburtsdatum /-Ort : 21.09.1982 Tehran / Iran

Nationalität : Iranisch

Studium:

- **2012-2018 / Anfertigung einer Dissertation in Anorganischer Chemie / Friedrich-Schiller- Jena Universität / in Jena / Deutschland**

  Betreuer: Professor Dr. Christian Robl

- **Thema der Doktorarbeit:** "Synthesis and characterization of ten new 1D, 2D and 3D-coordination polymers with oxygen and nitrogen containing ligands by using different metal cations".
- **2007 – 2010 / Master der Naturwissenschaft (MSc) in Anorganischer Chemie / Karaj Islamic Azad Universität / in Karaj / Tehran / Iran**

  Betreuer: Associate Professor Dr. Afshin Rajabi Khorrami

  Co- Betreuer: Professor Dr. Hamidreza Khavasi und Associate Professor

  Dr. Ali Mahmoudi

- **Thema der Masterarbeit:** "Synthesis and characterization of metal ion imprinted polymers for thallium and cadmium ions extraction from natural and industrial waters by SPE method".
- **2000 – 2005 / Bachelor der Naturwissenschaft (BSc) in Angewandter Chemie / Karaj Islamic Azad Universität/ in Karaj / Tehran / Iran**
- **Thema der Bachelorarbeit:** "Investigation of modifications' parameters of syrup in evaporation part".

  Betreuer: Assistant professor Dr. H. Baheri

Co- Betreuer: M. Sepaveh “Unternehmer der Zuckerfabrik ”.

- 1996 – 2000 / Moallem Schule , Rasht, Gilan, Iran
  Diploma in Experimenteller Wissenschaft

Publikationen:

- **Pyridine-Functionalized TiO2 Nanoparticles as a Sorbent for Preconcentration and Determination of Ultra-Trace Palladium Ions:**
  Mohammd Karimi[1], Mona Feizbakhsh Bazargani[2], Forouzan Aboufazeli[1], Hamidreza Lotfizadeh[1], Omid Sadeghi[1] and Ezzatollah Najafi[1].
  In Current World Environment Vol. **7**(2), 227-232 (2012).

- **2-[(1H-Imidazol-2-yl)disulfanyl]-1Himidazol:** Mona Feizbakhsh Bazargani, Laleh Talavat, SoheilaNaderi and Hamid Reza Khavasi,
  in Acta Crystallographica Section E Structure ,2012

- **Immobilization of Metalloporphyrin on Functionalized Magnetic Nanoparticles as a Catalyst in Oxidation of Cyclohexene: Novel Modified Fe3O4 Nanoparticles with Triethoxysilane Agent :**
  Omid Sadeghi, Mostafa M. Amini, Mona Feiz Bakhsh Bazargani, Azadeh Mehrani, Amineh Aghabali, Maryam Adineh, Vahid Amani, Kheirollah Mehrani,
  In J Inorg Organomet Polym, (2012) 22:530–535, DOI 10.1007/s10904-011-9563-x

Stipendien:

- April 2013-Juli 2017 Doktorandenstipendium des Deutschen akademischen Austauschdienst (DAAD)
- Juli - Januar 2019 Promotionsabschlussstipendien der Graduierten-Akademie der Friedrich-Schiller-Universität Jena

Jena 04.07.2018

Mona Feizbakhsh Bazargani

Declaration of authorship / Selbstständigkeitserklärung

I certify that the work presented here is, to the best of my knowledge, original and the result of my own investigation, except as acknowledged, and has not been submitted, either in part or whole, for a degree at this or any other university.

Ich erkläre, dass ich die vorliegende Arbeit selbstständig und nur unter Verwendung der angegebenen Hilfsmittel, persönlichen Mitteilungen und Quellen angefertigt habe und dass ich nicht die gleiche, eine in wesentlichen Teilen ähnliche oder eine andere Abhandlung bei einer anderen Hochschule als Dissertation eingereicht habe.

Jena, 04.07.2018

Mona Feizbakhsh Bazargani